Published in final edited form as:

Chem Rev. 2022 March 09; 122(5): 5233–5276. doi:10.1021/acs.chemrev.1c00365.

Dissecting Biological and Synthetic Soft–Hard Interfaces for Tissue-Like Systems

Yin Fang,
The James Franck Institute, University of Chicago, Chicago, Illinois 60637, United States; Present Address: School of Chemical and Biomedical Engineering, Nanyang Technological University, 70 Nanyang Drive, Singapore 637457, Singapore

Xiao Yang,
Department of Chemistry and Chemical Biology, Harvard University, Cambridge, Massachusetts 02138, United States

Yiliang Lin,
The James Franck Institute, University of Chicago, Chicago, Illinois 60637, United States; Department of Chemistry and The Institute for Biophysical Dynamics, University of Chicago, Chicago, Illinois 60637, United States

Jiuyun Shi,
The James Franck Institute, University of Chicago, Chicago, Illinois 60637, United States; Department of Chemistry and The Institute for Biophysical Dynamics, University of Chicago, Chicago, Illinois 60637, United State

Aleksander Prominski,
The James Franck Institute, University of Chicago, Chicago, Illinois 60637, United States; Department of Chemistry and The Institute for Biophysical Dynamics, University of Chicago, Chicago, Illinois 60637, United States

Clementene Clayton,
Department of Chemistry, University of Chicago, Chicago, Illinois 60637, United States

Ellie Ostroff,
Department of Chemistry, University of Chicago, Chicago, Illinois 60637, United States

Bozhi Tian
The James Franck Institute, University of Chicago, Chicago, Illinois 60637, United States; Department of Chemistry and The Institute for Biophysical Dynamics, University of Chicago, Chicago, Illinois 60637, United State

Corresponding Authors Yin Fang – The James Franck Institute, University of Chicago, Chicago, Illinois 60637, United States; Present Address: School of Chemical and Biomedical Engineering, Nanyang Technological University, 70 Nanyang Drive, Singapore 637457, Singapore; yin.fang@ntu.edu.sg; Bozhi Tian – The James Franck Institute, University of Chicago, Chicago, Illinois 60637, United States; Department of Chemistry and The Institute for Biophysical Dynamics, University of Chicago, Chicago, Illinois 60637, United States; btian@uchicago.edu.

Supporting Information

The Supporting Information is available free of charge at https://pubs.acs.org/doi/10.1021/acs.chemrev.1c00365.

Video illustrating the concept of the soft–hard “interaction framework”, where both the spatial and temporal aspects are discussed (MP4)

The authors declare no competing financial interest.

Abstract

Soft and hard materials at interfaces exhibit mismatched behaviors, such as mismatched chemical or biochemical reactivity, mechanical response, and environmental adaptability. Leveraging or mitigating these differences can yield interfacial processes difficult to achieve, or inapplicable, in pure soft or pure hard phases. Exploration of interfacial mismatches and their associated (bio)chemical, mechanical, or other physical processes may yield numerous opportunities in both fundamental studies and applications, in a manner similar to that of semiconductor heterojunctions and their contribution to solid-state physics and the semiconductor industry over the past few decades. In this review, we explore the fundamental chemical roles and principles involved in designing these interfaces, such as the (bio)chemical evolution of adaptive or buffer zones. We discuss the spectroscopic, microscopic, (bio)chemical, and computational tools required to uncover the chemical processes in these confined or hidden soft–hard interfaces. We propose a soft–hard interaction framework and use it to discuss soft–hard interfacial processes in multiple systems and across several spatiotemporal scales, focusing on tissue-like materials and devices. We end this review by proposing several new scientific and engineering approaches to leveraging the soft–hard interfacial processes involved in biointerfacing composites and exploring new applications for these composites.

Graphical Abstract

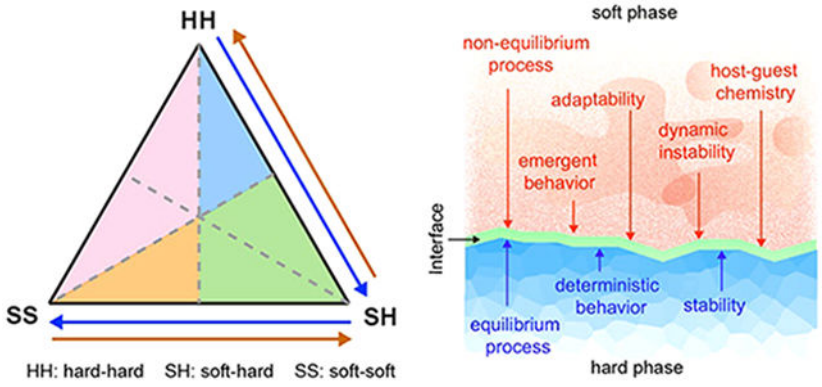

1. INTRODUCTION

1.1. Underexplored Dynamics at Soft–Hard Interfaces

Due to their diverse and tunable physical and chemical properties, soft[1-7] and hard[3,8-10] materials have been extensively explored in fundamental studies of biological and material dynamics and diverse applications. Elucidation of the underlying processes that yield either soft or hard materials or their individual behaviors has enabled numerous advances, such as the development of strain-adaptive stiffening triblock copolymers,[11] the discovery of hyper-expandable and self-healing macromolecular crystals[12] and other soft crystals,[13] and the synthesis of boron arsenide crystals[14] with ultrahigh thermal conductivity. However, our understanding of the dynamics at, or enabled by, soft–hard interfaces is surprisingly scattered (Figure 1a). There is a pressing need for a unified view of the processes at these soft–hard interfaces and understanding their implications across multiple disciplines, such

as basic materials science,[2,3,15-19] energy and environmental science,[2,20-22] catalysis,[23,24] biomedical research,[20,25] geobiology,[26,27] food science,[28] and even cosmetics.[20].

Several important interfacial mismatches exist at soft–hard interfaces, such as mismatches in mechanical properties, electrical conductivities, chemical diffusivity, and reactivity. These mismatches, while obstacles to our fundamental understanding of the interfaces, constitute a multifaceted platform for the discovery of novel smart materials. Chemical and physical processes at soft–hard interfaces may be distinct from those observed in homogeneous materials (e.g., molecular reaction-diffusion in a hydrogel matrix[29,30]) or other heterostructure interfaces used for catalysis[31] or electronics[32,33] (e.g., polyelemental nanoparticles[34] and high-order colloidal hybrid nanoparticles[35]).

1.2. Definition of “Soft” and “Hard” and Its Relevance to Materials Chemistry

In Chemistry literature, the definitions of “hard materials or phases” (H) and “soft materials or phases” (S) are sometimes confusing. Soft materials can include a large collection of materials, including droplets, hydrogels, polymers, foams, and most biological components[36] (Figure 2a). Additionally, the boundary between “soft” and “hard” is not clear-cut. For example, crystals are usually considered hard and brittle. However, the soft ionic bonding in organic–inorganic halide perovskite[37] crystals has yielded facile ion transport and defect tolerance, and the dynamic bonding between hydrogel matrix and ferritin molecules has produced self-healing and antifragmentation behaviors in hyper-expandable macromolecular crystals.[12]

Stiffness or rigidity describes the material’s capacity to resist deformation in response to an applied force. It is determined by the elastic modulus and the material structures (e.g., cross-sectional area and length). While the elastic modulus is a property (i.e., it is a constant within a certain range), the stiffness is dependent on the material’s geometry. For example, while the elastic modulus is the same (or quite close) in bulk silicon and silicon nanowire, the stiffness is drastically different such that a silicon nanowire can easily bend while the bulk material cannot. For uniaxial deformation, we typically use the Young’s modulus (E), as defined by the initial slope of the uniaxial stress–strain curve (Figure 2b). Chemical reactions such as in situ mineralization can stiffen a deformable matrix.[3,16] In contrast, chemical or biochemical degradation can eliminate the stiff components in a composite to improve compliance.

Strength represents the maximum stress a material can tolerate before it reaches a certain limit or a transition (Figure 2b). Specifically, ultimate tensile strength is the maximum stress on the stress–strain curve. Another strength, the yield strength is the stress that initiates plastic deformation of a material. Strength is related to the bulk or internal structures and the defects. Chemical approaches such as incorporation of self-healing[38,39] or ionic/covalent cross-linking[40] moieties inside the materials can increase the strength.

Hardness describes the resistance of a material surface to indentation. Chemical processes (e.g., cross-linkage) or coating strategies at the surface can be used to improve the surface hardness of a material.

Toughness quantifies the resistance of a material to fracture (Figure 2b). Toughness is usually calculated by integrating the area under a stress–strain curve, i.e., the energy consumed before the fracture point. Chemical interactions between multiple components in a hierarchical layout (such as the brick-and-mortar structure in nacre[3]) can integrate superb toughness and stiffness in a single composite material.

Based on these definitions, stiffness or modulus (Figure 2a) is the dominant figure-of-merit in Chemistry literature to define a hard or soft material and is highly relevant to a material's deformability. In particular, as the stiffness is size-dependent, one can create a highly deformable material that has intrinsically high modulus, such as a silicon nano-membrane.[41] Stiffness, strength, hardness, and toughness can all be tuned chemically. In this review, we define an interface as a soft–hard interface if the two phases have a modulus or bending stiffness difference of at least one order-of-magnitude.

1.3. Soft–Hard Interfaces Are Common to Both Living and Nonliving Systems

Soft–hard interfaces are critical for many life processes.[42] For example, studies of interfaces in nacre biogenesis revealed that epithelial cells produce all of the components required for the nacre composites and that several proteins[43,44] control the crystallization of aragonite (the hard granules in the composite).[3] In bone growth, the highly coordinated processes of chemical transport, storage, and release and resorption of phosphate and calcium ions confer strength, self-healing properties, and stability.[16] Perturbation of this homeostasis yields pathological mineralization or dissolution of bone.[16] The principles gleaned from studies of natural interfaces can be applied to synthetic materials to confer properties such as ultrahigh toughness and strength[3] and environmental adaptability.

Interfacial chemical processes can display cooperative assembly, periodic instability, or other dynamic activities necessary for material morphogenesis (Figure 3a). This principle underlies many mineralization processes where a biphasic interaction between the organic matrix and inorganic mineral precursors produces intricate three-dimensional (3D) architectures, including dodecahedral silica cages[45] (Figure 3b) or silica rings[46] over individual micelles and mesostructured materials.[47-52] In a nanowire growth system, the soft–hard interfacial chemistry produces periodic sawtooth faceting,[53] twin plane superlattices,[54] and the alloy droplet-assisted periodic deposition of atomic gold lines.[55]

1.4. Harnessing Soft–Hard Interactions to Improve Composite Performance or Signal Transduction

Biphasic behaviors[57,58] can be controlled by tuning the mechanical, electrical, and chemical interfacial interactions between soft and hard components, leading to improved material and device performance. In orthopedic applications, the ideal biomaterial surface (i.e., for the implant-tissue interface) should include surface interactions or topography that resist bacterial adhesion and enhance integration with host cells and tissues.[59] In energy research, the incorporation of both hard and soft material components can improve device performance. For example, the M13 virus forms a hydrogel with superaerophobic properties. When assembled over a photoelectrochemical device surface, the hydrogel layer promotes the elimination of the gas bubbles generated during the photoelectrochemical reaction. This

soft–hard composite significantly improves photoelectrode performance, as it helps maintain catalytic activity and reduces the overpotential for chemical reactions.[60]

van der Waals interactions, hydrogen bonding, electrostatic force, or chemical cross-linking at soft–hard interfaces are critical for stability, damage tolerance, and integration (Figure 3c) in heterogeneous materials or devices.[21,23,61-64] For example, in mechanical engineering, when hard particles or fibers are used to increase the stiffness of a polymer matrix, the interfacial interactions between the filler materials and the polymer are critical for mechanical durability and avoiding phase separation.[61] Likewise, conformal polymer coating over brittle ceramic mesostructures[64] has significantly improved compressive strength and toughness.

The intermolecular forces or chemical cross-linking at the interfaces can also improve bonding of hydrogels or elastomers onto various substrates, including metals, plastics, and even Teflon.[65,62] They can produce mineral sheet-based hydrogels capable of biocatalysis[23] or improve the longevity of a battery device[21,22] through dynamic processes (e.g., ring sliding of polyrotaxane[66]) at the interface between the binder (e.g., PAA,[21,66] alginate,[21,54,67] and PEDOT[21,68]) and the active material (e.g., Si,[21,66,67,69] $LiNi_xCo_yMn_{1-x-y}O_2$ [ref 68]). Preservation of soil organic matter (SOM) or tissue remains over mineral surfaces or in vertebrate fossils[70] represents another example of soft–hard interface-enabled stability. Samples from Cretaceous period dinosaur bones show structures indicative of endogenous collagen fibrils with 67 nm-wide periodic banding.[70]

Chemical, topographical, mechanical, and electrical processes at soft–hard interfaces underlie many sensing and modulation applications in biomaterials science, as they enable diverse signal transduction and cascade reactions[15,71,72] (Figure 3a). For example, nanopillars have been used to study the effect of cell-material interfacial curvature on the mechano-biochemistry of the plasma membrane. Using nanopillars to control plasma membrane curvatures (+50 nm to ~−500 nm), it was reported that only the positively curved membranes are hotspots for proteins such as clathrin and dynamin[56] (Figure 3c).

1.5. Aims of This Review

Here, we review the role and importance of mechanical, electrical, and chemical activities at the interfaces between soft and hard materials. We discuss the length and time scales for the interfacial processes. For many (bio)chemical events at the cell-bioelectronic device interface, these scales are the mesoscopic length scale and millisecond time scale. We describe the unique microenvironment of interfacial mechanical, electrical, and chemical processes, including ion accumulation in the cell-bioelectronics cleft and focal adhesion production at cell contact sites. We discuss the tools used to reveal interfacial processes, such as immunohistochemical labeling and focused-ion-beam (FIB) milling in biointerfaces. Next, we propose a new interaction framework to classify the soft–soft (SS), soft–hard (SH), and hard–hard (HH) interactions involved in diverse soft–hard composites. To prove the validity of this soft–hard interaction framework, we first discuss its relevance in chemical processes at both naturally occurring and synthetic soft–hard interfaces, such as the inflammatory biochemical response and the light-triggered faradaic modulation effect at cell-silicon interfaces. We then apply the validated interaction framework to rationalize

recent research advances in tissue-like materials, bioelectronics, and robotics, where SS, SH, and HH interactions beyond chemical ones (such as mechanical interactions) are involved. Finally, we use the validated interaction framework to predict new opportunities in tissue-like systems.

2. LENGTH AND TIME SCALES

Soft–hard interfaces are widely distributed throughout natural and synthetic systems (Figure 1). For example, through the interface between a soft mechanophore and a rigid ligand, macroscopic isotropic stress can be translated into atomic-level anisotropic strain for bond activation.[73] Soft–hard interfaces also play critical roles in the self-assembly[45] and transport properties[74,75] of nanocrystal solids, toughening in biominerals,[3,76] liquid alloy-catalyzed synthesis of semiconductor nanowires,[54,55,77-81] and precipitation of nanocrystals inside the alloy droplet.[77] In terms of mesoscopic level interfaces, tailored chemical interactions between the binder and the electrode[66,67,69] can increase the number of cycles in a battery, thereby improving battery performance;[21,22] cellular coordination can deposit renal stones at cell membranes and extracellular matrices;[82] and rapid ionic dynamics at cell/semiconductor interfaces can enable either electronic sensing[15,83,84] or modulation[85-88] in excitable tissues. Soft–hard interfaces at the macroscopic level can also influence the chemical and biochemical dynamics of SOM[89,90] at mineral surfaces and the formation of biofilms on the surface of medical implants[59] or naval equipment.

While these soft–hard interfaces cover a wide range of length scales, the critical chemical processes all occur at the molecular or nanoscopic level (Figure 1a). For example, bioelectronics devices operate through the modulation of ion channel dynamics,[86,91-93] and the proteins in SOM become stabilized through molecular interactions with mineral lattices.[90,94] The fact that diverse soft–hard interfaces overlap within such a unique size regime suggests several guiding principles for functional integration of soft and hard components in either naturally occurring or synthetic systems (Figure 4a).

The time scales of chemical processes at soft–hard interfaces cover an equally broad range (Figure 1b).[36] Fast processes include bond dissociation and electron transfer, which typically happen on the picosecond or subpicosecond time scale. As soft–hard interfaces can involve material growth and degradation, or cellular migration and development, some slow chemical processes can take hours to years.

3. UNIQUE (BIO)CHEMISTRY AT SOFT–HARD INTERFACES

Leveraging or mitigating the mismatches at soft–hard interfaces may yield new interfacial chemical processes. Additionally, interfacial chemical processes are influenced by both the activities of, and the interplay between, the soft and hard components. In this regard, the interfacial chemistry at soft–hard interfaces would be challenging to achieve, or inapplicable, in purely soft or hard media. Understanding unique interfacial properties, such as the confined space and the buffer zone, may guide our approach to exploring new chemical processes.

3.1. Utilizing the Confined Space to Mitigate Interfacial Mismatches

Many soft–hard interfaces are confined to the molecular or nanoscopic scale. This confinement is driven by the convergence of the amplitudes of many energy terms (e.g., electrostatic, mechanical, and chemical energies) at the molecular and nanoscopic scales (Figure 4a).[62,95] This energy convergence[36] represents one direct solution[17] to mismatches between soft and hard components. It can give rise to a wide range of intricate nanocomposites, such as a multifunctional hydrogel self-assembled from nanoclays and dendritic binders[23] (Figure 4b) and the silica-cetyltrimethylammonium bromide (CTAB) interface in the silica cage[45] (Figure 2b). The convergence also suggests a pathway for diverse or multimodal signal transductions at, or close to, the interfaces (Figure 4a), where nonchemical modulations such as mechanical deformation[12] or optoelectronic stimulation[15,36] could trigger interfacial chemical or biochemical processes. For example, in the presence of balanced magnetic force and electrostatic repulsion, optical illumination of titanate and niobate nanosheets triggers in situ vinyl polymerization to yield anisotropic hydrogel composites.[63]

3.2. Utilizing Buffer Zones to Mitigate Interfacial Mismatches

While multiple energies can converge at molecular-scale areas or volumes (Figure 4a), interfacial mismatches usually persist if the dimensions of the individual components are far above the molecular scale. Across different natural and synthetic soft–hard interfaces, we identify three chemical or biochemical buffer zone strategies (Figure 4c) to alleviate additional mismatch issues. These indirect solutions to mismatches can achieve seamless integration of soft and hard components.

3.2.1. Additive Strategy—Linkers or Deposits at the Interface.—At the interface between cells and a stiff substrate, linkers and deposits serve as the transition regime between the soft and hard components (Figure 4c, left). Chemical processes at this interface involve focal adhesion formation[71] and extracellular matrix (ECM) deposition at the rigid surface of the substrate. For example, integrin aggregates on ECM substrates serve as the interfacial additive in focal adhesion formation in biological systems.[97] Formation of the nascent adhesion is usually accompanied by traction forces that induce conformational changes in cytoskeletal proteins, such as talin and vinculin. Folding and unfolding of the intracellular proteins then triggers multiple phosphorylation events and enzymatic reactions, which activate cytoskeletal contractility and generate more traction force over the focal adhesion.[97] This series of events can “stiffen” the cellular contact, creating an adaptable transition from the cells to the rigid substrates. Another example involves the interfacial load-bearing protein linker Atrina pectinata foot protein-1 (APFP-1) which contains L-3,4-dihydroxyphenylalanine (DOPA)-containing and mannose-binding domains. APFP-1 is found at the junction between stiff byssus and soft tissue in the bivalve mollusk; the DOPA domain forms Fe^{3+}-DOPA complexes in the byssus and the mannose-binding domain attaches to the cells and tissues.[98] Other attachment linkers include microbial nanowires[99,100] that also facilitate electron transfer between minerals and microorganisms in soil.

3.2.2. Spatial Strategy—Graded Regime.—A modulus gradient over a long distance (up to centimeters) can efficiently reduce mechanical mismatch at a soft–hard interface for improved material or device durability and performance (Figure 4c, middle). At tendon-bone attachment sites, bone cells create a modulus gradient through precise control of mineralization across hard and soft tissues. Similar soft–hard gradients can be seen at interfaces between cranial sutures and the periodontal ligament,[16] in squid beak,[101,102] and in sucker ring teeth.[17] Another way to achieve the gradient is to establish an interpenetrating network in which the soft components are directly incorporated inside the hard component. This scenario is exemplified in the synthesis of mesostructured silica[50,51] (e.g., SBA-15). During self-assembly,[50] parts of the triblock copolymer chains are initially embedded inside the silica walls, producing a microporous "corona" upon template removal.[103] The interpenetrating network also increases the actual contact area, shrinks feature sizes at the interfaces, and enhances the interfacial roughness; similar principles have been used in promoting implant biointegration.[104]

3.2.3. Temporal Strategy—Hardening the Composite over Time.—Linkers or graded regimes facilitate the transition from soft to hard phases by adding new molecular materials at the interfaces or by increasing the spatial range of the interfaces. Robust and "minimally invasive" soft–hard integration can also be established through sequential chemical transformation from a soft–soft precursor (Figure 4c, right). The hardening process usually involves heterogeneous crystal nucleation and growth[105,106] over a soft matrix or cross-linking of a polymeric network to increase the local modulus.[101,102] For example, during bone mineralization, cell-mediated deposition of hydroxyapatite ($Ca_{10}(PO_4)_6(OH)_2$) begins with the production and distribution of initially soft and amorphous precursors, such as calcium-chelating polyPi matrix vesicles (an enzymatically cleavable substrate).[16] Synthetic equivalents include the sol–gel transition (i.e., the soft–hard transition) during precipitation of mesostructured silica.[50]

3.3. Leveraging Interfacial Mismatches for New Capabilities

Various interfacial mismatches may be mitigated through the convergence of energy amplitudes or establishment of a buffer zone; however, the interfaces still represent the transition between soft and hard components. Therefore, we can expect to find the largest gradients of mismatched properties or behaviors at soft–hard interfaces (i.e., the interfaces represent hotspots for triggered chemical processes), an aspect which can be explored for unconventional stimuli-responsive chemical processes.[73,107-109] Additionally, as soft and hard materials respond differently to external stimuli such as mechanical stress or electrical charging, temporary mechanical instability or chemical imbalance can occur locally at the interface, triggering (bio)chemical responses. In Si-based lithium batteries for example,[66] polyrotaxane has been incorporated into the poly(acrylic acid) (PAA) binder. This incorporation enables conversion of the large binder-Si interfacial strain into the ring sliding movement of polyrotaxane during a Si-based lithium-ion battery operation (Figure 4d); this triggered process has improved the anode cycling stability.

3.4. Rationale for Exploring New Chemistry at Soft–Hard Interfaces

Interfacial mismatches, and the natural and synthetic strategies to mitigate or leverage them, suggest a spectrum of exploratory pathways toward new chemical processes (Figure 5). New supramolecular chemistry may be discovered through the formation of soft–hard interfaces in a confined space. Examples include the electrochemical synthesis of monolayer atomic crystal molecular superlattices (MACMS).[110,111] Indirect seamless integration of soft and hard components through buffer zones can help reveal new homeostatic or biomimetic principles in coupled chemical reactions, by which the soft–hard interfaces evolve spatiotemporally. Finally, mismatches can be intentionally retained to yield mechanical instability[112] or chemical imbalance, because of the different responses of soft and hard components to external stimuli. These mismatches can then be used to explore new stimuli-responsive chemistry or chemical processes far from equilibrium.

4. TOOLS TO STUDY INTERFACIAL PROCESSES

Mechanical characterization methods, such as tensile and compressive deformation, dynamic mechanical analysis, shear rheometry, pipet or micropipette aspiration, (nano)-indentation, and atomic force microscopy, can provide important mechanical properties of the soft or hard components, or their integrated systems. These studies can yield the stress–strain behaviors upon uniaxial or dynamic deformation, and highly localized mechanical property probing and mapping. While it is challenging to use these tools to probe the interface mechanics directly, the mechanical information collected through a suite of such studies may provide clues for the interfacial processes.

Many conventional tools (Figure 6) can be used to study the chemical composition and chemical dynamics at soft–hard interfaces (Table 1). While these tools cannot reveal the mechanical properties of the soft or hard components, they provide essential molecular- or atomic-level chemical information that is responsible for the observed mechanical behaviors (which usually occur at scales above the micrometer level). Electron energy loss spectroscopy (EELS), energy-dispersive X-ray spectroscopy (EDS) and secondary ion mass spectrometry (SIMS) use electrons (i.e., EELS, EDS) or primary ions (i.e., SIMS) as the incident beam. They determine the elemental information (EELS, EDS, and SIMS) or even the state of valence electrons (EELS) by collecting inelastically scattered electrons (EELS), X-rays (EDS), and secondary ions (SIMS). Laser-assisted atom probe tomography (APT) can provide both elemental composition and subnanometer 3D imaging by decomposing the voltage-biased (DC voltage, 3–15 kV) sample with a laser beam. In addition to determining the composition, other tools can reveal the morphology, phase, and chemical bonding near soft–hard interfaces (Figure 6). Detailed descriptions of these tools, including their working principles and spatiotemporal resolutions, can be found in review papers published elsewhere.[113-116]

Biochemistry tools are particularly powerful when living systems are involved at soft–hard interfaces (Figure 6 and Table 1). For example, using time-of-flight secondary ion mass spectrometry, amino-acid fragments typical of collagen fibrils were found in Cretaceous period dinosaur bones, highlighting the fact that tissue residues can persist throughout the fossil record.[70] Integrated RNA-Seq and proteomics revealed two protein families,

chitin-binding proteins, and histidine-rich proteins, in the soft–hard transition region of squid beak.[101,102] In another example, immunohistochemical (IHC) staining[117,118] showed significant upregulation of glial intermediate filament proteins and the ECM molecules laminin and collagen IV, together with the softening of nearby tissue[118] upon insertion of rigid sharps into the brain.

Theoretical and computational tools (Figure 6), such as molecular dynamics simulations, have revealed numerous dynamic chemical processes at soft–hard interfaces,[61,119] including those that cannot be probed experimentally. These chemical processes include molecular wrapping over carbon nanotube sidewalls,[120-122] translocation of nanoparticles in cells and tissues,[123-125] and packing of nanowires in vesicles.[124,126]

4.1. Challenges in Characterizing Soft–Hard Interfaces

While the current tools have revealed important chemical insights, characterizations at soft–hard interfaces are generally more complicated than those performed on simple soft or hard components.

Soft–hard interfaces are usually embedded, requiring tools that can either directly visualize the interfaces nondestructively or provide 3D chemical or structural reconstruction of the interfaces after destructive sample preparations (e.g., APT[127] or computed X-ray tomography). Currently, tools capable of interfacial probing are limited, but we can expand the investigative tool kit by looking into existing approaches adopted in other areas. For example, optoacoustic imaging exploits ultrasonic acoustic waves that are generated by light-matter interactions. Optoacoustic imaging achieves a greater detection depth than imaging methods that rely on photons; the latter typically yields very limited depth of penetration due to photon scattering. While optoacoustic imaging has been used intensively for in vivo imaging[115,116,128] and has recently been used to reveal hidden underdrawings in paintings,[129,130] its utility in the study of dynamics at synthetic soft–hard interfaces is less explored and represents a promising tool. Other nondestructive methods to potentially reveal the mechanical properties at the soft–hard interfaces include magnetic resonance elastography and ultrasonic shear wave elastography,[131,132] which are usually used for probing biological tissues too. In particular, the ultrasonic elastography[131,132] uses ultrasonic pulses to generate shear waves through the material or biological tissues. While this technique is usually used to reveal various pathologies in biological tissues, it could be broadly extended to measure a composite’s mechanical heterogeneity through strain imaging and shear wave imaging.

Special preparation methods must be considered for samples that contain soft–hard interfaces. Certain characterizations require cutting through soft–hard interfaces, such as FIB milling for serial block imaging of 3D volumes in SEM[133] or generation of thin specimens for STEM and APT imaging. However, soft–hard interfaces display mechanical mismatches, which may necessitate cryogenic operations to produce fully hydrated frozen samples,[134] preserve the soft material structures, and avoid delamination at the soft–hard interfaces during FIB milling.

Finally, soft or hard materials usually use different sets of tools for their characterization. For example, while hard materials are usually stable under the electron beam in TEM, soft materials are prone to significant sample damage and artifact generation.[114,135,136] Likewise, confocal laser scanning microscopy (CLSM) is a powerful technique for solving the static or dynamic distribution of biomolecules in soft systems (Figure 6), but it usually provides minimal information on hard materials. In this regard, correlative microscopy and spectroscopy is needed to provide information on both the soft and hard phases at the interfaces.

4.2. Studying the Dynamics of Interfacial Chemical Processes

There are two broad approaches to investigating the dynamics of chemical processes at soft–hard interfaces (Figure 6).

First, in situ microscopy and spectroscopy have been widely used to probe chemical dynamics in directed organization, cooperative integration, or signal transduction at interfaces (Figure 6a). Tools such as cryo-TEM,[106,114] environmental TEM or TEM in liquid cells,[135,136,144] SAXS, CLSM, and field-effect transistor-based electrical recording display high spatial or temporal resolution and high sensitivity for capturing localized, transient, and weak chemical events. For example, using environmental TEM, the Ross group conducted multiple studies of the chemical dynamics at alloy droplet-semiconductor nanowire interfaces[33,53,77,78,80,81,145-150] (Figure 6a, second from left), including that of sawtooth faceting,[53] ledge flow,[81,148] twin plane or other defect formation,[137,148] and silicide quantum dot growth inside an alloy droplet and its stepwise merging into the nanowire backbone.[77] Electrical transport spectroscopy (ETS) was recently used for in situ recordings of molecular intercalation of 2D layered semiconductors,[111] representing a novel electronic method for studying soft–hard interfacial chemistry (Figure 6a, right).

Second, for a process that occurs over a longer duration (e.g., > a few days), single-shot, static and ex situ measurements are usually the best option (Figure 6b), as in situ recording is less feasible. The dynamic information can be inferred from measurements at multiple time points. In particular, correlative microscopies and spectroscopies alongside theory and computations studies can be used to integrate information on morphology, phase, molecular and elemental identity, and chemical bonding.

5. FRAMEWORK TO CLASSIFY SOFT-HARD INTERFACES

In this section, we move beyond chemical interfacial processes. Unique processes at the soft–hard interfaces are determined by the diverse soft material interactions (SS), the hard material interactions (HH), and the interactions between the soft and hard components (SH). Depending on the context of the discussion, the SS/HH could be the intramolecular interactions that hold the constituent phase together, the restoring forces upon elastic deformation, or physical or biological behaviors of the constituent. Likewise, the SH could be adhesion or bonding, chemical or biological recognition, or signal conversion (e.g., from photoelectrochemical to electrophysiological signals) at the soft–hard interfaces.

Based on the relative dominance of the roles played by the three interactions in determining the spatial organization or the temporal sequence of the soft–hard interface, we propose a soft–hard "interaction framework", which covers both the spatial and temporal aspects of the interactions (Figure 7, Supplementary Video 1).

Each color domain in Figure 7a-d (spatial aspect) is the overlapped area from two half-triangles which are defined by two inequalities that need to be satisfied simultaneously. The arrows in Figure 7e,f (temporal aspect) denote the signal transduction directions. This framework, especially the notion of "relative dominance" is primarily qualitative, although quantitative information like bending stiffness or power can inform the material choices for interface designs. For example, the bending stiffness of a brain tissue could be in the range of 10^{-4}~10^{-1} nN m. If we would like to establish very compliant brain interfaces (i.e., SS > HH) from pure silicon-based membranes, we could use a 10 nm-thick membrane (bending stiffness, ~10^{-5} nN m, ref 15). Another example is establishing a biointerface between a single bacterium and a single silicon nanowire for optically triggered metabolic control. The power consumption of a bacterial cell is ~10^{-12} W, while the power output from a coaxial silicon nanowire-based photovoltaic device is ~10^{-10}–10^{-9} W (ref 15). This power difference makes the signal transduction from silicon nanowire to bacterium possible, which has been proved experimentally.[151-153]

Additionally, as shown in Figure 4a, the energy amplitude is size-dependent except for the thermal energy. This provides a rationale to tune the "relative dominance" (i.e., SS, HH, and SH) and the domains within the interaction framework through size and shape control of the constituent materials. For example, an epidermal electronic device needs to follow the texture and mechanics of the skin tissues. The device composite usually contains both the high modulus materials and an elastomer substrate. This requires that the high modulus components, such as semiconductors or metals, would display low bending stiffness (i.e., to reduce the HH), so that the sensing or modulation functions enabled by these materials maintain during the stretching of the epidermal electronics. Reducing the "relative dominance" of HH can be achieved by using thin membranes and/or serpentine structures for the high modulus components. We wish that this framework could unify seemingly random and disconnected soft–hard examples in both the naturally occurring and the synthetic systems. This unified framework then may help us design new soft–hard interfaces by projecting the commonalities of the existing examples.

5.1. Spatial Aspect of the Interaction Framework

5.1.1. Deterministic Assembly.

5.1.1.1. Relative Dominance: SS > SH and HH > SH.: Deterministic assembly, shown in the first interaction domain (Figure 7a, pink area), combines the soft and hard phases via mechanical manipulation (e.g., folding, mixing, and layer-by-layer lamination) or top-down microfabrication. The role of the interaction between the soft and hard phases (i.e., SH, such as interfacial adhesion) is relatively minor in constructing the final composite, compared to that of the interaction within the soft phases (i.e., SS, such as dynamic hydrogen bonding in a double network hydrogel) or within the hard phases (i.e., HH, such as deformation of a Si membrane). Most composite materials can be fabricated following this framework, as

the original properties of the soft or hard phase can be well maintained upon composite formation.

5.1.2. Cooperative Integration.

5.1.2.1. Relative Dominance: SH > SS and SH > HH.: Cooperative integration (Figure 7b, green area) establishes a final composite structure that SS or HH alone cannot achieve. SS or HH cannot overrule SH, otherwise stable soft (i.e., dominated by SS) or hard phases (i.e., dominated by HH) will form.

5.1.3. Directed Organization–Initiated from the Soft Phase.

5.1.3.1. Relative Dominance: SS > SH > HH.: In this domain (Figure 7c, orange area), the structural or chemical information encoded in or dynamically displayed by the soft phase (i.e., SS) directs the organization of the final composite, forming a composite structure that cannot be achieved by HH alone. The soft phase must remain stable throughout the chemical processes. Therefore, SH cannot be the most significant interaction, as that would destabilize the soft template. However, SH is also essential as it transfers the information or dynamics from the soft phase to the hard phase. HH cannot overrule SH, otherwise stable hard phases (i.e., dominated by HH, such as uncontrolled crystallization) with structural or chemical properties that may not match those of the soft phase will form.

5.1.4. Directed Organization–Initiated from the Hard Phase.

5.1.4.1. Relative Dominance: HH > SH > SS.: In this last spatial aspect (Figure 7d, blue area), the static or dynamic information encoded in the hard phase (i.e., HH) guides the organization of the final composite, establishing a composite structure that cannot be achieved by SS alone. The hard phase must remain stable throughout the interfacial organization. Therefore, SH cannot be the most significant interaction, as that would destabilize the hard template. As above, SH is also essential as it transfers the information or dynamics from the hard phase to the soft phase. SS cannot overrule SH, otherwise stable soft phases (i.e., dominated by SS, such as uncontrolled polymerization) will form and "deterministic assembly" would dominate (i.e., SS > SH and HH > SH).

5.2. Temporal Aspect of the Interaction Framework

5.2.1. Signal Transduction–Initiated from the Soft Phase.

5.2.1.1. Temporal Sequence: SS → SH → HH.: Soft phase-initiated signal transduction (Figure 7e) typically deals with phenomena that involve biological components or stimuli-responsive synthetic materials, e.g., bacteria-enabled rapid degradation of materials in the soil. As HH, SH, and SS can be temporarily (and spatially) separated, represent different types of interactions (e.g., chemical, mechanical, and biological), and involve cascades of reactions (or signal amplification), their relative dominance is hard to define or arbitrary.

5.2.2. Signal Transduction–Initiated from the Hard Phase.

5.2.2.1. Temporal Sequence: HH → SH → SS.: The last interaction category (panel f) focuses on signal transduction that is initiated by the hard phase, e.g., tissue inflammatory response at a rigid implant surface. As above, as HH, SH, and SS can be temporarily

(and spatially) separated, represent different types of interactions (e.g., mechanical and biological), and involves a cascade of reactions (or signal amplification), their relative dominance is hard to define or arbitrary.

Multiple soft–hard interaction frameworks can coexist in a single material system, although they are often relevant to different stages of the system, such as material preparation or biointerface application. For example, many stretchable bioelectronic devices are organized through controlled buckling via compressive force from the elastomeric substrates. This 3D device preparation process can be classified as a directed organization that is initiated from the soft phase (i.e., $S_1S_1 > S_1H > HH$); S_1 and H denote the elastomer and the electronic circuits, respectively, and all three interactions are focused on mechanical behaviors. After the device is prepared, biointerfaces for either electronic sensing or stimulation can be established. In the case of sensing, the soft–hard framework follows signal transduction initiated from the soft phase, i.e., $S_2S_2 \rightarrow S_2H \rightarrow HH$. In the case of stimulation, the soft–hard framework instead would follow signal transduction initiated from the hard phase, i.e., $HH \rightarrow S_2H \rightarrow S_2S_2$. In these two signal transduction scenarios, S_2 and H denote electrogenic cells (e.g., neurons or cardiomyocytes) and the electronic circuits, respectively, and all of these interactions are relevant to (bio)electrical processes.

6. PROOF FOR THE INTERACTION FRAMEWORK

In section 5, we proposed an interaction framework to classify the SS, SH, and HH interactions involved in the structural formation or (bio)chemical dynamics of soft/hard composites. Section 6 will prove the utility of this new framework using established examples in both biological and synthetic systems.

6.1. Deterministic Assembly

Deterministic assembly (a) preserves the original properties of the soft and hard phases. Examples of deterministic assembly in biological systems are rare, as biological soft–hard interfaces are active and usually form via cooperative integration (b) or directed organization (c and d). However, numerous examples of deterministic assembly exist in synthetic systems, especially those prepared by homogeneous mixing (e.g., the process of preparing a blend of carbon nanotubes and conducting polymers for stretchable bioelectronic device[154,155]) or top-down fabrication (e.g., the process of fabricating a long-lived bioelectronic device[83,156]). Therein, SS and HH interactions dominate so that the stable performance of the soft and hard materials can persist upon the integration of the soft and hard components. The role of the SH interaction is relatively minor (SS > SH, HH > SH) in terms of the formation of the composite structure, although the SH interaction can improve bonding between the two phases and can yield improved physical properties like enhanced toughness. SH cannot override SS or HH; otherwise, disassembly of the original soft or hard phases would occur. To prove the validity of our proposed soft–hard interaction framework, we will focus on other interaction domains (b–f).

6.2. Cooperative Integration

In cooperative integration of soft–hard interfaces, phase separation into uncontrolled soft-only (i.e., SS > SH) or hard-only (i.e., HH > SH) domains must be inhibited. Therefore, the relative dominance of the three interactions (Figure 7b) usually follows SH > SS, SH > HH (Figure 8a). Both the hard and soft components display dynamic chemical or structural changes during the integration. The SH interaction usually involves coordinate covalent bonding, electrostatic interactions between charged groups, hydrogen bonding, or van der Waals interactions. The SH interaction can be reversible, suggesting a mechanism for environmental adaptability and stimuli responsiveness.

6.2.1. Naturally Occurring Process.—Numerous naturally occurring examples of soft–hard interfaces involve cooperative assembly, especially those related to morphogenesis and development.[3,16,57,157] The shape of the final complex composite depends on the dynamic organization of both the soft (e.g., intracellular membranes, collagen, gluten matrix, cytoplasm, or cellulose) and the hard (e.g., silica, hydroxyapatite, starch granules, cell walls, or ligin matrix) components. For example, in the tooth of a marine mollusc, the chiton *Chaetopleura apiculate*, the nanocrystalline magnetite (Fe_3O_4) is self-assembled with chiton-based organic fibers.[76] In another example of coccolithophore formation,[42,158] the coccoliths (i.e., the individual plates) are nucleated intracellularly and then are exocytosed and assembled over the surface of the single-cell algae. Given these topics have been reviewed elsewhere,[3,16,57,157] we will focus our discussion on synthetic chemical processes below (Table 1).

6.2.2. Synthetic Process.—Cooperative integration[50,51,75,159,160] underlies the synthesis of numerous organic–inorganic composites, such as the growth of ligand-protected nanocrystals and their ordered superstructures[75,157] (Figure 1a), the cross-linking of clay-dendrimer hydrogels[23] (Figure 4b), and the precipitation of mesostructured silica and transition metal oxides.[50,51] Composites formed via cooperative integration usually display molecularly integrated soft–hard interfaces with strong SH interactions (Figure 8). For example, in the block copolymer (e.g., Pluronic F127)-directed synthesis of mesostructured silica at low pH, the protonated hydrophilic segments of the polymer usually interact with the positively charged hydrolyzed silica oligomers through anion coupling (i.e., SH interaction). The hydrophobic moieties of the block copolymers self-assemble into micelle-like aggregates (i.e., SS interaction), while the silicate oligomers extend these aggregates into a 3D network (i.e., HH interaction) and form the precipitates (Figure 8b). Changes to the SH interaction though the addition of cosurfactants or other minor solvents can change the interfacial curvature and the resulting assembled structures (e.g., with a space group of $Im\bar{3}m$, $Fm\bar{3}m$, or $p6mm$, or $Ia\bar{3}d$; Figure 8b). Seamless integration is established via formation of a graded regime; portions of the hydrophilic block copolymer segments are incorporated inside the cross-linked silica matrix, making a transition from the soft copolymer core to the hard silica matrix. Hardening of the composite over time (i.e., additional HH interaction) can be accomplished by elongated sol–gel reactions and subsequent hydrothermal treatment.

Besides integration from molecular precursors, cooperativity among SS, SH, and HH interactions can be established through chemically induced organic phase incorporation which transforms existing inorganic aggregates (Figure 8c). This process is equivalent to the "swelling" of hard materials by soft components. One such example is the synthesis of a large range of MACMS.[110] Synthesis starts with bulking crystals (e.g., black phosphorus, $WeSe_2$, SnSe, and $NbSe_2$) and molecular intercalation species (e.g., lauryl- or cetyl- or octadecyl-trimethylammonium bromide), and the final superlattices consist of alternating layers of monolayer 2D atomic crystals (e.g., phosphorene) and molecular layers (Figure 8c). The intercalation of bulk crystals and ultimate monolayer formation is controlled by the electrochemical potential (Figure 8c). To further expand the family of MACMS, one can envision incorporating photosensitive,[161-163] thermosensitive or other responsive molecules[162,164-168] into the soft phases of MACMS. Other intercalation chemistry can be used to prepare soft–hard interfaces, such as those based on polyoxometalates[169] and layered hydroxides.[170-173]

Likewise, a transformation of existing soft aggregates (e.g., droplets and microgels) through their dynamic interactions with hard components can also yield cooperative syntheses, such as the spontaneous transformation from coacervates to vesicles by polyoxometalate-mediated protocell synthesis[174] and alloy droplet instability-induced growth of nanowire twin-plane superlattices[54,145] and sawtooth faceting.[53,147]

6.2.3. Takeaway Message.—By satisfying SH > SS and SH > HH, cooperative integration achieves materials or devices that are only possible when the interfacial interactions (SH) are most dominant. The cooperatively integrated systems usually display internal architectures or functions that are not a simple sum of the constituent materials, so it is a preferred approach for creating new materials or functions. If both SS and HH become more dominant than SH (i.e., SS > SH, and HH > SH), we would achieve the deterministic assembly and a sum of the constituent's properties and structures. If either SS or HH becomes more dominant than SH (i.e., SS > SH, or HH > SH), the soft (i.e., S) or the hard (i.e., H) phase becomes the stable template to guide the organization of the counterpart, yielding the directed organization.

6.3. Directed Organization

While cooperative integration produces composites de novo or from structurally different precursors, templated precipitation or cross-linking occurs at the predefined material surface or its interior (Table 1). In this class of chemical process, the strength of the three interactions usually follows SS > SH > HH if the soft materials are the template and define the growth (Figure 9a) or HH > SH > SS if the hard materials are the template (Figure 10a). The templates usually contain catalytic sites or heterogeneous nucleation sites for precipitation or cross-linking of the other components. Variation of the surface or the backbone chemistry of the templates can therefore yield different SH interfaces, producing a series of composites that preserve the template geometry (i.e., prescriptive or predictive[57]). This is in contrast to cooperative integration, where a change in interfacial chemistry usually accompanies a change in the entire composite, even yielding emergent structures.[57] Templated precipitation or cross-linking underlies many biomineralization

processes and biomimetic syntheses, such as those templated by polymer scaffolds,[139] DNA nanostructures,[175] or bacterial cells.[141]

6.3.1. Naturally Occurring Process.—Directed organization processes often use organic matrices as templates to build soft–hard interfaces. For example, during coccolith plate formation, macromolecular recognition (i.e., the SH interaction) directs calcium ions to coccolith organic backbone sites (formed via SS) and promotes calcite deposition (formed via SH and HH).[19] Bones grow and develop through cell-controlled local mineralization over a collagen fibril matrix,[138] a process which involves secretion and chemical transformation of precursor phosphate and calcium granules.[3] The bone composite consists of type-I collagen fibrils (formed via SS) and evenly distributed hydroxyapatite nanoplatelets (formed via SH and HH). Active inhibitors (such as pyrophosphate (PPi)[138]) throughout the soft tissues regulate bone growth by preventing unwanted mineral formation (i.e., suppressing HH).[138] When local mineralization over the collagen fibril matrix is desired, PPi is enzymatically degraded by osteoblasts to abolish the mineralization inhibition. Phosphate and calcium ions are then released from their reservoirs to promote nucleation and growth of hydroxyapatite nanoplatelets at the pre-established collagen sites and hardening of the bone tissues.

The directed organization occurs in many biological tissues that display a gradual and spatially defined hardening (Table 1). For example, in the biocomposite beak of the jumbo squid (*Dosidicus gigas*), there exists a 200-fold modulus gradient from the soft beak base to the hard distal rostrum[101,102] (Figure 9b). Through proteomics and transcriptomics, it was revealed that the chemical dynamics of chitin-binding proteins (DgCBPs), the histidine-rich proteins (DgHBPs), and water play major roles in this soft–hard transition. Specifically, DgCBPs and chitin fibers are biosynthesized and react into a hydrophilic scaffold (i.e., a process controlled by SS), producing the soft guiding component. As the jumbo squid ages, hydrophobic DgHBPs are expressed and condensed into coacervate droplets, followed by diffusion toward one end of the chitin-DgCBP scaffold. The His residues in the DgHBPs cross-link and dehydrate the chitin-DgCBPs scaffold[102] (i.e., the action of SH and HH). The variation in cross-linking density and water concentration across different parts of the beak, therefore, produces the modulus gradient (Figure 9b).

6.3.2. Synthetic Process.—Biomimetic synthesis often follows the directed organization approach (Table 1). Soft templates (such as hydrogels, polymeric scaffolds, or liquid crystals[52]) usually contain an accessible interior with active internal surface or domain chemistry to synthesize hard materials, with interactions following SS > SH > HH. Rigid materials can nucleate and grow over the internal surfaces of the soft materials, and ultimately develop into a soft–hard composite. For example, macroporous scaffolds can be made from naturally occurring polymers such as collagen or chitosan, or from synthetic materials with either designer backbones or surface modifications (e.g., with peptides screened from phage display[178-181] technologies). Synthetic nacre can be produced using a laminated chitosan matrix, made by freeze-drying, to form a chitosan-$CaCO_3$ composite.[139] To avoid matrix disintegration at soft–hard interfaces, the scaffold is stabilized by acetylation and transformation into β-chitin (i.e., enhancing **SS** interaction).

To enable a sufficient scaffold/mineral precursor interaction (i.e., SH interaction), a peristaltic pump-driven circulatory system delivers mineralization precursors including $Ca(HCO_3)_2$, PAA, and Mg^{2+}. Finally, silk fibroin infiltration and hot-pressing[139] are used to enhance the toughness and strength of the initial soft–hard interfaces. Besides porous scaffolds, nonporous lyotropic liquid crystals[52] have also been used to grow mesostructured semiconductors and metals.

In a different example of synthetic directed organization, Zheng and co-workers used a 3D printing method to prepare a mosaic of distinct surface charge regions (Figure 9c), which then served as a substrate for deposition of multiscale functional materials through electrostatic attraction (SS > SH > HH). This method allows volumetric production of several active materials such as metals, ceramics, semiconductors, and colloidal systems into site-specific architectures for applications such as tactile sensing and internal wave mapping.[176]

Hydrogels can respond to environmental changes through shape variations. This mechanism can be leveraged for dynamic actuation of inorganic components deposited within the hydrogel matrices or over their surfaces. Oran et al. used hydrogels[177] to direct nanostructured architectures made of metals and semiconductors with virtually any 3D geometry. The optically patternable hydrogels enabled volumetric deposition of hard material precursors at defined 3D locations. With volume shrinkage, the authors achieved nanoscale electronic components such as a 3D network of silver nanostructures and optical metamaterials. In this fabrication process, two steps involve soft–hard interfacial interactions (Figure 9d). The first step is the mineralization at defined hydrogel locations (S_1S_1 > S_1H > HH; S_1S_1 and S_1H focus on the soft template effect and interface-induced mineralization, respectively). The second step involves volume shrinkage of the hydrogel and densification of the inorganic components (S_2S_2 > S_2H > HH; S_2S_2 and S_2H focus on the hydrogel shrinkage and interfacial connection between the hydrogel and the mineralized species, respectively).

Soft templates are also found in micelles,[45,46] droplets,[80,140,150,182] self-assembled monolayers,[183,184] and DNA origami structures,[175] where the external surface triggers interface formation, and the relative dominance of three interactions follow SS > SH > HH. For example, it was recently demonstrated that a class of delicate but well-controlled silica nanostructures could be synthesized by coating the surface of DNA frameworks with silicate oligomers.[175] Spatial resolution down to ~3 nm was achieved. Upon silica coating, the Young's modulus of the composite increased 10-fold. Gallium-based eutectic alloys such as EGaIn (gallium + indium) and Galinstan (gallium + indium + tin) have been used as both the reactors and the templates[140] to grow oxide skins. The oxides that yield the lowest Gibbs free energy (ΔG_f) form the inorganic skins that encapsulate the alloy droplets (Figure 9e, right). This chemical process,[140] as well as many other surface solidification examples including the formation of an Au_4Si_8 sheet[80] over the surface of a Si/Au droplet (Figure 9e, left), exploits the minimization of free energy to form a soft–hard interface over an initially homogeneous soft substrate.

Biological cells can also serve as soft templates, for example, in the in situ synthesis of a CdS/bacterial hybrid for artificial photosynthesis at extracellular interfaces.[141] When Cd^{2+} and cysteine are supplied to the CO_2-reducing bacterium *M. thermoacetica*, CdS nanoparticles precipitate over the bacterium surface in situ. The precipitation of CdS involves the HH, the living behaviors of bacterium *M. thermoacetica* provides the SS, and the interfacial recognition and nucleation of the mineral species depend on the SH. In this way, nonphotosynthetic bacteria are converted to photosynthetic ones via soft–hard interfaces, which integrate the light responsiveness of the CdS nanoparticles and the biosynthetic properties of the bacteria.[141] Other examples include the use of polyphenol-based chemistry to assemble InP/yeast hybrids for light-driven regeneration of redox cofactors,[185] and the biogenic growth of iron sulfide over *Shewanella* for improved electron transfer in microbial fuel cells.[186]

Studies of hard templates with well-defined lattice structures[142,143] have recently revealed significant new chemical insights into biomolecule/substrate interactions (i.e., SH interaction), particularly in the nucleation and growth of 2D frameworks, tilings, and chiral structures. In these cases, free-standing biomolecular systems alone do not produce the patterns, confirming HH > SH > SS (Figure 10a). In one recent example, cleaved MoS_2 substrates were used to study the nucleation mechanism in 2D array assembly.[142] Tyr-Ser-Ala-Thr-Phe-Thr-Tyr peptides with acylated and amidated N and C termini formed 2D arrays along with three equivalent directions over freshly cleaved MoS_2 substrates.[142] Molecular dynamics simulations, atomic force microscopy, and theoretical studies were employed to uncover the chemical interaction and dynamics at the peptides/MoS_2 substrates interface. This work verified the long-standing speculation that nucleation of 1D structures, in contrast to that of 2D and 3D structures, occurs without a free energy barrier. Another recent study reported that de novo designed helical repeat (DHR) proteins assembled over a geometrically matched K^+ sublattice on muscovite mica (001) surfaces (Figure 10b)[143] (i.e., establishing the strength of SH). The concentration of the K^+ sublattice (i.e., tuning HH) affected the packing density and forms (individual proteins or liquid crystals) of the attached DHR proteins (i.e., tuning the area of SH). Additional modifications of interprotein chemical interactions (i.e., tuning SS) at the end-to-end or trimeric interfaces maintained the DHR/mica interfacial binding (i.e., SH > SS) but allowed for the extension of the attached DHR proteins into nanowire or honeycomb arrays.[143]

6.3.3. Takeaway Message.—In the directed organization, SS > SH > HH or HH > SH > SS should be satisfied. One of the phases, either the soft phase (i.e., S) or the hard phase (i.e.,H) serves as a template or a confined space to guide the nucleation, growth, or the dimension and size control of the counterpart phase. Depending on the context of the discussion, the SS/HH could be the intramolecular interactions that hold the constituent phase together, the restoring forces upon elastic deformation, or others.

A unique aspect of the directed organization is that the final material/device structure usually follows more closely to only one of the constituents, i.e., the template or the confined space. However, the final material/device structure would maintain that of both the soft and hard constituents in the deterministic assembly and should be different from both the soft and hard constituents in the cooperative integration.

Additionally, in the directed organization, the role of SH is still essential (i.e., it is not the least dominant interaction), because reactions or processes can only occur in the presence of the soft–hard interfaces. If the observed reactions or processes can happen without the interfaces (i.e., they are driven by purely SS or HH), they are not within the scope of this review.

6.4. Signal Transduction

The last functional chemical process, (bio)chemical signal transduction, predominantly applies to systems that contain biological components or stimuli-responsive polymers (Table 1). Signal transduction processes are distinct from cooperative integration and directed organization processes in several ways. First, effective signal generation, propagation, and even amplification usually require that multiple chemical, physical or biological processes are coupled together. This spatiotemporal complexity makes it challenging to define the relative dominance of SS, SH, and HH interactions. Second, in a signal transduction process, SS, SH, and HH interactions usually occur in temporal order, following a signal transduction sequence of either SS → SH → HH or HH → SH → SS. For example, HH-triggered processes (HH → SH → SS) involve final (bio)chemical changes to the soft components (i.e., SS) as a result of their interaction with the hard surfaces (i.e., SH; Figure 11a). Third, while the soft and hard components are usually tightly attached in cooperative integration and directed organization, they can be spatially distant in signal transduction processes as the transduction pathways can occur across a long distance and in a systemic manner.

6.4.1. Naturally Occurring Process.—Signal transduction involving SOM[27,89,90,94] and minerals is one example of an HH-triggered process. SOM is primarily formed through the decomposition of plant litter and its mineralization to inorganic carbon. Many SOM molecules can irreversibly absorb onto mineral surfaces (i.e., SH) to yield SOM-mineral complexes, with patchy domains (including aromatic carbon, aliphatic carbon, carboxylic/amide carbon, phenolic/pyrimidine carbon, or imidazole carbon) at the submicrometer level.[27] As the mineral sites are usually polar, strong electrostatic interactions occur between the minerals and the SOM molecules, triggering microbial signal transduction.[90] Specifically, absorption of the SOM molecules selectively promotes nitrogenous compound (particularly the amide) accumulation over mineral surfaces. The polar functional groups of the absorbed proteinaceous materials are exposed to the soil environment and recruit microbes from remote areas.

Renal crystal granuloma formation[82] is also an HH-triggered process. Type 2 crystal-induced kidney injuries arise from intratubular crystal deposition due to a series of sequential events[82] (Figure 11b) that involve the interfacial physicochemical behavior of the minerals, the mineralization regulators, and biochemical signaling pathways. Specifically, calcium oxalate (CaOx) crystal nuclei form upon supersaturation of CaOx in the urine. The CaOx crystals are phagocytized into the tubular cells, where they activate the TNF signaling pathway and produce crystal adhesion proteins (e.g., CD44 and annexin II) at the tubular cell membranes. The adhesion proteins next trigger attachment of more CaOx crystals and the crystal plug in the tubular lumen causes a tubular obstruction. Finally, cells proliferate on the

rigid CaOx plug surfaces and the crystal plug translocates to the interstitial compartment and forms the crystal granulomas.[82]

SS-triggered natural processes (i.e., SS → SH → HH) can involve cells that modulate the chemical or physical properties of inorganic materials. For example, electron transfer from *Geobacter metallireducens* GS-15 (i.e., SH) reduces minerals that contain Fe^{3+} or Mn^{4+} and modulates their redox activities in the soil environment (i.e., HH; ref 99). This mechanism and other redox microbiology processes are extensively reviewed elsewhere[99,187] and they are also the basis for many microbial fuel cell studies[187] in synthetic systems.

6.4.2. Synthetic Process.—HH-triggered synthetic signal transduction usually yields chemical or biochemical changes in soft phases (i.e., SS) due to interfacial delivery (i.e., SH) of chemical, mechanical,[71] topographical,[71] or electrical, electrochemical, and thermal stimuli[15,85-88] from hard phases (Figure 11a). Signal transduction can even be harnessed to stabilize special soft–hard interfaces, as in the synthesis of anisotropic hydrogels where photoexcitation of titanate or niobate nanosheets (i.e., HH) produces hydroxyl radicals to cross-link acrylamide derivatives.[63] Here, we focus on material-cell interfaces.[15,59,85-88,117,188,189]

In orthopedic implant infections, microbial community formation (i.e., SS) at the implant surface (i.e., HH) involves bacterial recognition of adhesive matrix molecules (i.e., SH) that are preconditioned at implant surfaces.[59] These recognition moieties include collagen-binding adhesion proteins and fibronectin-binding proteins.[59] Engineering the implant surface topography and chemistry[71,104] to inhibit this biochemical interaction can generate an antifouling effect or even bactericidal activity.[59] Another example of a material-induced biochemical effect in cells is the recruitment of curvature-sensing membrane proteins over nanopillar substrates.[56,190] These chemical processes usually occur over a time scale of minutes to weeks.

While the above two cases denote slow signal transductions, high-speed (i.e., submillisecond to seconds) neural or cardiac modulations[15,85-88,188,189,129] (i.e., SS) can be achieved by electrochemical or photoelectrochemical interfacial processes (i.e., SH) with semiconductor or metal devices (i.e., HH). For example, atomic gold-decorated coaxial p-type/intrinsic/n-type (PIN) silicon nanowires or gold nanoparticle-decorated PIN silicon nanomembranes were recently used as optically triggered biomaterials (Figure 11c). When interfaced with excitable cells, the atomic or nanostructured gold on the silicon surface facilitates a light-induced faradaic effect to depolarize cells and instigate action potentials.[86] The cleft between the silicon (or other modulation materials) and the isolated cells is usually very important, because local variations in ions or other chemicals could produce a larger modulation effect when in a confined volume.[191]

Finally, **SS**-triggered synthetic processes (i.e., SS → SH → HH) underlie essentially all electronic, electrochemical, or electromechanical sensing and energy conversion systems where the soft components are biological systems or stimuli-responsive polymers; these topics[15,164,168] will not be reviewed here.

6.4.3. Takeaway Message.—Different from the spatial aspect reflected in deterministic assembly, cooperative integration, and directed organization, the signal transduction focuses on the temporal aspect of the interaction framework. The signal can be triggered either by the soft phase or the hard phase. The soft–hard interface usually involves energy transduction, biosynthesis, or even signal amplification. In section 7, we will discuss the construction of devices or materials from the spatial aspect (i.e., using the language of deterministic assembly, the cooperative integration, and the directed organization), and analyze the sensing or modulation biointerfaces from the temporal aspect (i.e., the notion of signal transduction).

7. DISSECTION OF THE SOFT–HARD INTERFACES IN TISSUE-LIKE SYSTEMS

In section 6, we used diverse examples to validate the new soft–hard interaction framework. This section will apply this validated framework to dissect the soft–hard interfaces in several tissue-like systems such as bioelectronics and robotics. First, we will highlight a few biomechanical aspects of biological tissues and suggest opportunities for tissue-like synthetic materials.

7.1. Biomechanical Aspects of Biological Tissue

7.1.1. Mechanical Components for Building Living Soft–Hard Interfaces.—Biological tissues comprise spatially heterogeneous, mechanically rigid, hierarchical structures. Common ECM components include collagen, fibronectin, elastin, glycosaminoglycans (GAGs), laminin, tenascin, and vitronectin. Upon stretching or compression, the reorganization of collagen fibers contributes to dynamic and nonlinear tissue behavior, which activates a natural protection mechanism against tissue destruction. Elastin, another primary ECM component, is expressed in many organs, including the blood vessels, arteries, and lungs. Elastin displays high linear elastic extension, which contributes to the elastic deformation of the ECM. The elastin and collagen networks are highly entwined and work in unison to execute tissue mechanics.

Cells interact with the ECM through focal adhesion structures. They can remodel the ECM in response to mechanical, biochemical, and pathological cues. Cytoskeletal structures maintain and actuate cellular mechanics, while also helping the cell to adapt to the mechanics and dynamics of the ECM. For example, cytoskeletal intermediate filaments provide robust support against physical forces in the environment and help the cells resist mechanical stress. Highly cross-linked actin filaments undergo polymerization and depolymerization to remodel the cytoskeletal network in response to physical forces. Another set of critical cytoskeletal proteins, the microtubules, provides the molecular tracks for intracellular transport and displays the dynamic instability that shapes how cells respond to their mechanical environment.

7.1.2. Unique Behaviors in Biological Systems.—Biological tissues also exhibit complex rate-dependent and time-dependent mechanical responses, leading to “trainable behaviors.” These behaviors often rely on soft–hard interactions and the hierarchical

structure of the tissue. They can originate from the viscoelasticity, poroelasticity, plasticity, or other nonlinear strain–stress correlations, of the tissue.

Viscoelastic mechanical behavior is typical in biological tissues. Viscoelasticity comprises instantaneous elastic behavior and time-dependent viscous behavior. Viscoelastic materials display properties common to both pure elastic solids and viscous liquids. Energy dissipation in a classic elastic solid is completely in-phase in response to the input energy; the energy is stored and ultimately released without loss during cyclic loading. In contrast, energy dissipation in a viscous fluid is out-of-phase with the input energy because the input energy is dissipated by internal friction and reconfiguration. The features of viscoelasticity fall between these two extremes. The in-phase response of the elastic property defines a storage modulus, and the out-of-phase response of the viscous property yields a loss modulus. The deformation frequency can affect the ratio of the loss modulus-to-storage modulus, contributing to the dynamic mechanical behavior of biological tissues.

ECM viscoelasticity arises by breaking and reforming weak cross-links, releasing entanglements, and unfolding proteins. Most cross-links in the ECM network are noncovalent bonds that can break, slide, or slip and thus dissipate energy under mechanical stimuli with dissociation rates fast enough for stress relaxation or material creep within the relevant time frame. Release of polymer entanglements and unfolding of ECM proteins, such as fibrin and collagen, also dissipates energy and contributes to the viscoelasticity of ECM. The viscoelastic cytoskeleton is involved in numerous subcellular activities such as actomyosin-based contractility and actin polymerization-enabled pushing. The interplay between the cells and the ECM, together with inorganic components, determines the diverse and highly heterogeneous tissue mechanics.

Tissue poroelasticity is caused by the flow of water into or out of the ECM and the cells. Water in the tissue moves into or out of the ECM under tension or compression; the resulting ECM poroelasticity produces energy dissipation. A slightly different mechanism underlies cell poroelasticity as the less permeable cell membrane prevents substantial water movement. Instead, cytoskeleton deformation causes transient pressure gradients and results in intracellular water movement, leading to the poroelastic effect. Since poroelasticity operates through the movement of water, the dissipation of shear stress through poroelasticity is much less than that through viscoelasticity.

7.2. Need for Advanced Tissue-Like Materials

Traditional soft materials such as silicone are frequently used in bioelectronics and robotics applications. While silicone is typically deemed biocompatible, its mechanical properties still do not match biological tissues' viscoelasticity and strain-stiffening behavior. Recently, it was reported that the high surface stresses of silicone liquids and gels can stimulate the formation of multinucleated monocyte-derived cell masses, suggesting a foreign body response.[192] Several methods have also been proposed to mitigate the biocompatibility issues associated with silicone through surface topography[193] and modulus[194] control. In this regard, there is still a need for more biocompatible and tissue-like soft materials. This can usually be achieved by using composites to construct the soft phase, as different soft components can help tune the SS interactions.

Biological tissues possess a unique ECM structure, wherein the ECM provides mechanical and biochemical cues for cells and regulates intercellular communication. Thus, composite materials with structures similar to those of cell-ECM may provide dynamic and nonlinear tissue-like properties. For example, Rogers et al. demonstrated deterministic methods to achieve low-modulus thin films with nonlinear stress–strain responses precisely matched to those of skin.[195] Skin-like composites were achieved by integrating the wavy filamentary network of polyimide and a breathable elastomer; these two components mimicked the collagen/elastin structure and the biological ground substance, respectively. This example utilizes SS interactions to achieve better tissue-like biointerfaces.

Gong and co-workers developed “self-growing” polymeric materials comprising an effective mechanochemical transduction element for responding to external repeated mechanical stress (Figure 12a). They demonstrated that muscle-like hydrogel materials can generate self-growth behavior; these materials could be used for soft robotics and intelligent devices.[196] Fang et al. developed tissue-like materials by incorporating cellular-scale starch granules in a hydrogel matrix[197] (Figure 12b). The authors revealed that mechanical stress on the hydrogel matrix could induce reorganization and training dynamics of the incorporated starch granules. These dynamic responses enabled various tissue-like behaviors, including anisotropy, programmability, and trainability. The starch-based tissue-like materials have broad applications, including implantable devices, medical-surgical tools, and humanized robotics. He and co-workers recently presented a novel strategy toward a multi-length-scale hierarchical hydrogel architecture that mimicks natural tendons (Figure 12c). In their work, the authors prepared poly(vinyl alcohol) hydrogels with engineered structural anisotropy. With a freezing-assisted salting-out treatment, they discovered micrometer-scale honeycomb-like pore walls and interconnected nanofibril meshes. These hydrogels demonstrate outstanding fracture toughness and fatigue resistance.[198]

These recently reported tissue-like materials may serve as substitutes for conventional soft materials (e.g., PDMS) in future bioelectronics and robotics applications. In particular, these advanced tissue-like soft materials (i.e., an advanced soft phase, S) may help create more soft–hard composites (i.e., soft matrix-hard electronics) that follow the cooperative integration pathway, i.e., SH > SS, SH > HH, or the directed organization pathway, i.e., SS > SH > HH or HH > SH > SS, which is currently still lacking in bioelectronics and robotics.

7.3. Tissue-Like Deformable Electronics

In the previous section, we discussed a few of the components and properties that are unique to biological tissues. In the following sections, we will use the soft–hard interface framework (i.e., with notions of HH, SH, and SS) to present several biointerfaced materials and devices, in particular those related to bioelectronics and robotic systems (Table 2). We once again note that the definition of the soft and hard phases (i.e., S and H) that involve the same device depends on the context of the discussion. For example, the S can be the elastomer from a bioelectronic device if the whole device is treated as a soft–hard composite. Alternatively, the S can be the biological tissues if we discuss using the same bioelectronic device for sensing or modulation. In the following sections, we use S_1 and S_2, or H_1 and H_2, to indicate the differences if confusion may occur.

We will first look at the design and implementation of deformable electronics. Stretchability is a highly desirable electronics characteristic, especially when biointerfaces are concerned. For example, deformable electronics must accommodate the contraction of a muscle or the movement of the beating heart to faithfully and continuously map their electrical signals. Over the past few years, a collection of strain-tolerable stretchable electronics ranging from conductors to semiconductors have been developed.[199] Most of the designs involve SS > SH > HH (i.e., directed organization) or SH > SS/HH (i.e., cooperative integration) approaches, where SS denotes the physical or chemical processes in the deformable substrate that supports the electronic components (e.g., elastic deformation of PDMS), SH represents those at the substrate-electronics interface (e.g., interfacial covalent bonding between PDMS and Si), and HH represents those of the stretchable and deformable inorganic components (e.g., elastic deformation of Si ribbons). The general approach involves engineering designs that at least reduce the HH interactions (i.e., making the high modulus materials softer) through thickness reduction.

7.3.1. Stretchable Electronics through Geometric Engineering.—Stretchability in nonstretchable inorganic materials-based electronics is typically achieved through geometric engineering. When supported by an elastomeric substrate, structurally designed inorganic materials can be configured with the stretchability[41,200,201] needed to interface with, interrogate, and modulate the skin,[202-204] brain,[205-207] heart,[208] bladder,[209] and kidney.[210] In particular, the Rogers group has developed buckled thin strips of Si bonded in wavy structures to enable stretchable bioelectronics[200] (Figure 13a). According to the SS/SH/HH framework, the wavy structures are obtained via a cooperative self-patterning process between the Si nanoribbons and the elastomer substrate upon compression, i.e., SH > SS, and SH > HH (Figure 13b). SH is most dominant because the wavy elastomer/Si interface cannot be produced by the elastomer or the Si itself, i.e., the interface is generated through a cooperative process. Notably, this engineering approach is not limited to specific materials, but generically applicable to many material candidates. In these examples, the focus is to tailor the HH (i.e., the bendability of Si nanoribbons) and SH (i.e., the bonding between the elastomer and the Si nanoribbons) interactions, such that SH > SS and SH > HH can be satisfied to yield ideal device mechanics or morphology at the biointerface. In this case, the thickness of the high modulus materials (i.e., H) is usually on the order of micron or submicron meters to minimize the dominance of HH in the interaction framework.

More complex stretchability involves a geometric transformation of planar 2D structures into various extended 3D architectures (Figure 13c). From the SS/SH/HH framework, the $S_1S_1 > S_1H_1 > H_1H_1$ approach (i.e., directed organization, Figure 13d) is preferred over the $S_1H_1 > S_1S_1/H_1H_1$ approach(i.e., cooperative integration), where S_1S_1 and H_1H_1 denote the mechanical interaction within the elastomer and the electronic components, respectively. The contact regions for S_1H_1 action (i.e., the bonding between the elastomer and the electronic elements) only serve as focal points and the final soft substrate morphology is the same as the original; this is different from the wavy structure mentioned in the previous paragraph[200] where the soft substrate also largely deforms upon compression (i.e., SH is most dominant). In these 3D electronics designs, most of the stretchable interconnects are untethered from the elastomeric substrate such that out-of-plane deformations are

enabled for enhanced stretchability.[213] Based on the SS/SH/HH framework, the untethered components help reduce SH such that SS > SH > HH can be satisfied easily.

Xu and Rogers reported the assembly of complex 3D structures through compressive buckling to enable routes to previously inaccessible 3D constructs.[214] The resultant electronics with open network architectures—we now define the entire device as a hard phase, H_2—can be integrated with biological systems (a new soft phase, S_2) in 3D volumetric states for biophysical studies. For example, Rogers and co-workers showed that the microfabricated 3D networks can serve as compliant, electrical/chemical/thermal/optical signal transduction interfaces (i.e., S_2H_2) to neural spheroids and assembloids[211] (Figure 13c).

Moreover, to break the constraint of 2D integration, 3D integrated stretchable electronic devices were engineered by building electronic components layer-by-layer on elastomers and creating vertical interconnect accesses through the layers.[215] For example, Rogers and co-workers reported a vertical multilayer stack of arrays of electrodes and sensors that were integrated with catheters for minimally invasive cardiac therapy.[208]

7.3.2. 3D Bendable Electronics through Residual Stress Engineering.—

Residual stress can be harnessed to enable the fabrication of complex 3D inorganic materials from their 2D layered precursors. A similar approach has been used in the production of 3D bendable nanoelectronics for intracellular probing.[216] For example, several publications from the Lieber group showed that residual stress (i.e., HH) from Cr/Pd or Cr/Au metal layers, is sufficient to cause deformation of the SU-8 substrate (i.e., SS) via Cr-enabled metal/SU-8 adhesion[212,216,233-240] (i.e., SH interaction at the interface) (Figure 13e). In a typical fabrication, layers of SU-8 and metals were fabricated on ultrathin SU-8 polymer ribbons above a sacrificial layer (e.g., Ni or PMMA). The SU-8 substrate supported the nanoelectronic components, such as the semiconductor nanowires and the metal interconnects (e.g., Pd or Au). Upon the lift-off process, the interfacial stress between different layers (i.e., HH) would bend the supported nanoelectronic device components upward to a predictable height and angle.[216] This approach has also been used to fabricate a reticular scaffold-like nanoelectronic network for tissue engineering.[212] These examples follow the HH > SH > SS approach, as the residual stress from the metal layer interfaces (i.e., HH) actuates the 3D structure formation (Figure 13f). In these cases, the SU-8 or other polymeric substrate must be bendable enough (i.e., SS is small or its role in this interaction framework is least dominant) to allow for the 2D-3D shape transformation.

7.3.3. Stretchable Electronics through Nanoconfinement Effect.—

A different concept, self-assembly enabled nanoconfinement[241,242,217] (i.e., SH > SS, SH > HH), has been recently introduced for achieving intrinsically stretchable electronics. Organic thin-film transistors have been utilized extensively as wearable electronics. Notably, the Bao group utilized the nanoconfinement effect to achieve skin-like electronics based on polymer semiconductors with large stretchability, without compromising charge transport mobility. This was achieved *via* a nanoscale phase separation between the conjugated-polymer (i.e., the hard phase, H, as conjugated-polymers usually display larger modulus than that of elastomers) and the elastomer phase (i.e., the soft phase, S), where the interfacial interaction

between the two phases (i.e., SH) was key to maintaining the nanostructured architecture.[217] Moreover, a photopatterning method for stretchable devices that can be fabricated on a mass scale with high device density on flexible substrates was also developed.[243] Thousands of electronic circuits can be fabricated onto a stretchable platform. The high stretchability and minimal mechanical constraint of these intrinsically stretchable bioelectronics may enable many previously challenging biological applications, for example, morphing electronics that intimately interface with rapidly growing tissues during adolescent development.[244]

7.3.4. Stretchable Electronics through Interlayer Insertion.—A graded layer or buffer zone is established in many naturally occurring or synthetic soft–hard composites to promote seamless integration between mechanically different phases. This principle has recently been adopted in the design and application of stretchable electronics. Nam and co-workers showed that an-atomic-thick interlayer between a metallic film and a flexible substrate yields strain-resilient device conductivity (Figure 14a,b).[245] Without the interlayer, the metallic film is brittle and undergoes an unperturbed straight fracture under tensile strain. With the interlayer, the metal layer displayed progressive tortuous fractures, showing a ductile behavior. Overall, the addition of the interlayer enhanced the strain-resilient electrical property with a resistance-locking behavior. The authors employed this method and realized a stretchable electroluminescent light-emitting device. In this example, the soft–hard framework switches from $SS/SH_1/H_1H_1$ to $SS/SH_2/(H_2H_2 + H_1H_1)$, where H_1 and H_2 represent the metal and 2D materials, respectively. When the flexible substrate undergoes deformation (i.e., SS), the 2D interlayer bends readily (H_2H_2 is least dominant given the ultrasmall bending stiffness of the interlayer) through interfacial adhesion (i.e., SH_2) between the elastomer and the interlayer.

7.3.5. Stretchable Electronics through Stiffness Patterning.—Very recently, Wang et al. developed a strain-insensitive intrinsically stretchable transistor array using an elastomer substrate with patterned stiffnesses[218] (Figure 14c,d). This method is similar to the creation of graded mechanical zones between soft and hard phases. The authors increased local stiffness in the elastomer by increasing the local cross-linking density. The high stiffness elastomer domains supported the active regions of the devices and reduced their strain to preserve device performance. This method is general and has been used to fabricate high-gain amplifiers for sensing electrophysiological signals. In this example, the soft–hard framework switches from $S_1S_1/S_1H/HH$ to $S_1S_1/S_2S_2/S_2H/HH$, where S_1 and S_2 represent the soft and stiff elastomer, and H is the organic semiconductor device. In this case, S_1S_1, S_2S_2, S_2H, and HH interactions are related to material stretching or interfacial adhesion.

7.4. Tissue-Like Wearable and Epidermal Electronics

Living systems demonstrate highly sensitive, dynamic, and error-tolerant transmission of complex signals through two routes: bioelectrical signaling and biochemical signaling.[246] Bioelectrical signaling is achieved through ion fluxes and cell membrane potential charges and presents in many parts of the body such as the brain, heart, and muscle.[247] In these electrically active cells and tissues (neurons, cardiomyocytes, muscle cells, etc.), continuous recording and analysis of electrical signals can significantly help scientists understand

biological processes and further direct the diagnosis and treatment of diseases.[248] The past few decades have seen the development and wide application of bioelectronics devices for electro-signal recording and stimulation of brain, heart, and muscle. Bioelectrical signal recording devices typically include electroencephalography (EEG),[249] electrocardiography (ECG),[250] and electromyography (EMG).[251] One example of an electrical stimulating device is the transcutaneous electrical nerve stimulation (TENS) device, which reduces muscle spasms and pain using mild electrical current on a wide range of body parts, including the knee, neck, back, and pelvis.[252] Many of these devices require epidermal stimulation/recording electrodes to convert signals between ion flow in biological tissue and electron flow in the electronics at the skin-electrode interface. Impedance is significantly affected by a number of factors, including the degree of epidermis hydration and the electrode's conformal contact onto the skin.[253,254]

Epidermal electronics, electronic skin, or e-skin, refers to devices that can mimic and enhance the properties of human skin, such as stretchability, mechanical toughness, self-healing, and various sensing abilities.[255] To function properly, the e-skin needs to satisfy the following criteria: sufficient adhesion to moving surfaces such as human skin, prosthetics, and robotics; strong mechanical properties that can withstand lateral tension, compression, stretching, and twisting to cope with diverse movements; self-healing ability that enables long-term durability; biocompatibility which ensures no harm to the human body when applied on the skin; and various sensing capabilities including sensing of temperature, physical stimuli, chemicals, and electrophysiological signals. In the numerous studies carried out in this area, most of the epidermal electronics were prepared following deterministic assembly (i.e., HH > SH, SS > SH, where H and S denote the electronics components and the soft matrix, respectively; Figure 15). We highlight a few below (Table 2).

Rogers and co-workers used stretchable electronics with advanced physiological measurements for neonatal intensive care.[203] The devices provided continuous real-time monitoring of skin temperature, ECGs and photoplethysmograms (PPGs) that yielded measurements of a range of physiological parameters after on-board analysis. Xu and co-workers described a skin-attached ultrasonic device (Figure 15a,b) that was integrated into the conformal stretchable system to noninvasively and continuously capture blood pressure deep in the human body.[256]

Someya and co-workers reported ultrasoft and stretchable sensors for epidermal recording. Their conductive nanomesh structure consisted of PVA fibers and a thin-layer Au coating. The PVA/Au interface formation step followed SS > SH > HH, as PVA fibers (i.e., S) served as the template for the Au layers (i.e., H). The nanomesh system demonstrated promising tissue-like properties; it was inflammation-free, highly gas-permeable, and lightweight.[219]

Xu, Wang, and co-workers reported a skin-like and integrated wearable sensor that can monitor a series of physiological health indicators, such as blood pressure, glucose, and caffeine, among other biomarkers. They assembled polymer composites and piezoelectric lead zirconate titanate (PZT) ultrasound transducers to achieve highly integrated wearable conformal sensors.[257] Gao and co-workers reported a flexible and laser-engraved sensor for

monitoring essential biomarkers, such as uric acid (UA) and tyrosine (Tyr). In this case, the device formation follows SS > SH > HH, as the graphene layers were locally converted from the polymer substrate (template). The authors demonstrated that the laser-engraved graphene-based chemical sensor (LEG-CS) could precisely and simultaneously detect UA and Tyr in human sweat. This indicator can help clinical doctors diagnose cardiovascular disease, gout, type 2 diabetes, and renal disease.[220]

Current and future tissue-like materials are also suitable for e-skin or wearable electronics applications. The mechanical toughness and stretchability of tissue-like materials can ensure high e-skin performance even on the most flexible joints of the body/robotics/prosthetics. The adaptability, trainability, and even memory effects of the materials would further enhance the performance of the e-skin or wearable electronics. The self-healing ability of tissue-like materials would enable fast and spontaneous healing upon breakage and promote a longer service time. Last but not least, tissue-like materials consist of biocompatible components. Therefore long-term use on human skin would not lead to concerns related to inflammation or other toxicities.

7.5. Self-Healing Tissue-Like Electronic Systems

Living organisms can heal themselves naturally upon injury or damage.[258] The healing process includes the replacement of destroyed or damaged tissue with newly generated tissue. For example, when the skin is wounded, hemostasis is automatically triggered; platelets in the blood begin to stick to the injury site and form a clot to plug the broken vessel. The inflammation stage is then initiated to remove damaged and dead cells along with pathogens. The proliferation phase follows, and new tissue is grown. The entire healing process is wrapped up in the maturation phase, with the maturation and remodeling of collagen and cells.[259,260] The healing process of biological tissues can thus be summed up in four stages: formation of a primary clog to prevent further damage; removal of damaged/dead cells and pathogens; regeneration of new tissues; and realignment of new cells and collagen.

Various molecular interactions have been explored to realize self-healing behaviors in synthetic materials or devices (Table 2). Hydrogen bonds represent one type of reversible molecular force that can enable self-healing. When the material breaks, hydrogen bonds on the surfaces of the two pieces can automatically reform upon physical attachment. This creates a relinked structure that prevents further rupture, similar to the self-repair process in biological tissues. Many polymers possess extensive reversible Schiff bases that form a significant number of hydrogen and ionic bonds.[262-264] Ionic bonds can also automatically reform after breakage due to the reversible electrostatic interactions of oppositely charged ions.[265] Following the formation of the primary linkage by hydrogen or ionic bonds on the surface, further hydrogen bonds and ionic bonds are established in deeper layers. As more bonds form, the two pieces gradually become more firmly attached, similar to the regeneration of cells or ECM in tissue. In nervous tissue regeneration, bioelectrical signal transduction along neuronal processes can be partially or even fully recovered during the self-healing process through the regrowth of axons and the re-establishment of synaptic

connections. This serves as a biomimetic principle in many self-healing bioelectronics device designs.

The dynamic behaviors of molecularly designed polymers have enabled several advances in self-healing stretchable electronics and bioelectronics. For example, the Bao group developed a class of self-healing PDMS-based elastomers (PDMS-MPUx-IU1-x) using a one-pot polycondensation reaction of bis(3-aminopropyl)-terminated poly(dimethylsiloxane) with 4,4′-methylenebis(phenyl isocyanate) and isophor-one diisocyanate. This yields both strong and weak hydrogen networks within a single elastomer matrix, which can inhibit crack propagation along a defect and realize a highly stretchable, tough, and self-healing elastomer.[261] Using this PDMS-based elastomer (e.g., PDMS-$MPU_{0.4}$-$IU_{0.6}$) as the matrix, the Bao group embedded carbon nanotubes and silver nanowires on one side of the elastomer. They achieved self-healing electronics through the dynamic movement of the polymer chains upon physical contact with the broken parts of the devices[221] (Figure 16a,b). This example follows SS > SH > HH (Figure 16c), as the self-healing and nanostructure recontact (i.e., HH) is driven by the molecular motions of the elastomers (i.e., SS) and the elastomer-nanomaterials interactions (i.e., SH).

7.6. Tissue-Like Smart Wound Bandages

Skin, the first barrier against infection, possesses excellent regenerative abilities that enable rapid healing upon injury.[266,267] However, certain underlying health conditions, such as diabetes and severe burns, can cause significant skin damage and overwhelm the skin's regenerative ability, failing to complete the inflammation, proliferation, and maturation processes.[268] Such chronic wounds with slow healing speeds are at higher risk of infection; infection further slows the healing rate and increases the risk of recurrence.[269] Thus, chronic wounds are currently a critical cause of limb amputations and represent a global healthcare challenge.[270] Traditional wound management schemes can be time-consuming, costly, and passive and effective treatments that can address the following three aspects are greatly desired: (i) wound coverage and a physical barrier against environmental pathogens, (ii) continuous monitoring and timely reporting of infections, and (iii) timely and rapid localized treatment with drugs or antibiotics. In the past decade, hydrogels have received significant attention as components of wound dressings as they can maintain a moist environment and provide a physical barrier to protect wounds.[271] Hydrogels can also be merged with infection monitoring and drug-release systems. Among potential biomarkers for wound condition monitoring, pH and temperature are the most widely used as they are the most intimately linked with infections and inflammations.[272] Drugs and growth factors can also be combined with treatment patches to promote the healing process. Drug carriers that are thermoresponsive,[273] pH-responsive,[274] and electric-responsive[275-277] have been developed and incorporated into hydrogel-based wound dressings for controlled drug delivery. It has also been reported that external electrical stimulation at the wound site promotes cell migration and proliferation, thereby accelerating the wound healing process.[278,279]

Zhao and co-workers developed a dry double-sided tape (DST) made from a combination of biopolymers for tissue adhesion. Rapid covalent bonding with the amine groups on the tissue surface resulted in a soft–hard interface that further improved the robustness and

adhesion stability of the DST. The DST rapidly (<5 s) adhered to wet tissues *in vitro* and in *in vivo* animal models.[280] While these examples do not involve rigid materials, the DST system can be readily integrated with other electronics or optoelectronics for wound healing applications. Indeed, work from the same group demonstrated stretchable hydrogel electronics that served as a wearable bandaid, sensed temperature and light, and delivered medicine to the skin.[222] Conductive wires, semiconductor chips, light-emitting diodes (LEDs), and temperature sensors were embedded in the hydrogel to enable soft and stretchable electronic devices that function in the constantly changing environment of human body. In these examples, the soft–hard composite formation follows deterministic assembly, i.e., SS > SH, HH > SH as the hydrogels and the electronic/optoelectronic components are assembled manually.

Yu and co-workers developed an ultraconformal, customizable, and deformable thin layer conductive tape through direct drawing over a flexible mask (Figure 17a). In this case, the device assembly followed the directed organization pathway (Figure 17b), i.e., SS > SH > HH, because the local skin curvature and roughness defined that of the conductive device. The portable thin layer tape monitored electrophysiological signals during motion. Electrical stimulation from the conductive on-skin electrodes accelerated the healing of skin wounds[223] (Figure 17c).

For the development of precision medicine, the wound bandage can also be equipped with a closed-looped, dual drug release system that is both pH- and electrically responsive.[277] For example, a pH sensor can trigger drug release to the wound when infections are detected.[281-285] Looking forward, smart wound bandages based on more tissue-like hybrid materials would provide protection to the wound, continuously monitor infection and inflammation, and apply localized treatment through “smart” drug release upon infection.

7.7. Tissue-Like Neural and Cardiac Devices

Both 2D and 3D bioelectronics have been developed for neural and cardiac interfaces. While biointerface studies over conventional 2D cell layers can provide a mechanistic understanding of signal transduction at device-cell interfaces, interrogating the 3D cellular architectures or 3D tissue surfaces could more faithfully recapitulate endogenous biological processes in living animals. This goal necessitates interfacing bioelectronics with 3D tissue organizations. This section focuses on the discussion of nano-enabled neural and cardiac bioelectronics (Table 2), given the large volume of reviews on topics related to other types of devices.[286-289]

7.7.1. Neural Interfaces.—In the context of implantable neural probes for electrophysiology studies in live animals, evidence suggests that structural and mechanical differences between conventional neural probes and their cell targets can disrupt the native tissue and physiological processes[117,290-293] they are designed to interrogate, leading to neuronal loss and neuroinflammatory responses.[290,291] Disruption of the native tissue includes the proliferation of astrocytes and microglia and the depletion of neuronal nuclei and neurofilaments.[294,295] This foreign-body response acts as a barrier that precludes the device from stably recording and modulating neural circuits over a prolonged time.

Lieber and co-workers have been working toward minimally invasive neural probes by implanting 3D macroporous nanoelectronics with tissue-like flexibility into live animal brains and retinas to record electrophysiological activity.[233,296,297] The devices were fabricated through deterministic assembly, following $S_1S_1 > S_1H$, $HH > S_1H$ where S_1 and H denote SU-8 and metal layers, respectively (Figures 18). These mesh probes are robust and time-invariant in their properties, exhibiting sustained stability with a long lifetime that allows for functional long-term single-unit recordings (signal transduction: $S_2S_2 \rightarrow S_2H \rightarrow HH$, S_2 and H are brain tissues and metal layers, Figure 18d) over 8 months and stable tissue interface over a year[298,299] (Figure 18c). To further address the baseline structural and mechanical distinctions between neural probes and their neuron targets, Yang and Lieber implemented a bioinspired neural probe design, neuron-like electronics (NeuE) (Figure 18a), where the key building blocks mimic the subcellular structural features and mechanical properties of neurons.[224] NeuE is structurally indistinguishable and intimately interpenetrated with neurons, and exhibits a functionally stable interface with the neural tissue following implantation (Figure 18b). Moreover, the NeuE subcellular structural features were shown to facilitate association of endogenous neural progenitor cells (enhanced SH). Hong and Lieber reported tissue-like mesh electronics that formed seamless contact with the curved retina upon injection. The tissue-like mesh electronics have high-density channels that can stably record retinal ganglion cell (RGC) activity for at least 2 weeks, and substantial data revealed periodical circadian rhythms in RGC response.[299] Overall, these tissue-like neural interface devices possess integrated tissue-like properties that enable high-quality electrical performance and long-term use without rejection.

In addition, a mesh-like flexible silicon membrane allowed for conformal attachment and sufficient adhesion on the surface of a mouse brain, enabling control of brain activity in the somatosensory cortex (signal transduction: $HH \rightarrow S_1H \rightarrow S_1S_1$, S_1 and H are brain tissues and silicon membranes, respectively). [85] In the device fabrication, Jiang et al. started with the synthesis of nanocrystalline p-type/intrinsic/n-type multilayered Si membranes, followed by microfabrication to achieve mesh-like geometry. Upon attaching the Si mesh onto a porous PDMS substrate, a soft–hard composite was made for neuromodulation. The device fabrication follows a deterministic assembly, i.e., $HH > S_2H$, $S_2S_2 > S_2H$; S_2 and H are PDMS and Si membranes, respectively.

7.7.2. Cardiac Interfaces.—Tian and Lieber developed 3D macroporous flexible nanoelectronics as bioactive synthetic scaffolds to electrically probe the biophysical and biochemical microenvironments of engineered cardiac tissues in 3D.[212] The microporous nanoelectronics were fabricated either through deterministic assembly (SS > SH, HH > SH; where S and H denote the SU-8 and electronic components, respectively) via conventional lithography, or guided organization(HH > SH > SS, where S and H denote the SU-8 and the multilayered metals, respectively) via residual stress. The nanoelectronic scaffolds exhibited integrated sensory capabilities, enabling real-time monitoring of pH changes, electrical activity, as well as tissue dynamics in response to drugs. These “cyborg” cardiac tissues may be useful for in vitro drug screening. Moreover, 3D mapping and regulation of real-time action potential propagation in nanoelectronics-innervated tissues was achieved, and the dynamics and characteristics of action potential conduction in a transient arrhythmia disease

model was also probed using this model.[84] In addition, these multifunctional electronics can be applied as cardiac patches to online monitor and regulate cardiac function.[300] In addition to electrical recording, the integration of electroactive polymer enables on-demand electrical stimulation and drug release.

In a different approach, Liu and co-workers implanted prefabricated stretchable bioelectronics into developing cardiac tissues for tissue-wide electrophysiological mapping throughout organogenesis (Figure 19). Uniquely, the biomechanical forces produced during organogenesis drove transformation of the 2D stretchable devices into a tissue-integrated 3D layout, following SS > SH > HH where S is the growing cardiac organoid and H is the stretchable electronics (Figure 19b). The authors used this technique to chronically and systematically study the evolution, propagation, and synchronization of the bursting dynamics in human cardiac organoids during development (Figure 19c).

Besides electrical sensing, several soft–hard composites have been developed for cardiac pacing or stimulation. For example, Parameswaran et al. assembled Si nanowires over SU-8-based polymer mesh (deterministic assembly, $S_1S_1 > S_1H$, $HH > S_1H$; S_1 and H denote SU-8 and Si nanowires, respectively) for optically triggered cardiac training and pacing (signal transduction, $HH \rightarrow HS_2 \rightarrow S_2S_2$; S_2 and H denote cardiomyocytes and Si nanowires, respectively).[188] The Si nanowires produced photoelectrochemical output upon laser scanning, whereas the SU-8 mesh supported the Si nanowires and contributed to device adhesion over the heart surface.

Future soft–hard composites for multifunctional cardiac interfaces may achieve both stimulation and recording of the electrical signals for heart disease therapies, enable energy harvesting from the heart's beating motion,[301] possess tissue-like mechanical properties, and even display adaptability and trainability.

7.8. Tissue-Like Living Hybrid System

Biological components are adaptable and can produce signaling processes or molecules that are easily recognizable by cells and tissues. Bioelectronics are designed to interface with cells and tissues for electronic sensing or control of their electrical activities. While most efforts have focused on achieving bioelectronics that are nonliving or produced by physical methods, recent progress has involved the so-called "living bioelectronics". In living bioelectronics, the cells and tissues are seamlessly integrated with the electronic materials, for example, through cellular internalization-enabled integration[226] or cell-driven growth of the electronic materials[229] (Table 2).

Zimmerman et al. showed that Si nanowires could be internalized by many mammalian cells such as endothelial cells, smooth muscles, and many cancer cell lines.[226] With biophysical studies at the single-cell and ensemble levels, and with several drug assays, they found that the Si nanowire internalization was mediated by phagocytosis (Figures 20a,b). This composite formation follows SH > HH and SH > SS in the soft–hard framework, as the internalization (i.e., cell-Si nanowire interaction, SH) drives the translocation of nanowires from the extracellular to intracellular spaces (Figure 20c). Initially, the internalized Si nanowires were used to measure intracellular force dynamics. Jiang et al. later showed

that the Si nanowires, when internalized by satellite glial cells (Figure 20d), could trigger calcium flux from the intracellular space of the glia upon optical excitation.[85] More importantly, the calcium signal from the glia elicited neuronal responses in a neuron-glia coculture (Figure 20e). In this example, the photothermal effect of the Si nanowires may have contributed to the observed calcium flux initiation, as the transient heating would cause poration of calcium storage organelles such as the endoplasmic reticulum and mitochondria. It is also possible that the transient heating could produce reactive oxygen species (ROS) that stress the glial cells and elevate their intracellular calcium concentration. As minimal cytotoxicity was observed in this intracellularly integrated bioelectrical control, Rotenberg et al. expanded this modulation method to the cardiovascular system with a myofibroblast/Si nanowire composite.[227,228] The cellular composite was made via phagocytosis of Si nanowires into the myofibroblasts (Figure 20f). Upon lasing, calcium signals were produced in the myofibroblast, which were transmitted to the adjacent cardiomyocytes. With controlled frequency of the light pulses, Rotenberg et al. achieved cardiac training and pacing[227,228] (Figure 20f).

The above examples of living hybrid systems integrate cells with semiconductor materials through phagocytosis, and are potentially limited by the lack of cellular specificity. A more advanced method was recently demonstrated by Liu et al.,[229] where living neurons were genetically modified to produce electrically functional semiconducting and insulating polymers over plasma membranes (Figure 21a). The authors used adeno-associated virus (AAV) vectors and expressed peroxidase enzyme on the extracellular surface of plasma membranes. In the presence of the polymer precursors (such as that for PANI conducting polymers), peroxidases catalyzed the polymerization at the cell surfaces and produced polymer networks. In this example of the formation of a living composite, the soft–hard framework follows SS > SH > HH, as peroxidase production from the targeted cells (i.e., SS) and plasma membrane-associated polymerization (i.e., SH) are the key drivers behind the formation of the cellular composite (Figure 21b). The authors used various electrophysiological and behavior studies and demonstrated that the genetically targeted assembly of polymers could remodel the cell membranes' electrical properties and modulate the biological activities even in freely moving animals. This method has opened up many new opportunities in electroceuticals where the electronic materials or devices can be produced de novo from target cell populations. This method can seamlessly integrate cell-type-specific functional polymers into tissues or organs, which could help tissue regeneration if injury or disease occurs. In particular, the conductive polymers produced in this way can apply exogenous electrical fields for enhanced nerve regrowth or directed cell migration.

7.9. Tissue-Like Robotics

The human body is highly efficient and capable of performing precise and delicate movements. We have long been trying to replicate human biology to create autonomous forms that match or exceed human capabilities, whether carrying heavy loads or creating small inscriptions. Machines have entered the conversation for such a task, with computers and artificial intelligence and robots dominating technological advancements. Factories and other large industrial environments often utilize robots to increase labor efficiency while

lowering costs. Now, scientists have set their sights on developing robots that can achieve more deft and irregular movements that would allow robotics to enter fields that require more intimate interactions with humans, such as biomedical settings.

As robotics rapidly advances, increasing attention has been directed toward the development of soft robotics. Typical robots are composed of hard, unyielding material that allows them to carry out preplanned tasks precisely. However, while rigid-bodied robots have excelled in a factory and industrial settings, they lack the capabilities to interface with softer living organisms in unstructured environments[292] safely. Soft robotics utilizes bioinspired soft technologies to allow for morphologically adaptive interactions with different tissue-based systems. Such robots may surpass natural organisms in performing multifunctional and versatile tasks, thereby opening the door for numerous applications. The healthcare field,[302] in particular, is a virtual gold mine for soft robotics opportunities, motivating the desire for high biocompatibility and precision in these robots.

Soft robotics design revolves around three primary components: an actuator, a sensor, and a control system. Unlike conventional hard robots, soft-bodied robots do not use a motor but instead rely upon a device, termed an actuator, that allows for the robot to move and interact with the surrounding environment. Sensors take in external stimuli, such as pressure or temperature, and communicate that information to the actuator. The control system works to enhance and direct the activity of the robot through the information taken in by the sensor. These systems replace the rigid modular systems that perform and determine movement in hard robotics to allow for irregular and delicate movements.[303]

In designing these key pieces, material selection becomes extremely important. Soft and compliant materials with elastic moduli similar to that of tissue in biological systems (i.e., tissue-like materials) are chosen as the primary components of the robot to work in conjunction with harder components (Table 2). In choosing these tissue-like systems, researchers can develop robots that can safely interact with humans and other living systems, such as in surgical procedures, drug delivery, or even child supervision. Typical soft material components that could yield the tissue-like behaviors include, but are not limited to, hydrogels, silicone-based elastomers, urethanes, hydraulic fluids, and gases. Many of these soft materials are elastic or viscoelastic with nearly infinite degrees of freedom, allowing for energy dissipation and stable motion under dynamic loading forces.[304]

Soft robotic actuators have been developed to move in response to various external stimuli, including magnetic, thermal, electrical, chemical, and light stimuli. The material composition can be anything from shape memory alloys to papers or fluids. The desired application often determines the material composition, with biomedical applications requiring materials activated in the near-infrared region (NIR) and environmental ones preferring sunlight-stimulated materials.[305] Responsive hydrogels[306] have gained great attention due to their adaptive responses to various stimuli in the environment, including pH, temperature, light, and glucose. These hydrogel materials have the potential to be used as bioelectronics platforms for sensing physiological changes in the environment. An example of this is the phototactic self-sustained hydrogel oscillator[230] demonstrated by Zhao et al. Visible light directs and fuels the Au nanoparticle-embedded PNIPAAm (AuNP/PNIPAAm)

hydrogel pillar by converting absorbed light to heat, and causing different portions of the hydrogel to expand or contract, resulting in oscillatory locomotion (Figure 22). In this example, the Au nanoparticles are the hard materials, and they produce a rapid and robust photothermal effect through plasmonic heating. The soft PNIPAAm hydrogels are thermally responsive and produce strong shape changes upon heating and cooling (Figure 22c,d). Given that robotic actuation follows a clear temporal sequence, the soft–hard framework would follow HH → SH → SS, where H and S are Au nanoparticles and the hydrogel and the heat-induced shape changes *via* the Au/PNIPAAm interfaces (Figure 22b).

Magnetically responsive shape-programmable materials have also recently gained interest due to their ability to form small complex shapes that can be tuned over time *via* shifts in the direction, magnitude, and spatial gradients of the applied magnetics field.[307] One of the primary issues that arise in designing magnetic soft robots lies in the large rigid nature of the embedded magnets necessary to generate deflection.[231] This requirement impedes any attempts at miniaturization and hinders the robot's movement, thereby limiting the potential applications for magnetic soft robots. However, as fabrication technology has improved, scientists have developed magnetic soft robot designs[231,307,308] that circumvent these previous issues. Kim et al. reported a ferromagnetic soft continuum robot[231] for biomedical applications composed of polymer matrices embedded with magnetic microparticles (also following HH → SH → SS). The robot possessed self-lubrication, submillimeter scale, omnidirectional steering, and navigating capabilities that allowed it to move throughout complex environments.

Similar to the construction of living bioelectronics, magnetic particles can integrate with cells intracellularly. Yasa et al. showed that magnetically steerable helical microswimmers can be internalized by mouse macrophages and primary splenocytes.[232] They found that the macrophages and splenocytes interacted differently with microswimmers with different helix turn numbers (i.e., SH is highly dependent on the material design). This study suggests a new design perspective for biohybrid robotic implementation (following SH > HH, and SH > SS).

Sensors work to take in information on the environment surrounding the robot, whether that be light, pressure, or heat. Such technology is necessary to generate responsive and more bio-like soft robots. Silica-based distributed fiber-optic (DFOS) systems have been long used for their abilities to sense strain, pressure, temperature, and other external stimuli.[309] However, classic DFOS systems are not compatible with soft robotics due to their inability to deal with large strains present in the soft materials. Bai et al. demonstrated a "stretchable" DFOS system[309] that can sense locations, magnitudes, and modes of mechanical deformation through frustrated total internal reflection and absorption. They integrated the stretchable sensor into a soft glove to illustrate the capabilities and applications of such material in soft robotics. You et al. produced a deformable ionic receptor[310] that can take in and cleanly distinguish thermal and mechanical signals without interference. The receptor works through ion relaxation dynamics by regulating charge relaxation time to measure absolute temperature and normalized capacitance as a measure of mechanical strain. This sensor can then be integrated into a synthetic electronic-skin (e-skin)[311] system for more biorealistic soft robotics.

As technology continues to advance in soft robotics, efforts toward more faithful biomimicry begin to emerge. With actuators and sensors producing more life-like movement and responsiveness, scientists have devoted time to developing soft robotics that addresses an array of different natural processes through the endowment of tissue-like materials with unique properties. Pikul et al. published work delineating a synthetic 3D textural camouflage design on stretchable surfaces.[312] Inspired by the ability of cephalopods' musculature to change the organism's skin texture, this elastomeric structure can complete programmable transformations of 2D surfaces into 3D shapes depending on the spatial distribution of the mechanically heterogeneous components. Mishra et al. developed a hydrogel-based actuator[313] to maintain stable temperatures through autonomic perspiration, thereby endowing soft robotics with thermal homeostasis. Pena-Francesch et al. reported synthetic soft materials with self-healing capabilities[314] for both micro- and macro-scale mechanical damage. Such innovations will continue to emerge as tissue-like soft robotics progresses further toward and even surpasses conventional biological functionality.

8. OUTLOOK

Chemical processes at soft–hard interfaces are ubiquitous in both naturally occurring and synthetic systems. Despite the diversity of these interfaces, they share common principles (Figure 7) and can be understood in a coherent framework. Future chemical studies at soft–hard interfaces can benefit from interdisciplinary studies and advanced in situ characterization tools. Directions that may bring immediate impacts are suggested as follows:

8.1. Nature-Inspired Synthetic Interfaces

Naturally occurring soft–hard interfaces have evolved to display high performance, adaptability, and durability. They represent numerous sources of inspiration for synthetic soft–hard interface designs.

Nature displays remarkable gradient strategies for solving mechanical mismatch issues at heterogeneous tissue interfaces or transition zones. These chemical strategies involve graded mineralization[16] (Figure 23a, 1), diffusion of coacervates for uneven cross-linking and hardening,[101,102] formation of interpenetrated and spatially varying (bio)polymer networks,[102] or molecular linkers that display load-bearing moieties and asymmetric chemical bonding sites to both soft and hard components.[98] These strategies could be used in the synthesis of coating materials for stiff biomaterial implants, such as osseo-integrated prosthetic limbs.

Naturally occurring soft–hard hybrids demonstrate elegant solutions for mass transport (Figure 23a, 2) necessary for (bio)chemical processes in functional tissues or organs. For example, many natural materials, hard or soft, are porous or display loose interiors with dense surfaces to balance strength and flexibility.[3] Alternatively, molecules and ions are efficiently delivered to the target domains through vascular networks.[3,315] These strategies could be considered when designing chemical reactions at synthetic soft–hard interfaces (e.g., tissue-bioelectronics interfaces).

In contrast to most synthetic methods, biologically derived interfaces are processed with natural molecules[7] and ions under physiological conditions (i.e., at ambient or body temperature, at close to atmospheric pressure, in a salty solution, at close to neutral pH). If the biochemical pathways for these natural soft–hard interfaces are resolved, greener[7] and more robust chemical synthesis (Figure 23a, 3) may be developed for future materials or devices where soft–hard interfaces are desirable.

Finally, naturally occurring soft–hard interfaces usually have unique homeostatic functions (Figure 23a, 4) and can precisely control the interfacial microenvironment. This control is maintained by autoregulatory feedback loops that are distributed hierarchically at multiple spatiotemporal scales. However, most synthetic soft–hard interfaces are unable to self-sense or self-modulate their behaviors. Future studies should incorporate these homeostatic principles, identify the essential physical and chemical elements, and seek new customizable and scalable materials synthesis that would enable autonomous interfaces.

8.2. Emergent Behavior in Synergistic Interfacial Mismatches

Soft materials commonly present motile, nonlinear, and emergent properties, which are sensitive to subtle external perturbations such as reaction-diffusion processes and dynamic defect flows.[1,5,29,30,57] The exclusive behaviors of soft materials are acquired at far-from-equilibrium conditions and later preserved by energy dissipation.[57] In particular, biological tissues and synthetic soft materials are adaptable,[6,161,163,166-168,316] self-healing and regenerative,[12,38,39,69,161] and symmetry-breaking.[57] In contrast, hard materials display constant and well-defined behaviors, and most of their properties are generated at or close to equilibrium conditions. These differences, in addition to the mismatches in mass transport and mechanical and electrical properties, represent several unique and exploitable design opportunities for future chemical studies.

The contrasting behaviors and properties of soft and hard components can be integrated for synergistic outputs (Figure 23b, left). In this way, the information-generating or information-processing capacity can be drastically expanded as both nonequilibrium/emergent (in the soft phase) and equilibrium/deterministic (in the hard phase) pathways can be adopted and seamlessly integrated (Figure 23b, left). For example, a soft–hard composite made of ferromagnetic nanowires with nematic order and a light-responsive polymer network can respond to both the optical and magnetic fields in a synergistic manner. This has yielded rapid walking of a robot made from this composite in water and delivery of cargo by rolling and light-induced geometry variation.[317]

Soft and hard materials may display mismatched responses upon external stimulation, yielding energy dissipation domains[62] or temporarily imbalanced potential energy (V) levels across soft–hard interfaces. This would produce a gradient of properties and a driving force (i.e., following $F = -\mathrm{d}V/\mathrm{d}r$, r is the distance) of transition, as long as there are finite interactions between the soft and hard components at the interfaces. The hard component sets unique boundary conditions for any behaviors and properties from the soft component as the former has, for example, a much smaller chemical diffusivity and much larger modulus. The gradient of properties or force at the interface can serve as a localized zone (Figure 23b, right) to trigger directional chemical diffusion or bias reaction pathways based

on stimuli-responsive chemical groups.[6,161,166,167,316] For example, the force produced by a temporary difference in electric potential across the soft–hard interface (e.g., through the photovoltaic effect of a cell-interfacing semiconductor[15]) can affect ions or molecules and their transition states that display polarity.[318] One can also appreciate this possibility when considering ion channels and plasma membranes. The ~5 nm thick plasma membrane separates intra- and extra-cellular domains, and it establishes an electrical field on the order of ~10^7 V/m (ref 36). The ion channels and many other membrane proteins can sense this large electrical field,[91] display conformational changes, and trigger cellular signaling. While fields, gradients, and forces occur in many other interfacial domains, such as the electrical double layer at the solid/liquid interface or the charge depletion region of a p-type/n-type silicon junction,[15] these interfaces usually have limited room for exploring new chemical processes, as opposed to the multiple exploratory domains at soft–hard interfaces (Figure 5).

From an applications point of view, the mismatches at soft–hard interfaces can be leveraged for sensing and self-regulation, such as radiation or damage sensing (e.g., with a mechanophore[319] at the interface) and self-healing electronics (e.g., with mechanically induced free radical generation for polymerization[196]).

8.3. Tissue-Like System for Human-Machine Interfaces and Neuromorphic Computing

8.3.1. Human-Machine Interface.—Human-machine interfaces (HMIs) form direct connections between the human body and external electronic machines. According to the direction of information flow, HMIs can be divided into two types: the input type HMI in which artificial signals are transmitted into the central nervous system,[320] and the output type HMI in which signals generated in the human body are transmitted to external devices.[321] While both types of HMIs contribute greatly to the biomedical field, the output type HMIs, in particular, support restoration of mobility in paralyzed and amputated patients by bypassing lost or nonfunctional nerves and rerouting signals from the sensory-motor area in the cerebral cortex to manipulate prosthetic limbs. Thus, the key functions of output HMIs are to establish steady communication between the brain and signal-collecting electrodes, and between the HMIs and the electronic devices.[322] For example, Bao and co-workers demonstrated an artificial afferent nerve, which collects tactile information (1 to 80 kilopascals) from integrated pressure sensors. The artificial afferent nerve can convert the tactile information into a neuron-like action potential (0 to 100 Hz) achieved by ring oscillators. A series of ring oscillators can be used to construct a synaptic transistor that reflects complicated neural communication behavior, which is potentially useful for neurorobotics and neuroprosthetics.[323] Rogers and co-workers developed a highly integrated millimeter-scale pressure sensor. The three-dimensional design of the small-scale pressure sensor integrates a hard metal strain gauge on a soft, thin polyimide substrate with a battery-free and wireless platform. The unique hard–soft integration is similar to biological tissue and can be imperceptibly laminated onto skin-prosthesis interfaces.[324] Unfortunately, many currently developed HMIs display mechanical and biological mismatch with the human brain,[325] which restricts signal transmission efficiency and long-term performance. Noninvasive approaches are one potential solution; however, the relatively low spatial resolution and low signal-to-noise ratio of noninvasive approaches are not suitable for

practical control.[326] Thus, the development of tissue-like, minimally invasive HMIs that can integrate with compliant brain tissue is greatly desired.

8.3.2. Neuromorphic Computing.—Driven by the dream of building an artificial manmade brain, the field of computer science and neurobiology have become intricately linked.[327] As the science of neuromorphic computing has flourished in the past years, material scientists have been drawn to investigate technologies and materials that can ultimately apply neuromorphic computing to living organisms. Unlike conventional hard semiconductor materials, soft organic semiconductors may be used to craft neuromorphic devices for biomedical applications due to their biocompatibility, soft mechanical properties, and inherent sensitivity.[328] Soft organic semiconductors have been used to craft organic neurons,[329] memristive devices,[330] neuromorphic electrolyte-gated transistors,[331] and organic synapses.[332] Salleo and co-workers reported an electrochemical neuromorphic organic device (ENODe) that demonstrates neuromorphic functionality in stretchable electronic systems. The working principle of ENODe is different from the traditional inorganic memristor. The mechanical flexibility of ENODe makes the memristor more brain-like.[333] Santoro and co-workers reported a multifunctional biohybrid synapse, which coupled a conventional organic neuromorphic device to a PC-12 cell containing the dopaminergic presynaptic domain. They demonstrated a seamlessly integrated soft–hard interface-coupled tissue-like neuromorphic device and revealed the essential functions of dopamine during cell-to-cell transmission. On the other hand, dopamine can also manipulate synaptic plasticity. Therefore, the synaptic network produced by dopamine signaling created an unprecedented neuromorphic device.[334] Biological synapses are the functional connection points between neurons, and are responsible for transmitting, storing, and processing information simultaneously through changes in synaptic weight, which is the foundation of learning and memory in the biological brain.[335] Thus, synapse-like devices with seamlessly integrated soft–hard interfaces are critical to developing neuromorphic devices and essential for building up brain-like neuromorphic architectures. Current artificial neuromorphic devices include three-terminal organic synaptic transistors that consist purely of manmade organic materials[336] and biohybrid synapses that combine living cells as presynaptic neurons and organic materials as postsynaptic neurons.[334] These synaptic devices focus on mimicking the working behaviors of a biological synapse, such as long-term potentiation (LTP), short-term potentiation (STP), and spike-timing-dependent plasticity (STDP).[333] However, they do not consider other biological features equally important for crafting implantable or wearable devices. In the future, emulation of the working behaviors of synapses will be achieved through the development of tissue-like neuromorphic computing devices with sophisticated soft–hard components.

8.4. Living Components

The field of living bioelectronics or robotics will continue to expand, especially given the need for cellular specificity, biocompatibility, and extended lifetime in the next generation of devices. Future living bioelectronics will strive for truly seamless integration of biological circuits. Recent progress in fabricating purely biological “electrodes” has suggested that this seamless integration is feasible. For example, implantable “living electrodes” were achieved by growing living cortical neurons in biocompatible hydrogel cylinders, where the axonal

tracts were extended along the cylinder axis (Figures 24a, 24b). The “living electrodes” were highly biocompatible, could survive for a long time in the rat brain, and were capable of optical sensing and modulation of brain activity.[337] While no electronics components were included in this first study, the barriers are low to integrate these “living electrodes” with electronic circuits for closed-loop and highly efficient neural interfacing.

Many living subcellular components are conductive, which could be explored for future bioelectronics and robotics. For example, with electrical stimulation from electrodes, *Geobacter sulfurreducens* biofilms can produce cytochrome OmcZ nanowires. These nanowires have 1,000-fold higher conductivity and 3-fold higher stiffness than the naturally occurring cytochrome OmcS nanowires.[339] In this case, through signal transduction HH → SH → SS, *Geobacter sulfurreducens* produces living components that can be potentially integrated into a bioelectronics circuit for either sensing or modulation applications.

Future bioelectronics or robotics designs should also consider the incorporation of biological vasculature. This could potentially enhance biointegration and cell viability near the device surfaces. In tissue engineering and regenerative medicine, several methods have been proposed for enhanced vascular regeneration. For example, Baker and coauthors recently found that biomechanical conditioning, together with pharmacological treatment, can synergistically enrich the vascular regenerative potential of mesenchymal stem cells (Figure 24c). The proposed mechanism for the enhanced blood vessel growth involved elevated angiogenic paracrine signaling and an increase in the endothelia–pericytes population.[340]

9. CONCLUSION

This review proposed a soft–hard interaction framework to classify diverse structures and dynamic processes involved in soft–hard composites (Figure 7 and Video 1). A deeper and more coherent understanding of the interfacial processes at soft–hard interfaces will yield numerous opportunities for diverse research fields.

Given that soft–hard interfaces[42] are functional across a wide range of length and time scales, future efforts should include formulating a theoretical framework or a dimensionless description that covers the mechanical, electrical, and chemical processes in the majority of soft–hard interfaces. Additionally, a ‘total synthesis framework[35] could be developed for coupling the soft–hard components into functional structures. Such a framework would explore chemoselective reactions, substituent effects, regiospecificity, and many other rational designs. Moreover, since soft–hard interfaces are usually embedded, new tools that can either directly visualize the interfaces nondestructively or provide 3D chemical or structural reconstruction of the interfaces are highly desirable. Correlative microscopy or spectroscopy may also contribute to a future understanding of the structures and dynamics of both the soft and hard phases near the interfaces.

With the notion of SS, HH, and SH, we hope that the new interaction framework can unify seemingly random and disconnected soft–hard examples in both the naturally occurring and the synthetic systems. Looking forward, we anticipate that this framework may point to new directions for formulating new soft–hard interfaces. For example, while there

is numerous material and device progress in bioelectronics and robotics, most of these systems were constructed with a deterministic assembly approach. However, given that directed organization or cooperative integration makes most biological systems, we envision a significant increase in this effort by designing and implementing the SH interactions given their relative dominance in the interaction frameworks for directed organization or cooperative integration. Chemists, biochemists, and materials scientists would play a significant role in this regard, given they would help achieve new SH interactions involving coordinate covalent bonding, electrostatic interactions between charged groups, hydrogen bonding, or van der Waals interactions, etc.

Regarding biointerfacing materials, diverse approaches to building soft–hard interfaces have generated living composites or engineered tissues with moduli ranging from a few kilopascals to tens of gigapascals, with diverse stimuli-responsive or adaptable behaviors. Improvements in soft–hard interfaces may also yield new devices for clinical applications, such as engineered cartilage or meniscus. We believe that future chemical, mechanical, electrical, and medical exploration at soft–hard interfaces will yield breakthroughs in bioengineering, materials science, regenerative medicine, artificial intelligence, and future robotics design.

Supplementary Material

Refer to Web version on PubMed Central for supplementary material.

ACKNOWLEDGMENTS

We thank Karen Watters for scientific editing of the manuscript. This work is supported by National Institutes of Health (NIH NS101488), Army Research Office (W911NF2110090), Air Force Office of Scientific Research (FA9550-20-1-0387), the US Office of Naval Research (N000141612958), and the National Science Foundation (NSF CMMI-1848613, DMR-2105321). A.P. acknowledges support from the NSF MRSEC Graduate Fellowship (NSF DMR-2011854). B.T. and X.Y. would like to dedicate this article to Dr. C. M. Lieber for his mentorship.

Biography

Yin Fang is currently an assistant professor in the School of Chemical and Biomedical Engineering at Nanyang Technological University. He received his Ph.D. in chemical engineering from the University of Florida in 2016. His Ph.D. research with Professor Peng Jiang focused on self-assembled photonic crystals, shape memory polymers, smart windows, and plasmonic sensing in photonic structures. He worked with Professor Bozhi Tian as a postdoctoral scholar in tissue-like hybrid systems and bioelectronics at the University of Chicago. His current focus is on soft materials, tissue-like electronics, shape memory materials, and soft medical robotics for therapeutic applications. Professor Fang’s accolades include the MRS graduate student award (2015) and Chinese government award for outstanding self-financed Ph.D. students (2016). In 2020, his work was selected as the top 7 stories in the chemistry department. Meanwhile, his work was also selected as “ten cool research stories” on Uchicago news at the University of Chicago.

Xiao Yang received her Ph.D. degree in Chemistry from Harvard University in 2020 under the supervision of Professor Charles M. Lieber. Currently she is a postdoctoral fellow in the

laboratories of Professor Sergiu P. Paşca. and Professor Bianxiao Cui at Stanford University. She is interested in developing novel bioelectronics for neural interfaces.

Yiliang Lin received his B.S. in polymer science and engineering in 2013 from Zhejiang University in China. Later he obtained his Ph.D. in chemical engineering in 2018 from North Carolina State University in the U.S.A., under the guidance of Prof. Michael D. Dickey and Prof. Jan Genzer. He is currently a postdoctoral fellow in the lab of Prof. Bozhi Tian at the University of Chicago in the U.S.A. Yiliang's research interests include designing and engineering soft matter or soft–hard composites for bioelectronics and hybrid living materials.

Jiuyun Shi received his B.S. in chemistry in 2018 from Zhejiang University in China. Currently, he is a graduate student at the University of Chicago supervised by Prof. Bozhi Tian. His research involves the development of novel functional hydrogels for biomedical regenerative therapy and bioelectronics.

Aleksander Prominski received his B.Sc. from the University of Warsaw, Poland, in 2016 and M.Sc. from the University of Chicago in 2017 He entered the Ph.D. program in Chemistry at the University of Chicago in 2016. His current research involves the synthesis of new nanostructured materials for application in biomodulation and the development of machine-intelligence-assisted bioelectronic systems.

Clementene Clayton is an undergraduate student at the University of Chicago in the Chemistry and Molecular Engineering Departments. Her research centers around biomimetic materials, namely those involving hydrogels and starch-based systems. Her family currently resides in Sydney, Australia, but she is originally from the California Bay Area.

Eleanor Ostroff is an undergraduate student majoring in Chemistry at the University of Chicago. In the Tian Lab, she works on nanostructured materials and their applications to biomodulation. She is interested in pursuing a career in medicine and hopes to continue researching the biomedical applications of nanomaterials as her career progresses.

Bozhi Tian received B.Sc. and M.Sc. degrees in chemistry from Fudan University Shanghai, China, and A.M. and Ph.D. degrees in physical chemistry from Harvard University in 2010. His current research focuses on the semiconductor-enabled understanding of subcellular biophysics, as well as studies of dynamics at soft–hard interfaces.

REFERENCES

(1). Kato T; Yoshio M; Ichikawa T; Soberats B; Ohno H; Funahashi M Transport of ions and electrons in nanostructured liquid crystals. Nat. Rev. Mater 2017, 2, 1–20.

(2). Yang CH; Suo ZG Hydrogel ionotronics. Nat. Rev. Mater 2018, 3, 125–142.

(3). Wegst UGK; Bai H; Saiz E; Tomsia AP; Ritchie RO Bioinspired structural materials. Nat. Mater 2015, 14, 23–36. [PubMed: 25344782]

(4). Whittell GR; Hager MD; Schubert US; Manners I Functional soft materials from metallopolymers and metallosupramolecular polymers. Nat. Mater 2011, 10, 176–188. [PubMed: 21336298]

(5). Weiss RG The past, present, and future of molecular gels. what is the status of the field, and where is it going? J. Am. Chem. Soc 2014, 136, 7519–7530. [PubMed: 24836858]

(6). Merindol R; Walther A Materials learning from life: concepts for active, adaptive and autonomous molecular systems. Chem. Soc. Rev 2017, 46, 5588–5619. [PubMed: 28134366]

(7). Shen XP; Shamshina JL; Berton P; Gurau G; Rogers R D Hydrogels based on cellulose and chitin: fabrication, properties, and applications. Green Chem. 2016, 18, 53–75.

(8). Kim SH; Kim H; Kim NJ Brittle intermetallic compound makes ultrastrong low-density steel with large ductility. Nature 2015, 518, 77–79. [PubMed: 25652998]

(9). Cheng Z; Zhou HF; Lu QH; Gao HJ; Lu L Extra strengthening and work hardening in gradient nanotwinned metals. Science 2018, 362, 559.

(10). Ovid'ko IA; Valiev RZ; Zhu YT Review on superior strength and enhanced ductility of metallic nanomaterials. Prog. Mater. Sci 2018, 94, 462–540.

(11). Vatankhah-Varnosfaderani M; Keith AN; Cong YD; Liang HY; Rosenthal M; Sztucki M; Clair C; Magonov S; Ivanov DA; Dobrynin AV; et al. Chameleon-like elastomers with molecularly encoded strain-adaptive stiffening and coloration. Science 2018, 359, 1509–1513. [PubMed: 29599240]

(12). Zhang L; Bailey JB; Subramanian RH; Groisman A; Tezcan FA Hyperexpandable, self-healing macromolecular crystals with integrated polymer networks. Nature 2018, 557, 86–91. [PubMed: 29720635]

(13). Spanopoulos I; Hadar I; Ke WJ; Tu Q; Chen M; Tsai H; He YH; Shekhawat G; Dravid VP; Wasielewski MR; et al. Uniaxial expansion of the 2D ruddlesden-popper perovskite family for improved environmental stability. J.Am. Chem. Soc 2019, 141, 5518–5534. [PubMed: 30827098]

(14). Kang JS; Li M; Wu HA; Nguyen H; Hu YJ Experimental observation of high thermal conductivity in boron arsenide. Science 2018, 361, 575–578. [PubMed: 29976798]

(15). Jiang YW; Tian BZ Inorganic semiconductor biointerfaces. Nat. Rev. Mater 2018, 3, 473–490. [PubMed: 31656635]

(16). Reznikov N; Steele JAM; Fratzl P; Stevens MM A materials science vision of extracellular matrix mineralization. Nat. Rev. Mater 2016, 1, 1–14.

(17). Eder M; Amini S; Fratzl P Biological composites-complex structures for functional diversity. Science 2018, 362, 543–547. [PubMed: 30385570]

(18). Kim YY; Carloni JD; Demarchi B; Sparks D; Reid DG; Kunitake ME; Tang CC; Duer MJ; Freeman CL; Pokroy B; et al. Tuning hardness in calcite by incorporation of amino acids. Nat. Mater 2016, 15, 903–910. [PubMed: 27135858]

(19). Gal A; Wirth R; Kopka J; Fratzl P; Faivre D; Scheffel A Macromolecular recognition directs calcium ions to coccolith mineralization sites. Science 2016, 353, 590–593. [PubMed: 27493186]

(20). Nel A; Xia T; Madler L; Li N Toxic potential of materials at the nanolevel. Science 2006, 311, 622–627. [PubMed: 16456071]

(21). Lopez J; Mackanic DG; Cui Y; Bao ZN Designing polymers for advanced battery chemistries. Nat. Rev. Mater 2019, 4, 312–330.

(22). Sun YM; Liu NA; Cui Y Promises and challenges of nanomaterials for lithium-based rechargeable batteries. Nat. Energy 2016, 1, 1–12.

(23). Wang Q; Mynar JL; Yoshida M; Lee E; Lee M; Okuro K; Kinbara K; Aida T High-water-content mouldable hydrogels by mixing clay and a dendritic molecular binder. Nature 2010, 463, 339–343. [PubMed: 20090750]

(24). Serrano-Luginbuhl S; Ruiz-Mirazo K; Ostaszewski R; Gallou F; Walde P Soft and dispersed interface-rich aqueous systems that promote and guide chemical reactions. Nat. Rev. Chem 2018, 2, 306–327.

(25). Cianchetti M; Laschi C; Menciassi A; Dario P Biomedical applications of soft robotics. Nat. Rev. Mater 2018, 3, 143–153.

(26). Newcomb CJ; Qafoku NP; Grate JW; Bailey VL; De Yoreo JJ Developing a molecular picture of soil organic matter-mineral interactions by quantifying organo-mineral binding. Nat. Commun 2017, 8, 1–8. [PubMed: 28232747]

(27). Lehmann J; Solomon D; Kinyangi J; Dathe L; Wirick S; Jacobsen C Spatial complexity of soil organic matter forms at nanometre scales. Nat. Geosci 2008, 1, 238–242.

(28). Mezzenga R; Schurtenberger P; Burbidge A; Michel M Understanding foods as soft materials. Nat. Mater 2005, 4, 729–740. [PubMed: 16195765]

(29). Lovrak M; Hendriksen WEJ; Maity C; Mytnyk S; van Steijn V; Eelkema R; van Esch JH Free-standing supramolecular hydrogel objects by reaction-diffusion. Nat. Commun 2017, 8, 1–10. [PubMed: 28232747]

(30). Epstein IR; Xu B Reaction-diffusion processes at the nano- and microscales. Nat. Nanotechnol 2016, 11, 312–319. [PubMed: 27045215]

(31). Zhang Z-C; Xu B; Wang X Engineering nanointerfaces for nanocatalysis. Chem. Soc. Rev 2014, 43, 7870–7886. [PubMed: 24745032]

(32). Novoselov KS; Mishchenko A; Carvalho A; Castro Neto AH 2D materials and van der Waals heterostructures. Science 2016, 353, 353. [PubMed: 27417493]

(33). Wen CY; Reuter MC; Bruley J; Tersoff J; Kodambaka S; Stach EA; Ross FM Formation of Compositionally Abrupt Axial Heterojunctions in Silicon-Germanium Nanowires. Science 2009, 326, 1247–1250. [PubMed: 19965471]

(34). Chen PC; Liu MH; Du JSS; Meckes B; Wang SZ; Lin HX; Dravid VP; Wolverton C; Mirkin CA Interface and heterostructure design in polyelemental nanoparticles. Science 2019, 363, 959–964. [PubMed: 30819959]

(35). Buck MR; Bondi JF; Schaak RE A total-synthesis framework for the construction of high-order colloidal hybrid nanoparticles. Nat. Chem 2012, 4, 37–44.

(36). Milo R; Phillips R Cell biology by the numbers; Garland Science, Taylor & Francis Group, 2016.

(37). Ball JM; Petrozza A Defects in perovskite-halides and their effects in solar cells. Nat. Energy 2016, 1, 1–13.

(38). Li C-H; Wang C; Keplinger C; Zuo J-L; Jin L; Sun Y; Zheng P; Cao Y; Lissel F; Linder C; You X-Z; Bao Z; et al. A highly stretchable autonomous self-healing elastomer. Nat. Chem 2016, 8, 618–624. [PubMed: 27219708]

(39). Tee BCK; Wang C; Allen R; Bao ZN An electrically and mechanically self-healing composite with pressure- and flexion-sensitive properties for electronic skin applications. Nat. Nanotechnol 2012, 7, 825–832. [PubMed: 23142944]

(40). Sun JY; Zhao XH; Illeperuma WRK; Chaudhuri O; Oh KH; Mooney DJ; Vlassak JJ; Suo ZG Highly stretchable and tough hydrogels. Nature 2012, 489, 133–136. [PubMed: 22955625]

(41). Rogers JA; Lagally MG; Nuzzo RG Synthesis, assembly and applications of semiconductor nanomembranes. Nature 2011, 477, 45–53. [PubMed: 21886156]

(42). Lin YL; Fang Y; Yue JP; Tian BZ Soft–hard composites for bioelectric interfaces. Trends Chem. 2020, 2, 519–534. [PubMed: 34296076]

(43). Kroger N The Molecular Basis of Nacre Formation. Science 2009, 325, 1351–1352. [PubMed: 19679772]

(44). Suzuki M; Saruwatari K; Kogure T; Yamamoto Y; Nishimura T; Kato T; Nagasawa H An Acidic Matrix Protein, Pif, Is a Key Macromolecule for Nacre Formation. Science 2009, 325, 1388–1390. [PubMed: 19679771]

(45). Ma K; Gong YY; Aubert T; Turker MZ; Kao T; Doerschuk PC; Wiesner U Self-assembly of highly symmetrical, ultrasmall inorganic cages directed by surfactant micelles. Nature 2018, 558, 577–580. [PubMed: 29925942]

(46). Ma K; Spoth KA; Cong Y; Zhang DH; Aubert T; Turker MZ; Kourkoutis LF; Mendes E; Wiesner U Early formation pathways of surfactant micelle directed ultrasmall silica ring and cage structures. J. Am. Chem. Soc 2018, 140, 17343–17348. [PubMed: 30457849]

(47). Armatas GS; Kanatzidis MG Mesostructured germanium with cubic pore symmetry. Nature 2006, 441, 1122–1125. [PubMed: 16810250]

(48). Trikalitis PN; Rangan KK; Bakas T; Kanatzidis MG Varied pore organization in mesostructured semiconductors based on the SnSe4 (4-) anion. Nature 2001, 410, 671–675. [PubMed: 11287949]

(49). Shopsowitz KE; Qi H; Hamad WY; MacLachlan MJ Free-standing mesoporous silica films with tunable chiral nematic structures. Nature 2010, 468, 422–U246. [PubMed: 21085176]

(50). Wan Y; Zhao DY On the controllable soft-templating approach to mesoporous silicates. Chem. Rev 2007, 107, 2821–2860. [PubMed: 17580976]

(51). Wei J; Sun ZK; Luo W; Li YH; Elzatahry AA; Al-Enizi AM; Deng YH; Zhao DY New insight into the synthesis of large-pore ordered mesoporous materials. J. Am. Chem. Soc 2017, 139, 1706–1713. [PubMed: 28085258]

(52). Shi YF; Wan Y; Zhao DY Ordered mesoporous non-oxide materials. Chem. Soc. Rev 2011, 40, 3854–3878. [PubMed: 21423925]

(53). Ross FM; Tersoff J; Reuter MC Sawtooth faceting in silicon nanowires. Phys. Rev. Lett 2005, 95, 146104. [PubMed: 16241673]

(54). Caroff P; Dick KA; Johansson J; Messing ME; Deppert K; Samuelson L Controlled polytypic and twin-plane superlattices in III-V nanowires. Nat. Nanotechnol 2009, 4, 50–55. [PubMed: 19119283]

(55). Fang Y; Jiang Y; Cherukara MJ; Shi F; Koehler K; Freyermuth G; Isheim D; Narayanan B; Nicholls AW; Seidman DN; Sankaranarayanan SKRS; Tian B; et al. Alloy-assisted deposition of three-dimensional arrays of atomic gold catalyst for crystal growth studies. Nat. Commun 2017, 8, 1–10. [PubMed: 28232747]

(56). Zhao WT; Hanson L; Lou HY; Akamatsu M; Chowdary PD; Santoro F; Marks JR; Grassart A; Drubin DG; Cui Y; et al. Nanoscale manipulation of membrane curvature for probing endocytosis in live cells. Nat. Nanotechnol 2017, 12, 750–756. [PubMed: 28581510]

(57). Mann S Self-assembly and transformation of hybrid nano-objects and nanostructures under equilibrium and non-equilibrium conditions. Nat. Mater 2009, 8, 781–792. [PubMed: 19734883]

(58). Limo MJ; Sola-Rabada A; Boix E; Thota V; Westcott ZC; Puddu V; Perry CC Interactions between metal oxides and biomolecules: from fundamental understanding to applications. Chem. Rev 2018, 118, 11118–11193. [PubMed: 30362737]

(59). Arciola CR; Campoccia D; Montanaro L Implant infections: adhesion, biofilm formation and immune evasion. Nat. Rev. Microbiol 2018, 16, 397–409. [PubMed: 29720707]

(60). Jeon D; Park J; Shin C; Kim H; Jang JW; Lee DW; Ryu J Superaerophobic hydrogels for enhanced electrochemical and photoelectrochemical hydrogen production. Sci. Adv 2020, 6, 6.

(61). Naskar AK; Keum JK; Boeman RG Polymer matrix nanocomposites for automotive structural components. Nat. Nanotechnol 2016, 11, 1026–1030. [PubMed: 27920443]

(62). Yuk H; Zhang T; Lin ST; Parada GA; Zhao XH Tough bonding of hydrogels to diverse non-porous surfaces. Nat. Mater 2016, 15, 190–196. [PubMed: 26552058]

(63). Liu MJ; Ishida Y; Ebina Y; Sasaki T; Hikima T; Takata M; Aida T An anisotropic hydrogel with electrostatic repulsion between cofacially aligned nanosheets. Nature 2015, 517, 68–72. [PubMed: 25557713]

(64). Sajadi SM; Vásárhelyi L; Mousavi R; Rahmati AH; Kónya Z; Kukovecz A; Arif T; Filleter T; Vajtai R; Boul P; et al. Damage-tolerant 3D-printed ceramics via conformal coating. Sci. Adv 2021, 7, No. eabc5028. [PubMed: 34233870]

(65). Liu MJ; Wang ZY; Liu P; Wang ZK; Yao HM; Yao X Supramolecular silicone coating capable of strong substrate bonding, readily damage healing, and easy oil sliding. Sci. Adv 2019, 5, 5.

(66). Choi S; Kwon TW; Coskun A; Choi JW Highly elastic binders integrating polyrotaxanes for silicon microparticle anodes in lithium ion batteries. Science 2017, 357, 279–283. [PubMed: 28729506]

(67). Kovalenko I; Zdyrko B; Magasinski A; Hertzberg B; Milicev Z; Burtovyy R; Luzinov I; Yushin G A Major Constituent of Brown Algae for Use in High-Capacity Li-Ion Batteries. Science 2011, 334, 75–79. [PubMed: 21903777]

(68). Xu G-L; Liu Q; Lau KKS; Liu Y; Liu X; Gao H; Zhou X; Zhuang M; Ren Y; Li J; Shao M; Ouyang M; Pan F; Chen Z; Amine K; Chen G Building ultraconformal protective layers on both secondary and primary particles of layered lithium transition metal oxide cathodes. Nat. Energy 2019, 4, 484.

(69). Wang C; Wu H; Chen Z; McDowell MT; Cui Y; Bao ZA Self-healing chemistry enables the stable operation of silicon microparticle anodes for high-energy lithium-ion batteries. Nat. Chem 2013, 5, 1042–1048. [PubMed: 24256869]

(70). Bertazzo S; Maidment SCR; Kallepitis C; Fearn S; Stevens MM; Xie HN Fibres and cellular structures preserved in 75-million-year-old dinosaur specimens. Nat. Commun 2015, 6, 1–8.

(71). Dalby MJ; Gadegaard N; Oreffo ROC Harnessing nanotopography and integrin-matrix interactions to influence stem cell fate. Nat. Mater 2014, 13, 558–569. [PubMed: 24845995]

(72). Murphy WL; McDevitt TC; Engler AJ Materials as stem cell regulators. Nat. Mater 2014, 13, 547–557. [PubMed: 24845994]

(73). Yan H; Yang F; Pan D; Lin Y; Hohman JN; Solis-Ibarra D; Li FH; Dahl JEP; Carlson RMK; Tkachenko BA; et al. Sterically controlled mechanochemistry under hydrostatic pressure. Nature 2018, 554, 505–510. [PubMed: 29469090]

(74). Ong WL; Rupich SM; Talapin DV; McGaughey AJH; Malen JA Surface chemistry mediates thermal transport in three-dimensional nanocrystal arrays. Nat. Mater 2013, 12, 410–415. [PubMed: 23503009]

(75). Boles MA; Engel M; Talapin DV Self-assembly of colloidal nanocrystals: from intricate structures to functional materials. Chem. Rev 2016, 116, 11220–11289. [PubMed: 27552640]

(76). Gordon LM; Joester D Nanoscale chemical tomography of buried organic-inorganic interfaces in the chiton tooth. Nature 2011, 469, 194–197. [PubMed: 21228873]

(77). Panciera F; Chou YC; Reuter MC; Zakharov D; Stach EA; Hofmann S; Ross FM Synthesis of nanostructures in nanowires using sequential catalyst reactions. Nat. Mater 2015, 14, 820–825. [PubMed: 26168344]

(78). Kim BJ; Tersoff J; Kodambaka S; Reuter MC; Stach EA; Ross FM Kinetics of Individual Nucleation Events Observed in Nanoscale Vapor-Liquid-Solid Growth. Science 2008, 322, 1070–1073. [PubMed: 19008438]

(79). Luo ZQ; Jiang YW; Myers BD; Isheim D; Wu JS; Zimmerman JF; Wang ZG; Li QQ; Wang YC; Chen XQ; et al. Atomic gold-enabled three-dimensional lithography for silicon mesostructures. Science 2015, 348, 1451–1455. [PubMed: 26113718]

(80). Panciera F; Tersoff J; Gamalski AD; Reuter MC; Zakharov D; Stach EA; Hofmann S; Ross FM Surface crystallization of liquid Au-Si and its impact on catalysis. Adv. Mater 2019, 31, 1806544.

(81). Wen CY; Tersoff J; Reuter MC; Stach EA; Ross FM Step-flow kinetics in nanowire growth. Phys. Rev. Lett 2010, 105, 195502. [PubMed: 21231182]

(82). Mulay SR; Anders HJ Crystal nephropathies: mechanisms of crystal-induced kidney injury. Nat. Rev. Nephrol 2017, 13, 226–240. [PubMed: 28218266]

(83). Fang H; Yu KJ; Gloschat C; Yang Z; Song E; Chiang C-H; Zhao J; Won SM; Xu S; Trumpis M; Zhong Y; Han SW; Xue Y; Xu D; Choi SW; Cauwenberghs G; Kay M; Huang Y; Viventi J; Efimov IR; Rogers JA; et al. Capacitively coupled arrays of multiplexed flexible silicon transistors for long-term cardiac electrophysiology. Nat. Biomed. Eng 2017, 1, 1–12.

(84). Dai XC; Zhou W; Gao T; Liu J; Lieber CM Three-dimensional mapping and regulation of action potential propagation in nanoelectronics-innervated tissues. Nat. Nanotechnol 2016, 11, 776–782. [PubMed: 27347837]

(85). Jiang YW; Li XJ; Liu B; Yi J; Fang Y; Shi FY; Gao X; Sudzilovsky E; Parameswaran R; Koehler K; et al. Rational design of silicon structures for optically controlled multiscale biointerfaces. Nat. Biomed. Eng 2018, 2, 508–521. [PubMed: 30906646]

(86). Parameswaran R; Carvalho-de-Souza JL; Jiang YW; Burke MJ; Zimmerman JF; Koehler K; Phillips AW; Yi J; Adams EJ; Bezanilla F; et al. Photoelectrochemical modulation of neuronal activity with free-standing coaxial silicon nanowires. Nat. Nanotechnol 2018, 13, 260–266. [PubMed: 29459654]

(87). Lorach H; Goetz G; Smith R; Lei X; Mandel Y; Kamins T; Mathieson K; Huie P; Harris J; Sher A; et al. Photovoltaic restoration of sight with high visual acuity. Nat. Med 2015, 21, 476–U254. [PubMed: 25915832]

(88). Ghezzi D; Antognazza MR; Dal Maschio M; Lanzarini E; Benfenati F; Lanzani G A hybrid bioorganic interface for neuronal photoactivation. Nat. Commun 2011, 2, 1–7.

(89). Cotrufo MF; Soong JL; Horton AJ; Campbell EE; Haddix ML; Wall DH; Parton AJ Formation of soil organic matter via biochemical and physical pathways of litter mass loss. Nat. Geosci 2015, 8, 776–779.

(90). Kleber M; Sollins P; Sutton R A conceptual model of organo-mineral interactions in soils: self-assembly of organic molecular fragments into zonal structures on mineral surfaces. Biogeochemistry 2007, 85, 9–24.

(91). Bezanilla F How membrane proteins sense voltage. Nat. Rev. Mol. Cell Biol 2008, 9, 323–332. [PubMed: 18354422]

(92). Carvalho-de-Souza JL; Treger JS; Dang B; Kent SBH; Pepperberg DR; Bezanilla F Photosensitivity of neurons enabled by cell-targeted gold nanoparticles. Neuron 2015, 86, 207–217. [PubMed: 25772189]

(93). Jiang YW; Carvalho-de-Souza JL; Wong RCS; Luo ZQ; Isheim D; Zuo XB; Nicholls AW; Jung IW; Yue JP; Liu DJ; et al. Heterogeneous silicon rnesostructures for lipid-supported bioelectric interfaces. Nat. Mater 2016, 15, 1023–1030. [PubMed: 27348576]

(94). Schmidt MWI; Torn MS; Abiven S; Dittmar T; Guggenberger G; Janssens IA; Kleber M; Kogel-Knabner I; Lehmann J; Manning DAC; et al. Persistence of soil organic matter as an ecosystem property. Nature 2011, 478, 49–56. [PubMed: 21979045]

(95). Phillips R; Quake SR The biological frontier of physics. Phys. Today 2006, 59, 38–43.

(96). Acaron Ledesma H; Li X; Carvalho-de-Souza JL; Wei W; Bezanilla F; Tian B An atlas of nano-enabled neural interfaces. Nat. Nanotechnol 2019, 14, 645–657. [PubMed: 31270446]

(97). Li LQ; Eyckmans J; Chen CS Designer biomaterials for mechanobiology. Nat. Mater 2017, 16, 1164–1168. [PubMed: 29170549]

(98). Yoo HY; Iordachescu M; Huang J; Hennebert E; Kim S; Rho S; Foo M; Flammang P; Zeng H; Hwang D; Waite JH; Hwang DS; et al. Sugary interfaces mitigate contact damage where stiff meets soft. Nat. Commun 2016, 7, 1–8.

(99). Shi L; Dong HL; Reguera G; Beyenal H; Lu AH; Liu J; Yu HQ; Fredrickson JK Extracellular electron transfer mechanisms between microorganisms and minerals. Nat. Rev. Microbiol 2016, 14, 651–662. [PubMed: 27573579]

(100). Wang FB; Gu YQ; O'Brien JP; Yi SM; Yalcin SE; Srikanth V; Shen C; Vu D; Ing NL; Hochbaum AI; et al. Structure of microbial nanowires reveals stacked hemes that transport electrons over micrometers. Cell 2019, 177, 361–369. [PubMed: 30951668]

(101). Miserez A; Schneberk T; Sun CJ; Zok FW; Waite JH The transition from stiff to compliant materials in squid beaks. Science 2008, 319, 1816–1819. [PubMed: 18369144]

(102). Tan YP; Hoon S; Guerette PA; Wei W; Ghadban A; Hao C; Miserez A; Waite JH Infiltration of chitin by protein coacervates defines the squid beak mechanical gradient. Nat. Chem. Biol 2015, 11, 488–495. [PubMed: 26053298]

(103). Imperor-Clerc M; Davidson P; Davidson A Existence of a microporous corona around the mesopores of silica-based SBA-15 materials templated by triblock copolymers. J. Am. Chem. Soc 2000, 122, 11925–11933.

(104). Kang CG; Park YB; Choi H; Oh S; Lee KW; Choi SH; Shim JS Osseointegration of implants surface-treated with various diameters of TiO2 nanotubes in rabbit. J. Nanomater 2015, 2015, 1.

(105). Gebauer D; Kellermeier M; Gale JD; Bergstrom L; Colfen H Pre-nucleation clusters as solute precursors in crystallisation. Chem. Soc. Rev 2014, 43, 2348–2371. [PubMed: 24457316]

(106). De Yoreo JJ; Sommerdijk NAJM; Dove PM In New perspectives on mineral nucleation and growth, from solution precursors to solid materials; Kellermeier M, Benning LG, Gebauer D, Eds.; Springer International Publishing: Switzerland, 2017.

(107). Garcia-Manyes S; Beedle AEM Steering chemical reactions with force. Nat. Rev. Chem 2017, 1, 1–16.

(108). Avdoshenko SM; Makarov DE Reaction coordinates and pathways of mechanochemical transformations. J. Phys. Chem. B 2016, 120, 1537–1545. [PubMed: 26401617]

(109). Quapp W; Bofill JM; Ribas-Arino J Analysis of the acting forces in a theory of catalysis and mechanochemistry. J. Phys. Chem. A 2017, 121, 2820–2838. [PubMed: 28338327]

(110). Wang C; He QY; Halim U; Liu YY; Zhu EB; Lin ZY; Xiao H; Duan XD; Feng ZY; Cheng R; et al. Monolayer atomic crystal molecular superlattices. Nature 2018, 555, 231–236. [PubMed: 29517002]

(111). He QY; Lin ZY; Ding MN; Yin AX; Halim U; Wang C; Liu Y; Cheng HC; Huang Y; Duan XF In Situ probing molecular intercalation in two-dimensional layered semiconductors. Nano Lett. 2019, 19, 6819–6826. [PubMed: 31498650]

(112). Fu HR; Nan KW; Bai WB; Huang W; Bai K; Lu LY; Zhou CQ; Liu YP; Liu F; Wang JT; et al. Morphable 3D mesostructures and microelectronic devices by multistable buckling mechanics. Nat. Mater 2018, 17, 268–276. [PubMed: 29379201]

(113). Burnett TL; Withers PJ Completing the picture through correlative characterization. Nat. Mater 2019, 18, 1041–1049. [PubMed: 31209389]

(114). Kashin AS; Ananikov VP Monitoring chemical reactions in liquid media using electron microscopy. Nat. Rev. Chem 2019, 3, 624–637.

(115). Jiang Y; Parameswaran R; Li X; Carvalho-de-Souza JL; Gao X; Meng L; Bezanilla F; Shepherd GMG; Tian B Nongenetic optical neuromodulation with silicon-based materials. Nat. Protoc 2019, 14, 1339–1376. [PubMed: 30980031]

(116). Wang LHV; Yao JJ A practical guide to photoacoustic tomography in the life sciences. Nat. Methods 2016, 13, 627–638. [PubMed: 27467726]

(117). Salatino JW; Ludwig KA; Kozai TDY; Purcell EK Glial responses to implanted electrodes in the brain. Nat. Biomed. Eng 2017, 1, 862–877. [PubMed: 30505625]

(118). Moeendarbary E; Weber IP; Sheridan GK; Koser DE; Soleman S; Haenzi B; Bradbury EJ; Fawcett J; Franze K The soft mechanical signature of glial scars in the central nervous system. Nat. Commun 2017, 8, 1–11. [PubMed: 28232747]

(119). Gebauer D; Wolf SE Designing solid materials from their solute state: a shift in paradigms toward a holistic approach in functional materials chemistry. J. Am. Chem. Soc 2019, 141, 4490–4504. [PubMed: 30753066]

(120). Liu W; Yang CL; Zhu YT; Wang MS Interactions between single-walled carbon nanotubes and polyethylene/polypropylene/polystyrene/poly(phenylacetylene)/poly(p-phen ylenevinylene) considering repeat unit arrangements and conformations: a molecular dynamics simulation study. J. Phys. Chem. C 2008, 112, 1803–1811.

(121). Yu BW; Fu SR; Wu ZQ; Bai HW; Ning NY; Fu Q Molecular dynamics simulations of orientation induced interfacial enhancement between single walled carbon nanotube and aromatic polymers chains. Composites Part A 2015, 73, 155–165.

(122). Sindu BS; Sasmal S Evaluation of mechanical characteristics of nano modified epoxy based polymers using molecular dynamics. Comput. Mater. Sci 2015, 96, 146–158.

(123). Yi X; Gao HJ Kinetics of receptor-mediated endocytosis of elastic nanoparticles. Nanoscale 2017, 9, 454–463. [PubMed: 27934990]

(124). Yi X; Zou GJ; Gao HJ Mechanics of cellular packing of nanorods with finite and non-uniform diameters. Nanoscale 2018, 10, 14090–14099. [PubMed: 29999084]

(125). Yu MR; Wang JL; Yang YW; Zhu CL; Su Q; Guo SY; Sun JS; Gan Y; Shi XH; Gao HJ Rotation-facilitated rapid transport of nanorods in mucosal tissues. Nano Lett. 2016, 16, 7176–7182. [PubMed: 27700115]

(126). Zou GJ; Yi X; Zhu WP; Gao HJ Packing of flexible nanofibers in vesicles. Extreme Mech. Lett 2018, 19, 20–26.

(127). Vurpillot F; Danoix F; Gilbert M; Koelling S; Dagan M; Seidman DN True atomic-scale imaging in three dimensions: a review of the rebirth of field-ion microscopy. Microsc. Microanal 2017, 23, 210–220. [PubMed: 28337951]

(128). Dean-Ben XL; Gottschalk S; Mc Larney B; Shoham S; Razansky D Advanced optoacoustic methods for multiscale imaging of in vivo dynamics. Chem. Soc. Rev 2017, 46, 2158–2198. [PubMed: 28276544]

(129). Tserevelakis GJ; Tsafas V; Melessanaki K; Zacharakis G; Filippidis G Combined multiphoton fluorescence microscopy and photoacoustic imaging for stratigraphic analysis of paintings. Opt. Lett 2019, 44, 1154–1157. [PubMed: 30821736]

(130). Tserevelakis GJ; Vrouvaki I; Siozos P; Melessanaki K; Hatzigiannakis K; Fotakis C; Zacharakis G Photoacoustic imaging reveals hidden underdrawings in paintings. Sci. Rep 2017, 7, 7. [PubMed: 28127057]

(131). Guimaraes CF; Gasperini L; Marques AP; Reis RL The stiffness of living tissues and its implications for tissue engineering. Nat. Rev. Mater 2020, 5, 351–370.

(132). Sigrist RMS; Liau J; Kaffas AE; Chammas MC; Willmann JK Ultrasound elastography: review of techniques and clinical applications. Theranostics 2017, 7, 1303–1329. [PubMed: 28435467]

(133). Zankel A; Wagner J; Poelt P Serial sectioning methods for 3D investigations in materials science. Micron 2014, 62, 66–78. [PubMed: 24811993]

(134). Grandfield K; Engqvist H Focused ion beam in the study of biomaterials and biological matter. Adv. Mater. Sci. Eng 2012, 2012, 1.

(135). de Jonge N; Houben L; Dunin-Borkowski RE; Ross FM Resolution and aberration correction in liquid cell transmission electron microscopy. Nat. Rev. Mater 2019, 4, 61–78.

(136). Ross FM Opportunities and challenges in liquid cell electron microscopy. Science 2015, 350, 350. [PubMed: 26472912]

(137). Wen CY; Tersoff J; Hillerich K; Reuter MC; Park JH; Kodambaka S; Stach EA; Ross FM Periodically changing morphology of the growth interface in Si, Ge, and GaP nanowires. Phys. Rev. Lett 2011, 107, 025503. [PubMed: 21797618]

(138). Nudelman F; Pieterse K; George A; Bomans PHH; Friedrich H; Brylka LJ; Hilbers PAJ; de With G; Sommerdijk NAJM The role of collagen in bone apatite formation in the presence of hydroxyapatite nucleation inhibitors. Nat. Mater 2010, 9, 1004–1009. [PubMed: 20972429]

(139). Mao LB; Gao HL; Yao HB; Liu L; Colfen H; Liu G; Chen SM; Li SK; Yan YX; Liu YY; et al. Synthetic nacre by predesigned matrix-directed mineralization. Science 2016, 354, 107–110. [PubMed: 27540008]

(140). Zavabeti A; Ou JZ; Carey BJ; Syed N; Orrell-Trigg R; Mayes ELH; Xu CL; Kavehei O; O'Mullane AP; Kaner RB; et al. A liquid metal reaction environment for the room-temperature synthesis of atomically thin metal oxides. Science 2017, 358, 332–335. [PubMed: 29051372]

(141). Sakimoto KK; Wong AB; Yang PD Self-photo-sensitization of nonphotosynthetic bacteria for solar-to-chemical production. Science 2016, 351, 74–77. [PubMed: 26721997]

(142). Chen JJ; Zhu EB; Liu J; Zhang S; Lin ZY; Duan XF; Heinz H; Huang Y; De Yoreo JJ Building two-dimensional materials one row at a time: Avoiding the nucleation barrier. Science 2018 362, 1135–1139. [PubMed: 30523105]

(143). Pyles H; Zhang S; De Yoreo JJ; Baker D Controlling protein assembly on inorganic crystals through designed protein interfaces. Nature 2019, 571, 251–256. [PubMed: 31292559]

(144). De Yoreo JJ; Sommerdijk NAJM Investigating materials formation with liquid-phase and cryogenic TEM. Nat. Rev. Mater 2016, 1, 1–18.

(145). Chou YC; Hillerich K; Tersoff J; Reuter MC; Dick KA; Ross FM Atomic-Scale Variability and Control of III-V Nanowire Growth Kinetics. Science 2014, 343, 281–284. [PubMed: 24436416]

(146). Chou YC; Panciera F; Reuter MC; Stach EA; Ross FM Nanowire growth kinetics in aberration corrected environmental transmission electron microscopy. Chem. Commun 2016, 52, 5686–5689.

(147). Hannon JB; Kodambaka S; Ross FM; Tromp RM The influence of the surface migration of gold on the growth of silicon nanowires. Nature 2006, 440, 69–71. [PubMed: 16452928]

(148). Jacobsson D; Panciera F; Tersoff J; Reuter MC; Lehmann S; Hofmann S; Dick KA; Ross FM Interface dynamics and crystal phase switching in GaAs nanowires. Nature 2016, 531, 317–322. [PubMed: 26983538]

(149). Kodambaka S; Tersoff J; Reuter MC; Ross FM Germanium nanowire growth below the eutectic temperature. Science 2007, 316, 729–732. [PubMed: 17478716]

(150). Panciera F; Norton MM; Alam SB; Hofmann S; Molhave K; Ross FM Controlling nanowire growth through electric field-induced deformation of the catalyst droplet. Nat. Commun 2016, 7, 1–8.

(151). Deng J; Su YD; Liu D; Yang PD; Liu B; Liu C Nanowire photoelectrochemistry. Chem. Rev 2019, 119, 9221–9259. [PubMed: 31333018]

(152). Liu C; Dasgupta NP; Yang PD Semiconductor nanowires for artificial photosynthesis. Chem. Mater 2014, 26, 415–422.

(153). Liu C; Gallagher JJ; Sakimoto KK; Nichols EM; Chang CJ; Chang MCY; Yang PD Nanowire-bacteria hybrids for unassisted solar carbon dioxide fixation to value-added chemicals. Nano Lett. 2015, 15, 3634–3639. [PubMed: 25848808]

(154). Fan X; Nie WY; Tsai SH; Wang NX; Huang HH; Cheng YJ; Wen RJ; Ma LJ; Yan F; Xia YG PEDOT:PSS for flexible and stretchable electronics: modifications, strategies, and applications. Adv. Sci 2019, 6, 1900813.

(155). Han JQ; Wang HX; Yue YY; Mei CT; Chen JZ; Huang CB; Wu QL; Xu XW A self-healable and highly flexible supercapacitor integrated by dynamically cross-linked electro-conductive hydrogels based on nanocellulose-templated carbon nanotubes embedded in a viscoelastic polymer network. Carbon 2019 149, 1–18.

(156). Rotenberg MY; Tian BZ Long-lived recordings. Nat. Biomed. Eng 2017, 1, 1–2.

(157). Bergstrom L; Sturm EV; Salazar-Alvarez G; Colfen H Mesocrystals in biominerals and colloidal arrays. Acc. Chem. Res 2015, 48, 1391–1402. [PubMed: 25938915]

(158). Young JR; Didymus JM; Brown PR; Prins B; Mann S Crystal assembly and phylogenetic evolution in heterococcoliths. Nature 1992, 356, 516–518.

(159). Hosono N; Kitagawa S Modular design of porous soft materials via self-organization of metal-organic cages. Acc. Chem. Res 2018, 51, 2437–2446. [PubMed: 30252435]

(160). Sun Y; Chen CY; Stang PJ Soft materials with diverse suprastructures via the self-assembly of metal-organic complexes. Acc. Chem. Res 2019, 52, 802–817. [PubMed: 30794371]

(161). Gu YW; Alt EA; Wang H; Li XP; Willard AP; Johnson JA Photoswitching topology in polymer networks with metal-organic cages as crosslinks. Nature 2018, 560, 65–69. [PubMed: 30022167]

(162). Yang ZJ; Wei JJ; Sobolev YI; Grzybowski BA Systems of mechanized and reactive droplets powered by multi-responsive surfactants. Nature 2018, 553, 313–318. [PubMed: 29320473]

(163). Klajn R Spiropyran-based dynamic materials. Chem. Soc. Rev 2014, 43, 148–184. [PubMed: 23979515]

(164). Grzelczak M; Liz-Marzan LM; Klajn R Stimuli-responsive self-assembly of nanoparticles. Chem. Soc. Rev 2019, 48, 1342–1361. [PubMed: 30688963]

(165). Kundu PK; Samanta D; Leizrowice R; Margulis B; Zhao H; Borner M; Udayabhaskararao T; Manna D; Klajn R Light-controlled self-assembly of non-photoresponsive nanoparticles. Nat. Chem 2015, 7, 646–652. [PubMed: 26201741]

(166). Appel EA; Loh XJ; Jones ST; Biedermann F; Dreiss CA; Scherman OA Ultrahigh-Water-Content supramolecular hydrogels exhibiting multistimuli responsiveness. J. Am. Chem. Soc 2012, 134, 11767–11773. [PubMed: 22758793]

(167). Kumpfer JR; Rowan SJ Thermo-, photo-, and chemo-responsive shape-memory properties from photo-cross-linked metallosupramolecular polymers. J.Am. Chem. Soc 2011, 133, 12866–12874. [PubMed: 21790172]

(168). Zarzar LD; Aizenberg J Stimuli-responsive chemo-mechanical actuation: a hybrid materials approach. Acc. Chem. Res 2014, 47, 530–539. [PubMed: 24283993]

(169). Ma PT; Hu F; Wang JP; Niu JY Carboxylate covalently modified polyoxometalates: From synthesis, structural diversity to applications. Coord. Chem. Rev 2019, 378, 281–309.

(170). Abellan G; Marti-Gastaldo C; Ribera A; Coronado E Hybrid materials based on magnetic layered double hydroxides: a molecular perspective. Acc. Chem. Res 2015, 48, 1601–1611. [PubMed: 25989182]

(171). Chiu CW; Huang TK; Wang YC; Alamani BG; Lin JJ Intercalation strategies in clay/polymer hybrids. Prog. Polym. Sci 2014, 39, 443–485.

(172). Okada T; Ide Y; Ogawa M Organic-Inorganic hybrids based on ultrathin xxide layers: designed nanostructures for molecular recognition. Chem. - Asian J 2012, 7, 1980–1992. [PubMed: 22615212]

(173). Rogez G; Massobrio C; Rabu P; Drillon M Layered hydroxide hybrid nanostructures: a route to multifunctionality. Chem. Soc. Rev 2011, 40, 1031–1058. [PubMed: 21221445]

(174). Williams DS; Patil AJ; Mann S Spontaneous structuration in coacervate-based protocells by polyoxometalate-mediated membrane assembly. Small 2014, 10, 1830–1840. [PubMed: 24515342]

(175). Liu XG; Zhang F; Jing XX; Pan MC; Liu P; Li W; Zhu BW; Li J; Chen H; Wang LH; et al. Complex silica composite nanomaterials templated with DNA origami. Nature 2018, 559, 593–598. [PubMed: 30013119]

(176). Hensleigh R; Cui HC; Xu ZP; Massman J; Yao DS; Berrigan J; Zheng XY Charge-programmed three-dimensional printing for multi-material electronic devices. Nat. Electron 2020, 3, 216–224.

(177). Oran D; Rodriques SG; Gao RX; Asano S; Skylar-Scott MA; Chen F; Tillberg PW; Marblestone AH; Boyden ES 3D nanofabrication by volumetric deposition and controlled shrinkage of patterned scaffolds. Science 2018, 362, 1281–1285. [PubMed: 30545883]

(178). Brown AC; Stabenfeldt SE; Ahn B; Hannan RT; Dhada KS; Herman ES; Stefanelli V; Guzzetta N; Alexeev A; Lam WA; et al. Ultrasoft microgels displaying emergent platelet-like behaviours. Nat. Mater 2014, 13, 1108–1114. [PubMed: 25194701]

(179). Sanghvi AB; Miller KPH; Belcher AM; Schmidt CE Biomaterials functionalization using a novel peptide that selectively binds to a conducting polymer. Nat. Mater 2005, 4, 496–502. [PubMed: 15895095]

(180). Wang SQ; Humphreys ES; Chung SY; Delduco DF; Lustig SR; Wang H; Parker KN; Rizzo NW; Subramoney S; Chiang YM; et al. Peptides with selective affinity for carbon nanotubes. Nat. Mater 2003, 2, 196–200. [PubMed: 12612679]

(181). Whaley SR; English DS; Hu EL; Barbara PF; Belcher AM Selection of peptides with semiconductor binding specificity for directed nanocrystal assembly. Nature 2000, 405, 665–668. [PubMed: 10864319]

(182). Li M; Harbron RL; Weaver JVM; Binks BP; Mann S Electrostatically gated membrane permeability in inorganic protocells. Nat. Chem 2013, 5, 529–536. [PubMed: 23695636]

(183). Love JC; Estroff LA; Kriebel JK; Nuzzo RG; Whitesides GM Self-assembled monolayers of thiolates on metals as a form of nanotechnology. Chem. Rev 2005, 105, 1103–1169. [PubMed: 15826011]

(184). Yan L; Huck WTS; Whitesides GM Self-assembled monolayers (SAMS) and synthesis of planar micro- and nanostructures. J. Macromol. Sci., Polym. Rev 2004, C44, 175–206.

(185). Guo JL; Suastegui M; Sakimoto KK; Moody VM; Xiao G; Nocera DG; Joshi NS Light-driven fine chemical production in yeast biohybrids. Science 2018, 362, 813–816. [PubMed: 30442806]

(186). Jiang XC; Hu JS; Lieber AM; Jackan CS; Biffinger JC; Fitzgerald LA; Ringeisen BR; Lieber CM Nanoparticle facilitated extracellular electron transfer in microbial fuel cells. Nano Lett. 2014, 14, 6737–6742. [PubMed: 25310721]

(187). Kumar A; Hsu LHH; Kavanagh P; Barriere F; Lens PNL; Lapinsonniere L; Lienhard JH; Schroder U; Jiang XC; Leech D The ins and outs of microorganism-electrode electron transfer reactions. Nat. Rev. Chem 2017, 1, 1–13.

(188). Parameswaran R; Koehler K; Rotenberg MY; Burke MJ; Kim J; Jeong KY; Hissa B; Paul MD; Moreno K; Sarma N; et al. Optical stimulation of cardiac cells with a polymer-supported silicon nanowire matrix. Proc. Natl. Acad. Sci. U. S. A 2019, 116, 413–421. [PubMed: 30538202]

(189). Parameswaran R; Tian BZ Rational design of semiconductor nanostructures for functional subcellular interfaces. Acc. Chem. Res 2018, 51, 1014–1022. [PubMed: 29668260]

(190). Lou HY; Zhao WT; Zeng YP; Cui BX The role of membrane curvature in nanoscale topography-induced intracellular signaling. Acc. Chem. Res 2018, 51, 1046–1053. [PubMed: 29648779]

(191). Zhao H; Sen S; Udayabhaskararao T; Sawczyk M; Kucanda K; Manna D; Kundu PK; Lee JW; Kral P; Klajn R Reversible trapping and reaction acceleration within dynamically self-assembling nanoflasks. Nat. Nanotechnol 2016, 11, 82–88. [PubMed: 26595335]

(192). Cheng Z; Shurer CR; Schmidt S; Gupta VK; Chuang G; Su J; Watkins AR; Shetty A; Spector JA; Hui C-Y; Reesink HL; Paszek MJ; et al. The surface stress of biomedical silicones is a stimulant of cellular response. Sci. Adv 2020, 6, 6.

(193). Doloff JC; Veiseh O; de Mezerville R; Sforza M; Perry TA; Haupt J; Jamiel M; Chambers C; Nash A; Aghlara-Fotovat S; et al. The surface topography of silicone breast implants mediates the foreign body response in mice, rabbits and humans. Nat. Biomed. Eng 2021, 1–16. [PubMed: 33483712]

(194). Noskovicova N; Schuster R; van Putten S; Ezzo M; Koehler A; Boo S; Coelho NM; Griggs D; Ruminski P; McCulloch CA; et al. Suppression of the fibrotic encapsulation of silicone implants by inhibiting the mechanical activation of pro-fibrotic TGF-β. Nat. Biomed. Eng 2021, 1–20. [PubMed: 33483712]

(195). Jang K-I; Chung HU; Xu S; Lee CH; Luan H; Jeong J; Cheng H; Kim G-T; Han SY; Lee JW; et al. Soft network composite materials with deterministic and bio-inspired designs. Nat. Commun 2015, 6, 6566. [PubMed: 25782446]

(196). Matsuda T; Kawakami R; Namba R; Nakajima T; Gong JP Mechanoresponsive self-growing hydrogels inspired by muscle training. Science 2019, 363, 504–508. [PubMed: 30705187]

(197). Fang Y; Han ED; Zhang XX; Jiang YW; Lin YL; Shi JY; Wu JB; Meng LY; Gao X; Griffin PJ; et al. Dynamic and programmable cellular-scale granules enable tissue-like materials. Matter 2020, 2, 948–964.

(198). Hua M; Wu S; Ma Y; Zhao Y; Chen Z; Frenkel I; Strzalka J; Zhou H; Zhu X; He X Strong tough hydrogels via the synergy of freeze-casting and salting out. Nature 2021, 590, 594–599. [PubMed: 33627812]

(199). Sekitani T; Someya T Stretchable, large-area organic electronics. Adv. Mater 2010, 22, 2228–2246. [PubMed: 20229571]

(200). Khang D-Y; Jiang H; Huang Y; Rogers JA A Stretchable Form of Single-Crystal Silicon for High-Performance Electronics on Rubber Substrates. Science 2006, 311, 208–212. [PubMed: 16357225]

(201). Liu Y; Wang X; Xu Y; Xue Z; Zhang Y; Ning X; Cheng X; Xue Y; Lu D; Zhang Q; et al. Harnessing the interface mechanics of hard films and soft substrates for 3D assembly by controlled buckling. Proc. Natl. Acad. Sci. U. S. A 2019, 116, 15368–15377. [PubMed: 31315983]

(202). Kim D-H; Lu N; Ma R; Kim Y-S; Kim R-H; Wang S; Wu J; Won SM; Tao H; Islam A; et al. Epidermal Electronics. Science 2011, 333, 838–843. [PubMed: 21836009]

(203). Chung HU; Kim BH; Lee JY; Lee J; Xie Z; Ibler EM; Lee K; Banks A; Jeong JY; Kim J; et al. Binodal, wireless epidermal electronic systems with in-sensor analytics for neonatal intensive care. Science 2019, 363, No. eaau0780. [PubMed: 30819934]

(204). Yu X; Xie Z; Yu Y; Lee J; Vazquez-Guardado A; Luan H; Ruban J; Ning X; Akhtar A; Li D; et al. Skin-integrated wireless haptic interfaces for virtual and augmented reality. Nature 2019 575, 473–479. [PubMed: 31748722]

(205). Viventi J; Kim DH; Vigeland L; Frechette ES; Blanco JA; Kim YS; Avrin AE; Tiruvadi VR; Hwang SW; Vanleer AC; et al. Flexible, foldable, actively multiplexed, high-density electrode array for mapping brain activity in vivo. Nat. Neurosci 2011, 14, 1599–1605. [PubMed: 22081157]

(206). Yu KJ; Kuzum D; Hwang S-W; Kim BH; Juul H; Kim NH; Won SM; Chiang K; Trumpis M; Richardson AG; et al. Bioresorbable silicon electronics for transient spatiotemporal mapping of electrical activity from the cerebral cortex. Nat. Mater 2016, 15, 782–791. [PubMed: 27088236]

(207). Kang S-K; Murphy RKJ; Hwang S-W; Lee SM; Harburg DV; Krueger NA; Shin J; Gamble P; Cheng H; Yu S; et al. Bioresorbable silicon electronic sensors for the brain. Nature 2016, 530, 71–76. [PubMed: 26779949]

(208). Kim D-H; Lu N; Ghaffari R; Kim Y-S; Lee SP; Xu L; Wu J; Kim R-H; Song J; Liu Z; et al. Materials for multifunctional balloon catheters with capabilities in cardiac electrophysiological mapping and ablation therapy. Nat. Mater 2011, 10, 316–323. [PubMed: 21378969]

(209). Mickle AD; Won SM; Noh KN; Yoon J; Meacham KW; Xue Y; McIlvried LA; Copits BA; Samineni VK; Crawford KE; et al. A wireless closed-loop system for optogenetic peripheral neuromodulation. Nature 2019, 565, 361–365. [PubMed: 30602791]

(210). Zhang Y; Guo H; Kim SB; Wu Y; Ostojich D; Park SH; Wang X; Weng Z; Li R; Bandodkar AJ; et al. Passive sweat collection and colorimetric analysis of biomarkers relevant to kidney disorders using a soft microfluidic system. Lab Chip 2019, 19, 1545–1555. [PubMed: 30912557]

(211). Park Y; Franz CK; Ryu H; Luan H; Cotton KY; Kim JU; Chung TS; Zhao S; Vazquez-Guardado A; Yang DS; Li K; Avila R; Phillips JK; Quezada MJ; Jang H; Kwak SS; Won SM; Kwon K; Jeong H; Bandodkar AJ; Han M; Zhao H; Osher GR; Wang H; Lee K; Zhang Y; Huang Y; Finan

JD; Rogers JA; et al. Three-dimensional, multifunctional neural interfaces for cortical spheroids and engineered assembloids. Sci. Adv 2021, 7, 7.

(212). Tian BZ; Liu J; Dvir T; Jin LH; Tsui JH; Qing Q; Suo ZG; Langer R; Kohane DS; Lieber CM Macroporous nanowire nanoelectronic scaffolds for synthetic tissues. Nat. Mater 2012, 11, 986–994. [PubMed: 22922448]

(213). Han MD; Chen L; Aras K; Liang CM; Chen XX; Zhao HB; Li K; Faye NR; Sun BH; Kim JH; et al. Catheter-integrated soft multilayer electronic arrays for multiplexed sensing and actuation during cardiac surgery. Nat. Biomed. Eng 2020, 4, 997–1009. [PubMed: 32895515]

(214). Xu S; Yan Z; Jang K-I; Huang W; Fu H; Kim J; Wei Z; Flavin M; McCracken J; Wang R; et al. Assembly of micro/nanomaterials into complex, three-dimensional architectures by compressive buckling. Science 2015, 347, 154–159. [PubMed: 25574018]

(215). Huang Z; Hao Y; Li Y; Hu H; Wang C; Nomoto A; Pan T; Gu Y; Chen Y; Zhang T; et al. Three-dimensional integrated stretchable electronics. Nat. Electron 2018, 1, 473–480.

(216). Tian BZ; Cohen-Karni T; Qing Q; Duan XJ; Xie P; Lieber CM Three-Dimensional, Flexible Nanoscale Field-Effect Transistors as Localized Bioprobes. Science 2010, 329, 830–834. [PubMed: 20705858]

(217). Xu J; Wang S; Wang G-JN; Zhu C; Luo S; Jin L; Gu X; Chen S; Feig VR; To JWF; et al. Highly stretchable polymer semiconductor films through the nanoconfinement effect. Science 2017, 355, 59–64. [PubMed: 28059762]

(218). Wang WC; Wang SH; Rastak R; Ochiai Y; Niu SM; Jiang YW; Arunachala PK; Zheng Y; Xu J; Matsuhisa N; et al. Strain-insensitive intrinsically stretchable transistors and circuits. Nat. Electron 2021, 4, 143–150.

(219). Miyamoto A; Lee S; Cooray NF; Lee S; Mori M; Matsuhisa N; Jin H; Yoda L; Yokota T; Itoh A; et al. Inflammation-free, gas-permeable, lightweight, stretchable on-skin electronics with nanomeshes. Nat. Nanotechnol 2017, 12, 907–913. [PubMed: 28737748]

(220). Yang Y; Song Y; Bo X; Min J; Pak OS; Zhu L; Wang M; Tu J; Kogan A; Zhang H; et al. A laser-engraved wearable sensor for sensitive detection of uric acid and tyrosine in sweat. Nat. Biotechnol 2020, 38, 217–224. [PubMed: 31768044]

(221). Son D; Kang J; Vardoulis O; Kim Y; Matsuhisa N; Oh JY; To JWF; Mun JW; Katsumata T; Liu YX; et al. An integrated self-healable electronic skin system fabricated via dynamic reconstruction of a nanostructured conducting network. Nat. Nanotechnol 2018, 13, 1057–1065. [PubMed: 30127474]

(222). Lin S; Yuk H; Zhang T; Parada GA; Koo H; Yu C; Zhao X Stretchable hydrogel electronics and devices. Adv. Mater 2016, 28, 4497–4505. [PubMed: 26639322]

(223). Ershad F; Thukral A; Yue J; Comeaux P; Lu Y; Shim H; Sim K; Kim N-I; Rao Z; Guevara R; Contreras L; Pan F; Zhang Y; Guan Y-S; Yang P; Wang X; Wang P; Wu X; Yu C; et al. Ultra-conformal drawn-on-skin electronics for multifunctional motion artifact-free sensing and point-of-care treatment. Nat. Commun 2020, 11, 3823. [PubMed: 32732934]

(224). Yang X; Zhou T; Zwang TJ; Hong G; Zhao Y; Viveros RD; Fu T-M; Gao T; Lieber CM Bioinspired neuron-like electronics. Nat. Mater 2019, 18, 510–517. [PubMed: 30804509]

(225). Li Q; Nan KW; Le Floch P; Lin ZW; Sheng H; Blum TS; Liu J Cyborg organoids: implantation of nanoelectronics via organogenesis for tissue-wide electrophysiology. Nano Lett. 2019, 19, 5781–5789. [PubMed: 31347851]

(226). Zimmerman JF; Parameswaran R; Murray G; Wang YC; Burke M; Tian BZ Cellular uptake and dynamics of unlabeled freestanding silicon nanowires. Sci. Adv 2016, 2, 2.

(227). Rotenberg MY; Elbaz B; Nair V; Schaumann EN; Yamamoto N; Sarma N; Matino L; Santoro F; Tian BZ Silicon nanowires for intracellular optical interrogation with subcellular resolution. Nano Lett. 2020, 20, 1226–1232. [PubMed: 31904975]

(228). Rotenberg MY; Yamamoto N; Schaumann EN; Matino L; Santoro F; Tian BZ Living myofibroblast-silicon composites for probing electrical coupling in cardiac systems. Proc. Natl. Acad. Sci. U. S. A 2019, 116, 22531–22539. [PubMed: 31624124]

(229). Liu J; Kim YS; Richardson CE; Tom A; Ramakrishnan C; Birey F; Katsumata T; Chen SC; Wang C; Wang X; et al. Genetically targeted chemical assembly of functional materials in living cells, tissues, and animals. Science 2020, 367, 1372–1376. [PubMed: 32193327]

(230). Zhao Y; Xuan C; Qian X; Alsaid Y; Hua M; Jin L; He X Soft phototactic swimmer based on self-sustained hydrogel oscillator. Sci. Robot 2019, 4, 4.

(231). Kim Y; Parada GA; Liu S; Zhao X Ferromagnetic soft continuum robots. Sci. Robot 2019, 4, 4.

(232). Yasa IC; Ceylan H; Bozuyuk U; Wild AM; Sitti M Elucidating the interaction dynamics between microswimmer body and immune system for medical microrobots. Sci. Robot 2020, 5, 5.

(233). Xie C; Liu J; Fu T-M; Dai X; Zhou W; Lieber CM Three-dimensional macroporous nanoelectronic networks as minimally invasive brain probes. Nat. Mater 2015, 14, 1286–1292. [PubMed: 26436341]

(234). Qing Q; Jiang Z; Xu L; Gao RX; Mai LQ; Lieber CM Free-standing kinked nanowire transistor probes for targeted intracellular recording in three dimensions. Nat. Nanotechnol 2014, 9, 142–147. [PubMed: 24336402]

(235). Zhao YL; You SS; Zhang AQ; Lee JH; Huang JL; Lieber CM Scalable ultrasmall three-dimensional nanowire transistor probes for intracellular recording. Nat. Nanotechnol 2019, 14, 783–790. [PubMed: 31263191]

(236). Duan XJ; Gao RX; Xie P; Cohen-Karni T; Qing Q; Choe HS; Tian BZ; Jiang XC; Lieber CM Intracellular recordings of action potentials by an extracellular nanoscale field-effect transistor. Nat. Nanotechnol 2012, 7, 174–179.

(237). Gao RX; Strehle S; Tian BZ; Cohen-Karni T; Xie P; Duan XJ; Qing Q; Lieber CM Outside looking in: nanotube transistor intracellular sensors. Nano Lett. 2012, 12, 3329–3333. [PubMed: 22583370]

(238). Jiang Z; Qing Q; Xie P; Gao RX; Lieber CM Kinked p–n junction nanowire probes for high spatial resolution sensing and intracellular recording. Nano Lett. 2012, 12, 1711–1716. [PubMed: 22309132]

(239). Tian BZ; Lieber CM Design, synthesis, and characterization of novel nanowire structures for photovoltaics and intracellular probes. Pure Appl Chem. 2011, 83, 2153–2169. [PubMed: 22707797]

(240). Tian BZ; Lieber CM In Annu. Rev. Anal. Chem; Cooks RG; Pemberton JE, Eds.; Annual Reviews, 2013; Vol. 6.

(241). Shin M; Oh JY; Byun KE; Lee YJ; Kim B; Baik HK; Park JJ; Jeong U Polythiophene nanofibril bundles surface-embedded in elastomer: a route to a highly stretchable active channel layer. Adv. Mater 2015, 27, 1255–1261. [PubMed: 25581228]

(242). Song E; Kang B; Choi HH; Sin DH; Lee H; Lee WH; Cho K Stretchable and transparent organic semiconducting thin film with conjugated polymer nanowires embedded in an elastomeric matrix. Adv. Electron. Mater 2016, 2, 1500250.

(243). Wang S; Xu J; Wang W; Wang G-JN; Rastak R; Molina-Lopez F; Chung JW; Niu S; Feig VR; Lopez J; et al. Skin electronics from scalable fabrication of an intrinsically stretchable transistor array. Nature 2018, 555, 83–88. [PubMed: 29466334]

(244). Liu Y; Li J; Song S; Kang J; Tsao Y; Chen S; Mottini V; McConnell K; Xu W; Zheng Y-Q; Tok JB-H; George PM; Bao Z; et al. Morphing electronics enable neuromodulation in growing tissue. Nat. Biotechnol 2020, 38, 1031–1036. [PubMed: 32313193]

(245). Cho C; Kang P; Taqieddin A; Jing YH; Yong K; Kim JM; Haque MF; Aluru NR; Nam S Strain-resilient electrical functionality in thin-film metal electrodes using two-dimensional interlayers. Nat. Electron 2021, 4, 126–133. [PubMed: 35136855]

(246). Caubet JC; Kaiser L; Lemaitre B; Fellay B; Gervaix A; Eigenmann PA The role of penicillin in benign skin rashes in childhood: a prospective study based on drug rechallenge. J. Allergy Clin. Immunol 2011, 127, 218–222. [PubMed: 21035175]

(247). Hong G; Lieber CM Novel electrode technologies for neural recordings. Nat. Rev. Neurosci 2019, 20, 330–345. [PubMed: 30833706]

(248). Cogan SF Neural stimulation and recording electrodes. Annu. Rev. Biomed. Eng 2008, 10, 275–309. [PubMed: 18429704]

(249). Bossi F; Willemse C; Cavazza J; Marchesi S; Murino V; Wykowska A The human brain reveals resting state activity patterns that are predictive of biases in attitudes toward robots. Sci. Robot 2020, 5, 5.

(250). Zhang L; Kumar KS; He H; Cai CJ; He X; Gao H; Yue S; Li C; Seet RC-S; Ren H; Ouyang J; et al. Fully organic compliant dry electrodes self-adhesive to skin for long-term motion-robust epidermal biopotential monitoring. Nat. Commun 2020, 11, 4683. [PubMed: 32943621]

(251). Furui A; Eto S; Nakagaki K; Shimada K; Nakamura G; Masuda A; Chin T; Tsuji T A myoelectric prosthetic hand with muscle synergy-based motion determination and impedance model-based biomimetic control. Sci. Robot 2019, 4, 4.

(252). Sluka KA; Walsh D Transcutaneous electrical nerve stimulation: basic science mechanisms and clinical effectiveness. J. Pain 2003, 4, 109–121. [PubMed: 14622708]

(253). Lin S; Yuk H; Zhang T; Parada GA; Koo H; Yu C; Zhao X Stretchable Hydrogel Electronics and Devices. Adv. Mater 2016, 28, 4497–4505. [PubMed: 26639322]

(254). Kim DH; Ghaffari R; Lu N; Rogers JA Flexible and stretchable electronics for biointegrated devices. Annu. Rev. Biomed. Eng 2012, 14, 113–128. [PubMed: 22524391]

(255). Yang JC; Mun J; Kwon SY; Park S; Bao Z; Park S Electronic skin: recent progress and future prospects for skin-attachable devices for health monitoring, robotics, and prosthetics. Adv. Mater 2019, 31, 1904765.

(256). Wang C; Li X; Hu H; Zhang L; Huang Z; Lin M; Zhang Z; Yin Z; Huang B; Gong H; et al. Monitoring of the central blood pressure waveform via a conformal ultrasonic device. Nat. Biomed. Eng 2018, 2, 687–695. [PubMed: 30906648]

(257). Sempionatto JR; Lin M; Yin L; De la paz E; Pei K; Sonsa-ard T; de Loyola Silva AN; Khorshed AA; Zhang F; Tostado N; Xu S; Wang J An epidermal patch for the simultaneous monitoring of haemodynamic and metabolic biomarkers. Nat. Biomed Eng 2021, 5, 737. [PubMed: 33589782]

(258). MacNeil S Biomaterials for tissue engineering of skin. Mater. Today 2008, 11, 26–35.

(259). Barrett S Wound-bed preparation: a vital step in the healing process. Br J. Nurs 2017, 26, S24–S31.

(260). Brown A Phases of the wound healing process. Nurs Times 2015, 111, 12–13.

(261). Kang J; Son D; Wang G-JN; Liu Y; Lopez J; Kim Y; Oh JY; Katsumata T; Mun J; Lee Y; et al. Tough and water-Insensitive self-healing elastomer for robust electronic skin. Adv. Mater 2018, 30, 1706846.

(262). Dominiak PM; Grech E; Barr G; Teat S; Mallinson P; Woźniak K Neutral and ionic hydrogen bonding in Schiff bases. Chem. - Eur. J 2003, 9, 963–970. [PubMed: 12584712]

(263). Darabi MA; Khosrozadeh A; Mbeleck R; Liu Y; Chang Q; Jiang J; Cai J; Wang Q; Luo G; Xing M Skin-inspired multifunctional autonomic-intrinsic conductive self-healing hydrogels with pressure sensitivity, stretchability, and 3D printability. Adv. Mater 2017, 29, 1700533.

(264). Riley L; Schirmer L; Segura T Granular hydrogels: emergent properties of jammed hydrogel microparticles and their applications in tissue repair and regeneration. Curr. Opin. Biotechnol 2019, 60, 1–8. [PubMed: 30481603]

(265). Li S; Pei M; Wan T; Yang H; Gu S; Tao Y; Liu X; Zhou Y; Xu W; Xiao P Self-healing hyaluronic acid hydrogels based on dynamic Schiff base linkages as biomaterials. Carbohydr. Polym 2020, 250, 116922. [PubMed: 33049836]

(266). Singer AJ; Clark RA Cutaneous wound healing. N. Engl. J. Med 1999, 341, 738–746. [PubMed: 10471461]

(267). Jarrahi M An experimental study of the effects of Matricaria chamomilla extract on cutaneous burn wound healing in albino rats. Nat. Prod. Res 2008, 22, 422–427. [PubMed: 18404562]

(268). Chen JS; Wong VW; Gurtner GC Therapeutic potential of bone marrow-derived mesenchymal stem cells for cutaneous wound healing. Front. Immunol 2012, 3, 192. [PubMed: 22787462]

(269). Bjarnsholt T; Kirketerp-Møller K; Jensen PØ; Madsen KG; Phipps R; Krogfelt K; Høiby N; Givskov M Why chronic wounds will not heal: a novel hypothesis. Wound repair and regeneration 2008, 16, 2–10. [PubMed: 18211573]

(270). Boateng JS; Matthews KH; Stevens HN; Eccleston GM Wound healing dressings and drug delivery systems: a review. J. Pharm. Sci 2008, 97, 2892–2923. [PubMed: 17963217]

(271). Mostafalu P; Tamayol A; Rahimi R; Ochoa M; Khalilpour A; Kiaee G; Yazdi IK; Bagherifard S; Dokmeci MR; Ziaie B; Sonkusale SR; Khademhosseini A Smart bandage for monitoring and treatment of chronic wounds. Small 2018, 14, No. e1703509.

(272). Kamoun EA; Kenawy ES; Chen X A review on polymeric hydrogel membranes for wound dressing applications: PVA-based hydrogel dressings. J. Adv. Res 2017, 8, 217–233. [PubMed: 28239493]

(273). Mi L; Xue H; Li Y; Jiang S A thermoresponsive antimicrobial wound dressing hydrogel based on a cationic betaine ester. Adv. Funct. Mater 2011, 21, 4028–4034.

(274). Zhang Y; Wang J; Yu J; Wen D; Kahkoska AR; Lu Y; Zhang X; Buse JB; Gu Z Bioresponsive microneedles with a sheath structure for H2 O2 and pH cascade-triggered insulin delivery. Small 2018, 14, No. e1704181. [PubMed: 29479811]

(275). Aili D; Stevens MM Bioresponsive peptide-inorganic hybrid nanomaterials. Chem. Soc. Rev 2010, 39, 3358–3370. [PubMed: 20596582]

(276). Wilson AN; Guiseppi-Elie A Bioresponsive hydrogels. Adv. Healthcare Mater 2013, 2, 520–532.

(277). Lu Y; Aimetti AA; Langer R; Gu Z Bioresponsive materials. Nat. Rev. Mater 2017, 2, 1–17.

(278). Blacklow SO; Li J; Freedman BR; Zeidi M; Chen C; Mooney DJ Bioinspired mechanically active adhesive dressings to accelerate wound closure. Sci. Adv 2019, 5, No. eaaw3963. [PubMed: 31355332]

(279). Kai H; Yamauchi T; Ogawa Y; Tsubota A; Magome T; Miyake T; Yamasaki K; Nishizawa M Accelerated wound healing on skin by electrical stimulation with a bioelectric plaster. Adv. Healthcare Mater 2017, 6, 6.

(280). Yuk H; Varela CE; Nabzdyk CS; Mao X; Padera RF; Roche ET; Zhao X Dry double-sided tape for adhesion of wet tissues and devices. Nature 2019, 575, 169–174. [PubMed: 31666696]

(281). Wang Z; Wang J; Li H; Yu J; Chen G; Kahkoska AR; Wu V; Zeng Y; Wen D; Miedema JR; et al. Dual self-regulated delivery of insulin and glucagon by a hybrid patch. Proc. Natl. Acad. Sci. U. S. A 2020, 117, 29512–29517. [PubMed: 33177238]

(282). Jiang H; Ochoa M; Waimin JF; Rahimi R; Ziaie B A pH-regulated drug delivery dermal patch for targeting infected regions in chronic wounds. Lab Chip 2019, 19, 2265–2274. [PubMed: 31179468]

(283). Santos LF; Correia IJ; Silva AS; Mano JF Biomaterials for drug delivery patches. Eur. J. Pharm. Sci 2018, 118, 49–66. [PubMed: 29572160]

(284). Than A; Liang K; Xu S; Sun L; Duan H; Xi F; Xu C; Chen P Transdermal delivery of anti-obesity compounds to subcutaneous adipose tissue with polymeric microneedle patches. Small Methods 2017, 1, 1700269.

(285). Than A; Zan P; Chen P Transdermal theranostics. View 2020, 1, No. e21.

(286). Song EM; Li JH; Won SM; Bai WB; Rogers JA Materials for flexible bioelectronic systems as chronic neural interfaces. Nat. Mater 2020, 19, 590–603. [PubMed: 32461684]

(287). Vazquez-Guardado A; Yang YY; Bandodkar AJ; Rogers JA Recent advances in neurotechnologies with broad potential for neuroscience research. Nat. Neurosci 2020, 23, 1522–1536. [PubMed: 33199897]

(288). Jiang Y; Li X; Liu B; Yi J; Fang Y; Shi F; Gao X; Sudzilovsky E; Parameswaran R; Koehler K; et al. Rational design of silicon structures for optically controlled multiscale biointerfaces. Nat. Biomed. Eng 2018, 2, 508–521. [PubMed: 30906646]

(289). Won SM; Song EM; Reeder JT; Rogers JA Emerging modalities and implantable technologies for neuromodulation. Cell 2020, 181, 115–135. [PubMed: 32220309]

(290). Chen R; Canales A; Anikeeva P Neural recording and modulation technologies. Nat. Rev. Mater 2017, 2, 16093. [PubMed: 31448131]

(291). Feiner R; Dvir T Tissue–electronics interfaces: from implantable devices to engineered tissues. Nat. Rev. Mater 2018, 3, 17076.

(292). Rivnay J; Wang H; Fenno L; Deisseroth K; Malliaras GG Next-generation probes, particles, and proteins for neural interfacing. Sci. Adv 2017, 3, No. e1601649. [PubMed: 28630894]

(293). Polikov VS; Tresco PA; Reichert WM Response of brain tissue to chronically implanted neural electrodes. J. Neurosci. Methods 2005, 148, 1–18. [PubMed: 16198003]

(294). Biran R; Martin DC; Tresco PA Neuronal cell loss accompanies the brain tissue response to chronically implanted silicon microelectrode arrays. Exp. Neurol 2005, 195, 115–126. [PubMed: 16045910]

(295). Chestek CA; Gilja V; Nuyujukian P; Foster JD; Fan JM; Kaufman MT; Churchland MM; Rivera-Alvidrez Z; Cunningham JP; Ryu SI; Shenoy KV; et al. Long-term stability of neural prosthetic control signals from silicon cortical arrays in rhesus macaque motor cortex. J. Neural Eng 2011, 8, 045005. [PubMed: 21775782]

(296). Liu J; Fu TM; Cheng ZG; Hong GS; Zhou T; Jin LH; Duvvuri M; Jiang Z; Kruskal P; Xie C; et al. Syringe-injectable electronics. Nat. Nanotechnol 2015, 10, 629–636. [PubMed: 26053995]

(297). Hong G; Fu T-M; Qiao M; Viveros RD; Yang X; Zhou T; Lee JM; Park H-G; Sanes JR; Lieber CM A method for single-neuron chronic recording from the retina in awake mice. Science 2018, 360, 1447–1451. [PubMed: 29954976]

(298). Fu T-M; Hong G; Zhou T; Schuhmann TG; Viveros RD; Lieber CM Stable long-term chronic brain mapping at the single-neuron level. Nat. Methods 2016, 13, 875–882. [PubMed: 27571550]

(299). Zhou T; Hong G; Fu T-M; Yang X; Schuhmann TG; Viveros RD; Lieber CM Syringe-injectable mesh electronics integrate seamlessly with minimal chronic immune response in the brain. Proc. Natl. Acad. Sci U. S. A 2017, 114, 5894–5899. [PubMed: 28533392]

(300). Feiner R; Engel L; Fleischer S; Malki M; Gal I; Shapira A; Shacham-Diamand Y; Dvir T Engineered hybrid cardiac patches with multifunctional electronics for online monitoring and regulation of tissue function. Nat. Mater 2016, 15, 679–685. [PubMed: 26974408]

(301). Sim K; Ershad F; Zhang YC; Yang PY; Shim H; Rao ZY; Lu YT; Thukral A; Elgalad A; Xi YT; et al. An epicardial bioelectronic patch made from soft rubbery materials and capable of spatiotemporal mapping of electrophysiological activity. Nat. Electron 2020, 3, 775–784.

(302). Cianchetti M; Laschi C; Menciassi A; Dario P Biomedical applications of soft robotics. Nat. Rev. Mater 2018, 3, 143–153.

(303). Sachyani Keneth E; Kamyshny A; Totaro M; Beccai L; Magdassi S 3D printing materials for soft robotics. Adv. Mater 2021, 33, 2003387.

(304). Coyle S; Majidi C; LeDuc P; Hsia KJ Bio-inspired soft robotics: Material selection, actuation, and design. Extreme Mech. Lett 2018, 22, 51–59.

(305). El-Atab N; Mishra RB; Al-Modaf F; Joharji L; Alsharif AA; Alamoudi H; Diaz M; Qaiser N; Hussain MM Soft ctuators for soft robotic applications: a review. Advanced Intelligent Systems 2020, 2, 2000128.

(306). Kim P; Zarzar LD; He X; Grinthal A; Aizenberg J Hydrogel-actuated integrated responsive systems (HAIRS): Moving towards adaptive materials. Curr. Opin. Solid State Mater. Sci 2011, 15, 236–245.

(307). Lum GZ; Ye Z; Dong X; Marvi H; Erin O; Hu W; Sitti M Shape-programmable magnetic soft matter. Proc. Natl. Acad. Sci. U. S. A 2016, 113, E6007–E6015. [PubMed: 27671658]

(308). Kim Y; Yuk H; Zhao R; Chester SA; Zhao X Printing ferromagnetic domains for untethered fast-transforming soft materials. Nature 2018, 558, 274–279. [PubMed: 29899476]

(309). Bai H; Li S; Barreiros J; Tu Y; Pollock CR; Shepherd RF Stretchable distributed fiber-optic sensors. Science 2020, 370, 848–852. [PubMed: 33184214]

(310). You I; Mackanic DG; Matsuhisa N; Kang J; Kwon J; Beker L; Mun J; Suh W; Kim TY; Tok JB; et al. Artificial multimodal receptors based on ion relaxation dynamics. Science 2020, 370, 961–965. [PubMed: 33214277]

(311). Boutry CM; Negre M; Jorda M; Vardoulis O; Chortos A; Khatib O; Bao Z A hierarchically patterned, bioinspired e-skin able to detect the direction of applied pressure for robotics. Sci. Robot 2018, 3, 3.

(312). Pikul JH; Li S; Bai H; Hanlon RT; Cohen I; Shepherd RF Stretchable surfaces with programmable 3D texture morphing for synthetic camouflaging skins. Science 2017, 358, 210–214. [PubMed: 29026040]

(313). Mishra AK; Wallin TJ; Pan W; Xu P; Wang K; Giannelis EP; Mazzolai B; Shepherd RF Autonomic perspiration in 3D-printed hydrogel actuators. Sci. Robot 2020, 5, 5.

(314). Pena-Francesch A; Jung H; Demirel MC; Sitti M Biosynthetic self-healing materials for soft machines. Nat. Mater 2020, 19, 1230–1235. [PubMed: 32719508]

(315). Grüneboom A; Hawwari I; Weidner D; Culemann S; Müller S; Henneberg S; Brenzel A; Merz S; Bornemann L; Zec K; et al. A network of trans-cortical capillaries as mainstay for blood circulation in long bones. Nat. Metab 2019, 1, 236–250. [PubMed: 31620676]

(316). Jones CD; Steed JW Gels with sense: supramolecular materials that respond to heat, light and sound. Chem. Soc. Rev 2016, 45, 6546–6596. [PubMed: 27711667]

(317). Li C; Lau GC; Yuan H; Aggarwal A; Dominguez VL; Liu S; Sai H; Palmer LC; Sather NA; Pearson TJ; Freedman DE; Amiri PK; de la Cruz MO; Stupp SI; et al. Fast and programmable locomotion of hydrogel-metal hybrids under light and magnetic fields. Sci. Robot 2020, 5, 5.

(318). Robertson JC; Coote ML; Bissember AC Synthetic applications of light, electricity, mechanical force and flow. Nat. Rev. Chem 2019, 3, 290–304.

(319). Davis DA; Hamilton A; Yang JL; Cremar LD; Van Gough D; Potisek SL; Ong MT; Braun PV; Martinez TJ; White SR; et al. Force-induced activation of covalent bonds in mechanoresponsive polymeric materials. Nature 2009, 459, 68–72. [PubMed: 19424152]

(320). Yokoi H; Sato Y; Suzuki M; Yabuki Y; Nakamura T; Mori T; Morishita S; Kato R; Yamamura O; Kubota M Clinical Systems Neuroscience; Springer, 2015.

(321). Lebedev MA; Nicolelis MA Brain–machine interfaces: past, present and future. Trends Neurosci. 2006, 29, 536–546. [PubMed: 16859758]

(322). Santhanam G; Ryu SI; Yu BM; Afshar A; Shenoy KV A high-performance brain–computer interface. Nature 2006, 442, 195–198. [PubMed: 16838020]

(323). Kim Y; Chortos A; Xu W; Liu Y; Oh JY; Son D; Kang J; Foudeh AM; Zhu C; Lee Y; et al. A bioinspired flexible organic artificial afferent nerve. Science 2018, 360, 998–1003. [PubMed: 29853682]

(324). Kwak JW; Han M; Xie Z; Chung HU; Lee JY; Avila R; Yohay J; Chen X; Liang C; Patel M; Jung I; Kim J; Namkoong M; Kwon K; Guo X; Ogle C; Grande D; Ryu D; Kim DH; Madhvapathy S; Liu C; Yang DS; Park Y; Caldwell R; Banks A; Xu S; Huang Y; Fatone S; Rogers JA Wireless sensors for continuous, multimodal measurements at the skin interface with lower limb prostheses. Sci. Transl. Med 2020, 12, 12.

(325). Griffith RW; Humphrey DR Long-term gliosis around chronically implanted platinum electrodes in the Rhesus macaque motor cortex. Neurosci. Lett 2006, 406, 81–86. [PubMed: 16905255]

(326). Morishita S; Sato K; Watanabe H; Nishimura Y; Isa T; Kato R; Nakamura T; Yokoi H Brain-machine interface to control a prosthetic arm with monkey ECoGs during periodic movements. Front. Neurosci 2014, 8, 417. [PubMed: 25565947]

(327). Von Neumann J; Kurzweil R Computer and the brain; Yale University Press, 2012.

(328). Tuchman Y; Mangoma TN; Gkoupidenis P; Van De Burgt Y; John RA; Mathews N; Shaheen SE; Daly R; Malliaras GG; Salleo A Organic neuromorphic devices: past, present, and future challenges. MRS Bull. 2020, 45, 619–630.

(329). Nawrocki RA; Voyles RM; Shaheen SE Neurons in polymer: Hardware neural units based on polymer memristive devices and polymer transistors. IEEE Trans. Electron Devices 2014, 61, 3513–3519.

(330). Battistoni S; Erokhin V; Iannotta S Organic memristive devices for perceptron applications. J. Phys. D: Appl Phys 2018, 51, 284002.

(331). Desbief S; di Lauro M; Casalini S; Guerin D; Tortorella S; Barbalinardo M; Kyndiah A; Murgia M; Cramer T; Biscarini F; Vuillaume D Electrolyte-gated organic synapse transistor interfaced with neurons. Org. Electron 2016, 38, 21–28.

(332). Juzekaeva E; Nasretdinov A; Battistoni S; Berzina T; Iannotta S; Khazipov R; Erokhin V; Mukhtarov M Coupling cortical neurons through electronic memristive synapse. Adv. Mater. Technol 2019, 4, 1800350.

(333). van de Burgt Y; Lubberman E; Fuller EJ; Keene ST; Faria GC; Agarwal S; Marinella MJ; Alec Talin A; Salleo A A non-volatile organic electrochemical device as a low-voltage artificial synapse for neuromorphic computing. Nat. Mater 2017, 16, 414–418. [PubMed: 28218920]

(334). Keene ST; Lubrano C; Kazemzadeh S; Melianas A; Tuchman Y; Polino G; Scognamiglio P; Cina L; Salleo A; van de Burgt Y; et al. A biohybrid synapse with neurotransmitter-mediated plasticity. Nat. Mater 2020, 19, 969–973. [PubMed: 32541935]

(335). Liu Q; Liu Y; Li J; Lau C; Wu F; Zhang A; Li Z; Chen M; Fu H; Draper J; Cao X; Zhou C Fully printed all-solid-state organic flexible artificial synapse for neuromorphic computing. ACS Appl. Mater. Interfaces 2019, 11, 16749–16757. [PubMed: 31025562]

(336). Yan Y; Wu X; Chen Q; Wang X; Li E; Liu Y; Chen H; Guo T An intrinsically healing artificial neuromorphic device. J. Mater. Chem. C 2020, 8, 6869–6876.

(337). Adewole DO; Struzyna LA; Burrell JC; Harris JP; Nemes AD; Petrov D; Kraft RH; Chen HI; Serruya MD; Wolf JA; Cullen DK; et al. Development of optically controlled “living electrodes” with long-projecting axon tracts for a synaptic brain-machine interface. Sci. Adv 2021, 7, 7.

(338). Simmons CA; Ireland RG Stretch-boosted cell-mediated vascularization. Nat. Biomed Eng 2021, 5, 6–7. [PubMed: 33483711]

(339). Yalcin SE; O’Brien JP; Gu YQ; Reiss K; Yi SM; Jain R; Srikanth V; Dahl PJ; Huynh W; Vu D; et al. Electric field stimulates production of highly conductive microbial OmcZ. nanowires. Nat. Chem. Biol 2020, 16, 1136–1142. [PubMed: 32807967]

(340). Lee J; Henderson K; Massidda MW; Armenta-Ochoa M; Im BG; Veith A; Lee BK; Kim M; Maceda P; Yoon E; et al. Mechanobiological conditioning of mesenchymal stem cells for enhanced vascular regeneration. Nat. Biomed. Eng 2021, 5, 89–102. [PubMed: 33483713]

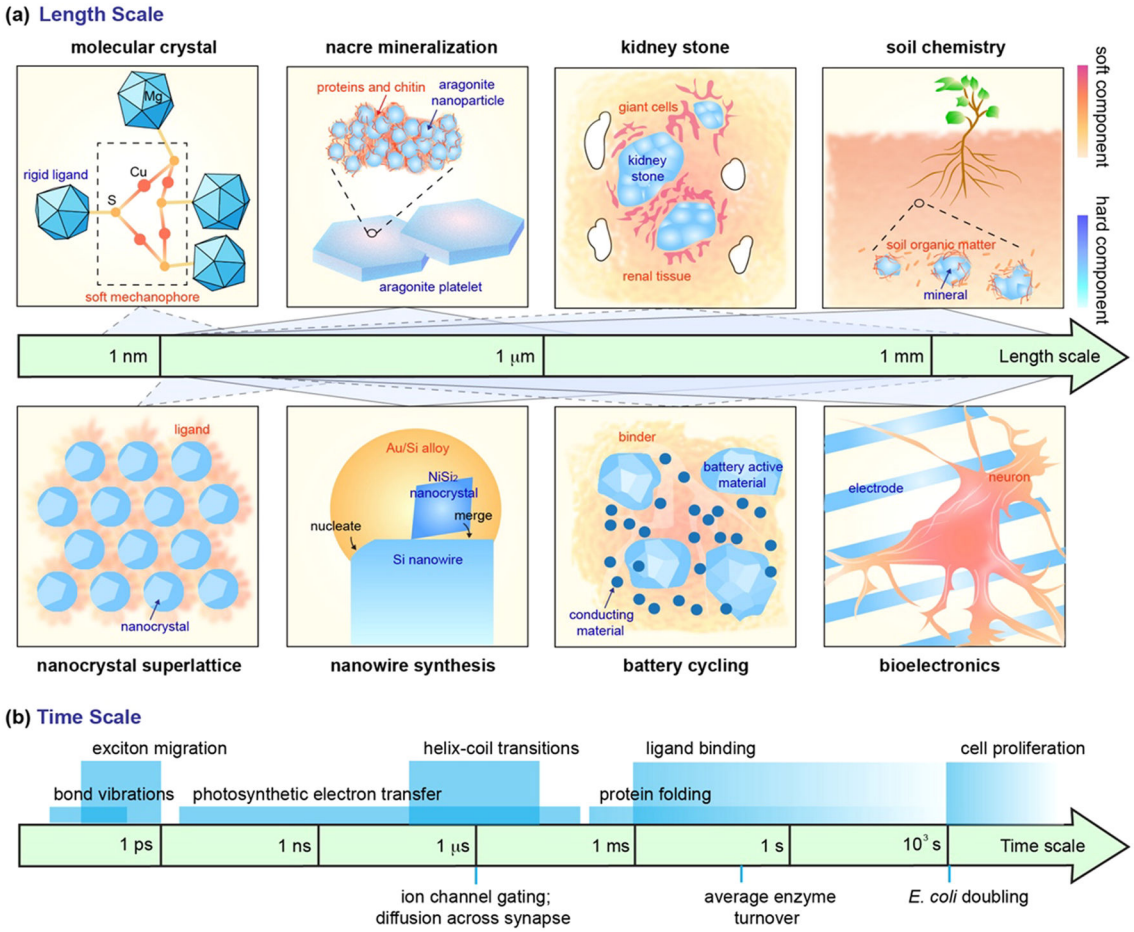

Figure 1.

Soft–hard interfaces cover a wide range of length and time scales. (a) The interfaces are diverse and cover those in molecular crystals, nanocrystal superlattices, nanowire nucleation and growth, biomineralization in both healthy and pathological conditions, active battery interfaces, soil chemistry and geobiology, and bioelectronics and implants. The soft and hard components are represented by colors within the range of the respective color bars (upper right). While the overall length scale ranges from subnanometer to above centimeter, the critical interfacial processes all occur at the molecular and nanometer scales where the interfacial mismatches are minimal. (b) Time scale is broad, and includes mechanical, electrical, and chemical events (shown here), such as bond vibration and enzyme turnover.

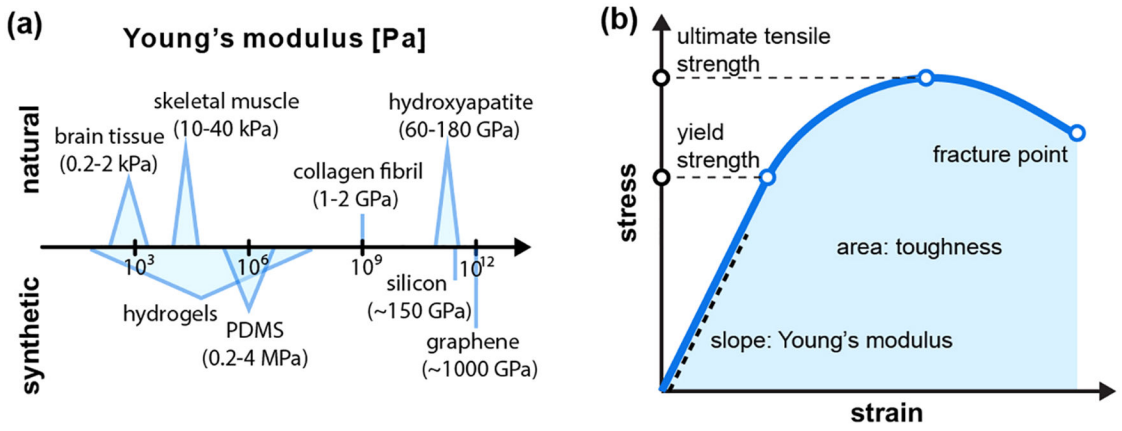

Figure 2.

Several figures-of-merit for material mechanics are relevant to this review. (a) Young's moduli of naturally occurring and synthetic materials. (b) Stress–strain curves and a few relevant definitions.

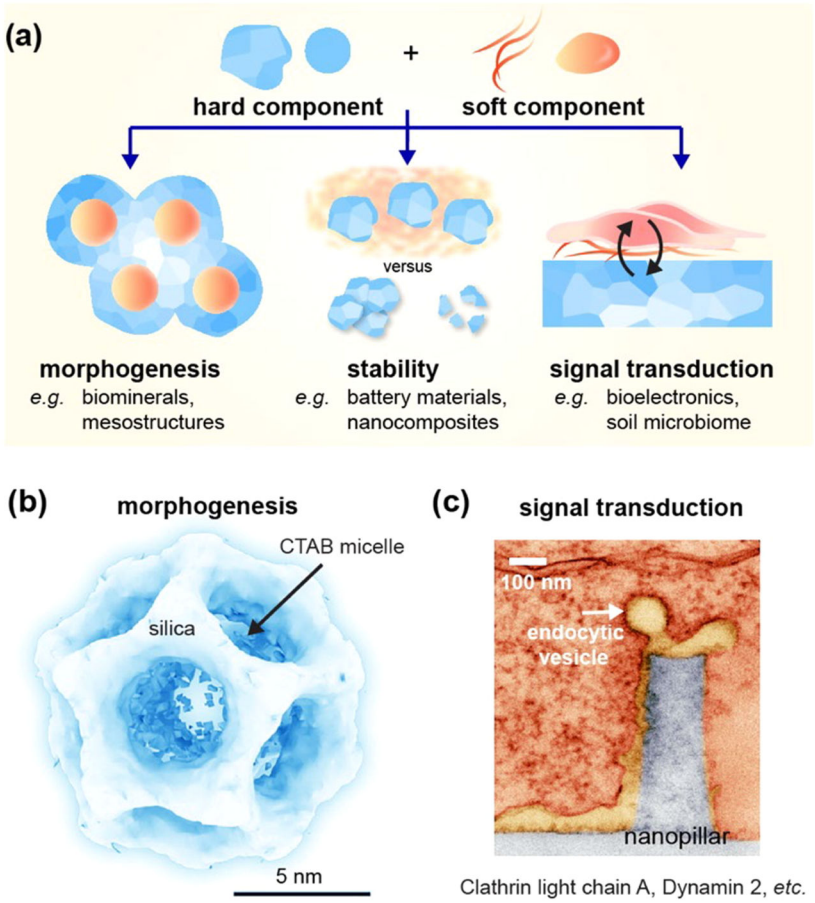

Figure 3.

Soft–hard interfacial processes have essential roles. (a) The interfacial process can yield new morphologies difficult to obtain with soft or hard components alone. It can stabilize the components against fragmentation, degradation, or disintegration. It also enables signal transductions between the soft and hard components. (b) 3D reconstructed cryo-TEM image of a dodecahedral silica cage, showing the intricate 3D architecture of the interface and the nanoscale feature size. The cryo-TEM image is modified with permission from ref 45. Copyright 2018 Springer Nature. (c) The high curvature from nanopillar structures recruits multiple curvature-sensing proteins, with protein names shown on the right. The image is modified with permission from ref 56. Copyright 2017 Springer Nature.

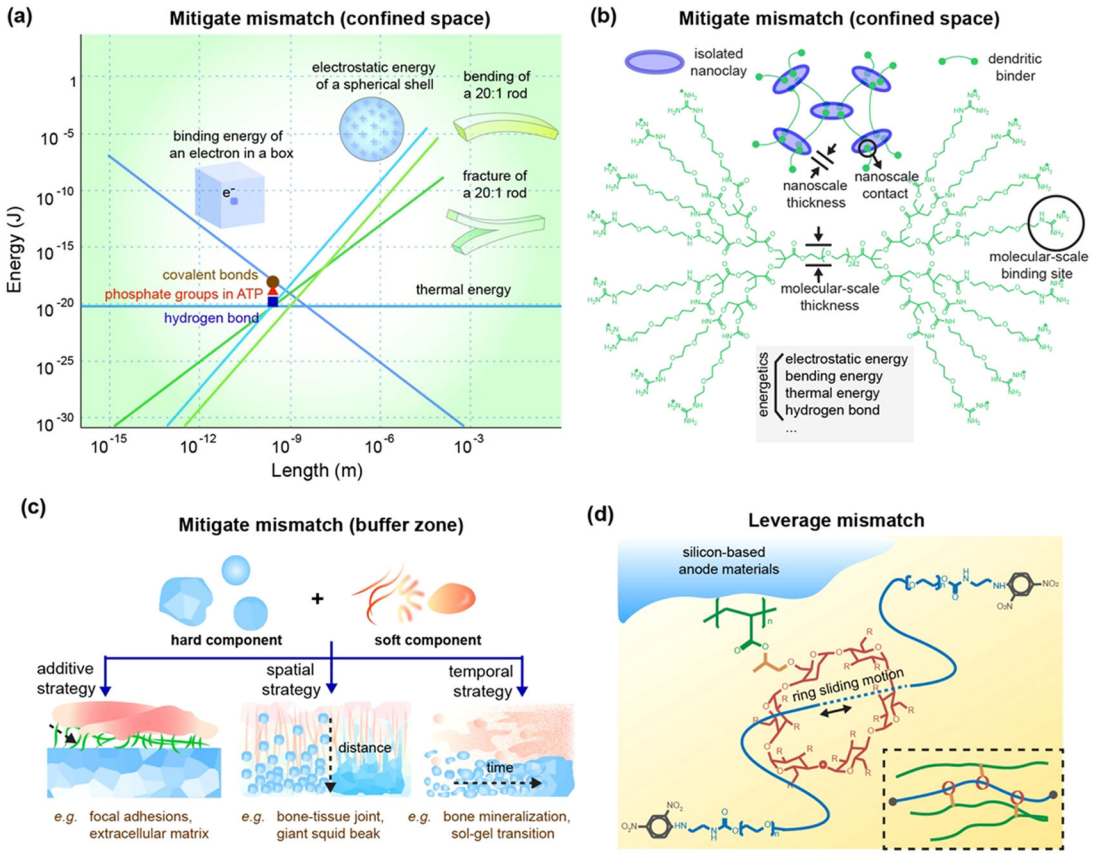

Figure 4.

Processes at soft–hard interfaces are unique. (a) Although different energies display different dependence on object size or dimensions, they converge at the molecular and nanoscopic scale. At this length scale, efficient signal transduction and minimal mismatches are expected at soft–hard interfaces. At this size regime, the boundaries between soft and hard materials, and the boundaries between living and nonliving systems, become blurred. This energy convergence can explain the critical roles of nanoscale interfacial processes at many soft–hard interfaces.[36] Reproduced with permission from ref 96. Copyright 2019 Nature Springer. (b) Dendritic binders and nanoclays self-assemble to form stable hydrogel. The feature sizes of the building blocks are at the molecular and nanoscopic levels, where multiple energy terms show similar amplitude such that the soft–hard interfaces can establish in a seamless manner. (c) To mitigate interfacial mismatches, additional buffer mechanisms are available. These mechanisms include the use of connecting linkers and deposits (additive strategy), the formation of a modulus gradient over the distance between the soft and hard phases (spatial strategy), and gradual and less perturbative condensation of the hard component at the interface (temporal strategy). (d) The soft–hard interfaces can produce the strain hotspots, which may be leveraged for special chemical processes or applications. For example, ring sliding of polyrotaxane close to the silicon/binder interfaces can be triggered during the operation of silicon-based battery anode.

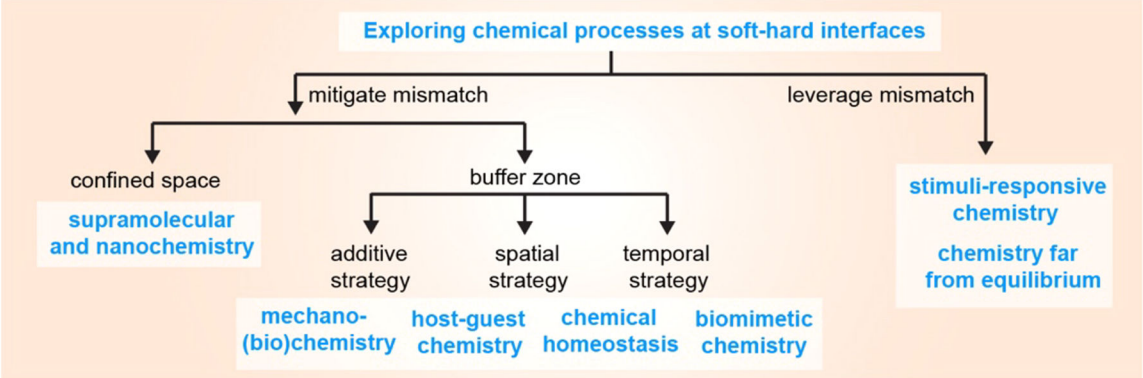

Figure 5.

Soft–hard interfaces present several pathways of exploring new interfacial processes, by either mitigating or leveraging the mismatches at the interfaces. Shown here only highlights the chemical processes.

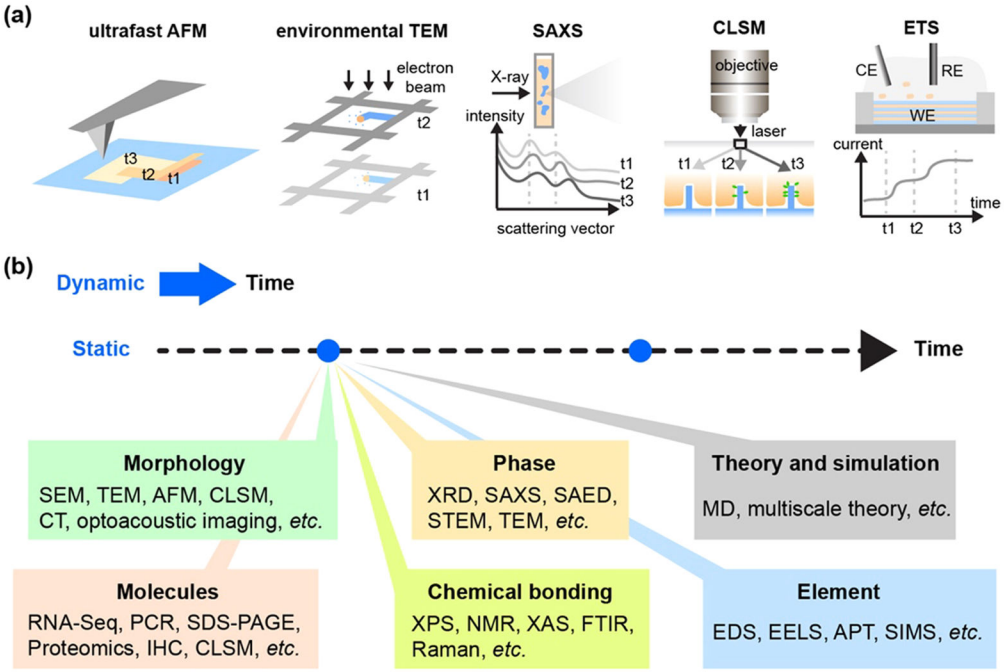

Figure 6.

Multiple characterization approaches have been developed to study the dynamic interfacial processes at the soft–hard interfaces. (a) In situ studies of short processes can be achieved with ultrafast atomic force microscopy (AFM), environmental transmission electron microscopy (TEM), small angle X-ray scattering (SAXS) and confocal laser scanning microscopy (CLSM). (b) While in situ experiments can capture the dynamics of short processes directly, ex situ studies can reveal the dynamics indirectly by recording static information at multiple time points (blue dots alone the dashed line arrow), with correlative microscopies and spectroscopies, and with input from theory and simulation. SEM: scanning electron microscope; TEM: transmission electron microscope; AFM: atomic force microscope; CLSM: confocal laser scanning microscopy; XRD: X-ray diffraction; SAXS: Small-angle X-ray scattering; SAED: selected area electron diffraction; STEM: scanning transmission electron microscopy; MD: molecular dynamics simulation; PCR: polymerase chain reaction; SDS-PAGE: sodium dodecyl sulfate polyacrylamide gel electrophoresis; IHC: immunohistochemistry; XPS: X-ray photoelectron spectroscopy; NMR: Nuclear magnetic resonance; FTIR; Fourier transform infrared spectroscopy; EDS: energy-dispersive X-ray spectroscopy; EELS: electron energy loss spectroscopy; APT: atom probe tomography; SIMS: secondary-ion mass spectrometry.

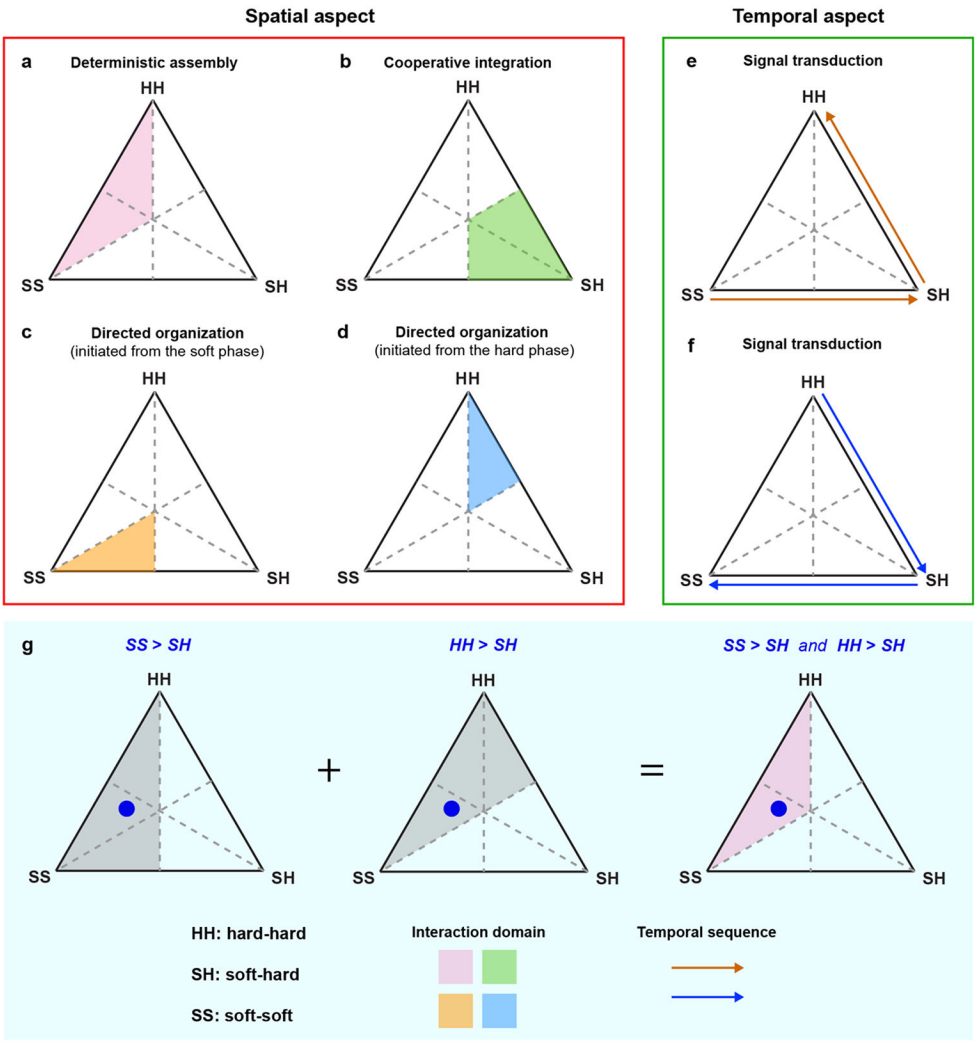

Figure 7.

We propose a new “Interaction Framework” at the soft–hard interfaces. The interactions can be (bio)chemical, mechanical, electrical, etc. (a–d) represent the spatial aspect, while panels e and f represent the temporal aspect of the interaction framework. Depending on the specific target/domain of a system, different interaction frameworks can coexist in a single system. (g) Similar to the interpretation of a conventional phase diagram, the relative distance from a point (blue dot) to the three corners of the framework triangle suggests the relative dominance of the roles of SS, SH, and HH interactions; the shorter the distance to one corner, the more dominant the interaction that is represented by the corner. Each color domains in a–d are the overlapped area from two half-triangles (in gray) as two inequalities need to be satisfied simultaneously. The approach to derive the domain for the case of “deterministic assembly” is given in panel g.

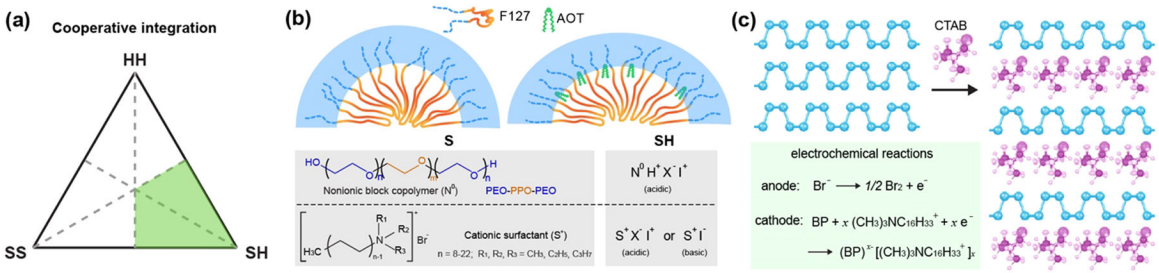

Figure 8.

Interaction framework–cooperative integration can be verified with existing examples. (a) The cooperative integration diagram. (b) Synthesis of mesostructured inorganic materials often involves self-assembly of inorganic precursors (positively charged I^+ or negatively charged I^-) with cationic surfactants (S^+) or nonionic block copolymers (N^0). The soft–hard (SH) interactions can involve protonation (H^+) and anion coupling (X^-), and occur in either acidic or basic conditions. In block copolymer-based synthesis, e.g., with pluronic F127, the hydrophilic segments such as PEO are inserted inside the inorganic walls, producing a graded regime. The addition of cosurfactant such as sodium bis(2-ethylhexyl) sulfosuccinate (AOT) can tune the interface chemistry and the curvature. (c) Electrochemical intercalation of black phosphorus (BP) by CTAB molecules produces a soft–hard superlattice structure. Electrochemical reactions are shown in the lower left panel. As the superstructure cannot be formed by either the black phosphorus or the CTAB molecules alone, the cooperativity at the soft–hard interfaces is the key to the final composite structure.

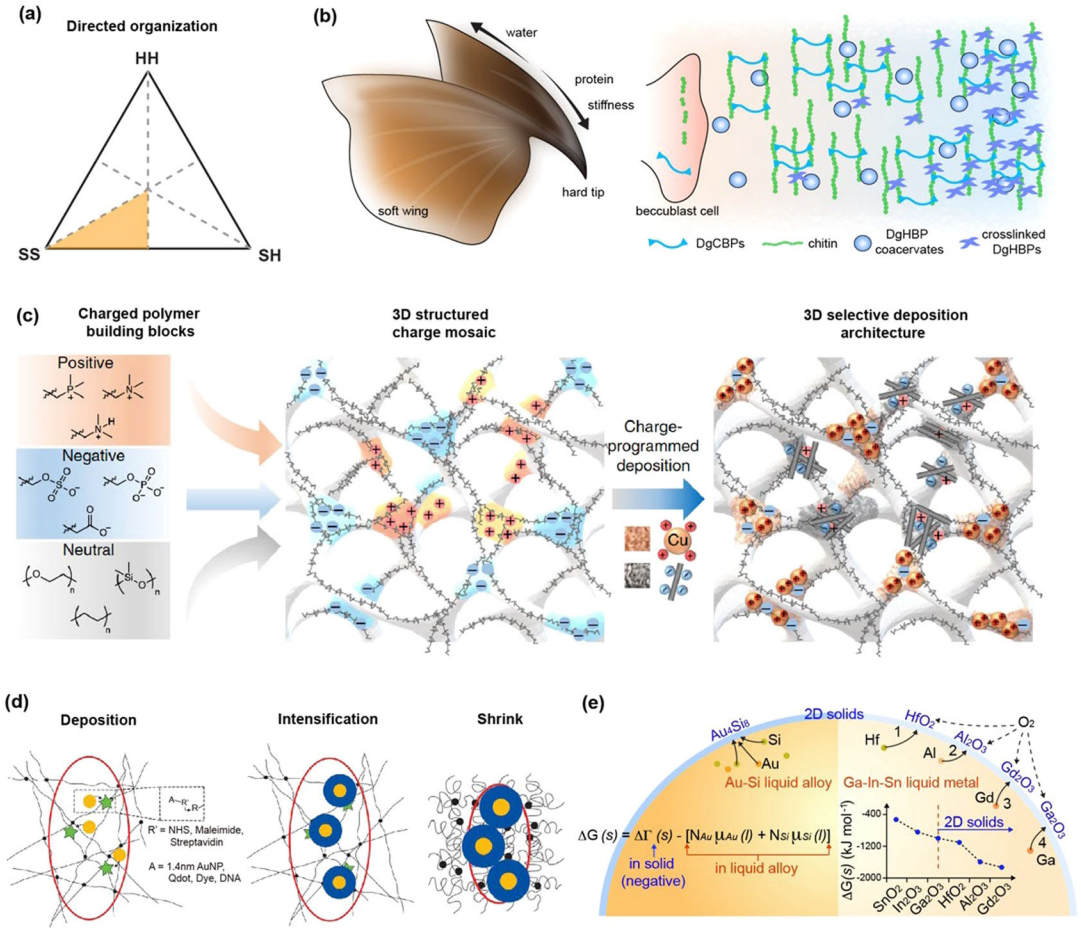

Figure 9.

Interaction framework–directed organization from the soft phase can be verified with existing examples. (a) The interaction framework for the soft phase-directed organization. (b) In a naturally occurring example, the production of chitin-binding proteins (DgCBPs) and histidine-rich proteins (DgHBPs) based coacervates, the dynamic interaction of these proteins with the chitin-based soft template, and hydration/dehydration create the modulus gradient. Panels c–e are synthetic examples. (c) Schematic of the strategy enabling programmed deposition of electrostatic charges. Patterns of positive, negative, and neutral patterns allow for selective material deposition and preserve the prescribed charge in 3D materials. Reproduced with permission from ref 176. Copyright 2020 Springer Nature. (d) The optically patternable hydrogels triggered volumetric metal deposition and intensification at defined 3D locations. Upon volume shrinkage, mineralized networks such as a silver nanostructure and optical metamaterials can be generated. Reproduced with permission from ref.[177] Copyright 2018 AAAS. (e) Liquid alloy droplets or liquid metal droplets can template the growth of 2D inorganic sheets over their surfaces. The droplets also serve as the chemical reactors where at least one chemical element is extracted from the droplets for the sheet production. $\Delta G(S)$ is the free energy change for the solid skin. N_{Au} and N_{Si} are the area density of Au and Si atoms in the skin layer. $\Delta\Gamma(S)$ is the change in free energy

upon taking $N_{Au} + N_{Si}$ atoms from the reference solids. $\mu_{Au}(l)$ and $\mu_{Si}(l)$ are the chemical potentials of the atoms in the liquid.

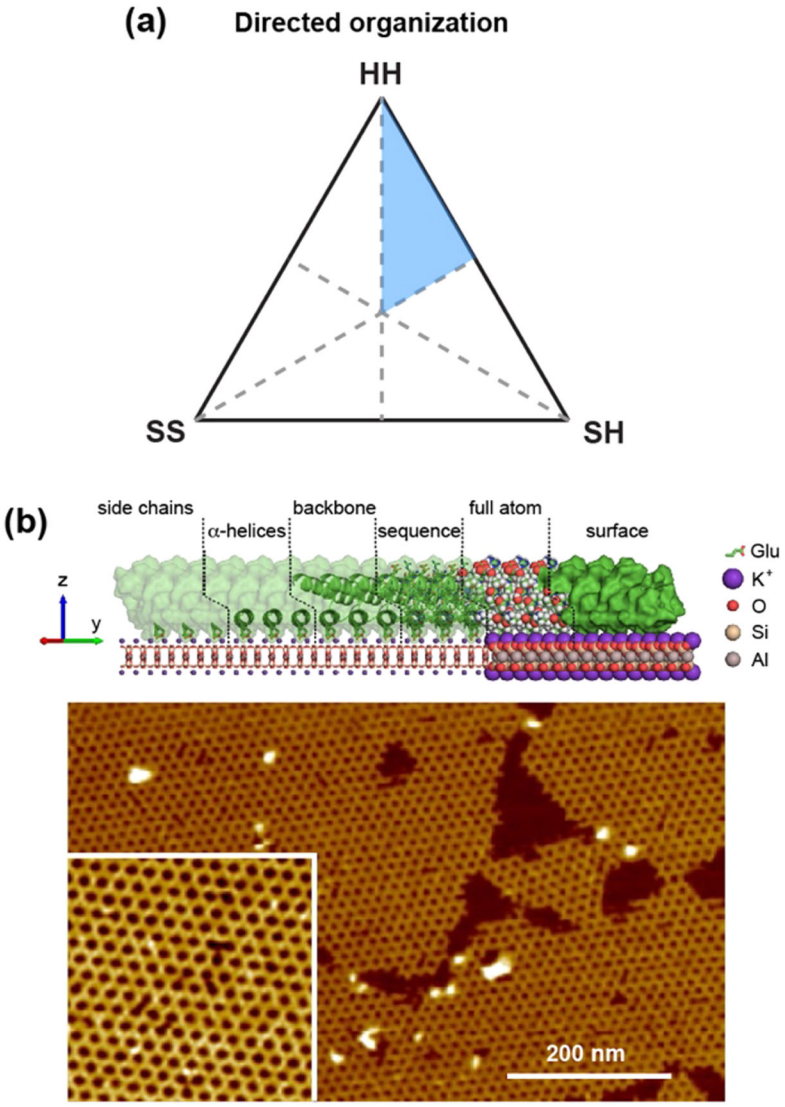

Figure 10.

Interaction framework–directed organization from the hard phase can be verified with existing examples. (a) The interaction framework for the hard phase-directed organization. (b) De novo designed proteins form ordered structures over the mica surface. The upper schematic shows the model of DHR-mica interface, with repeats 1–3 (glutamate, Glu, side chains), repeats 4–6 (α-helical secondary structures), repeats 7–9 (full DHR backbone), repeats 10–12 (backbone and amino acid side chains), repeats 13–15 (all atoms), and repeats 16–18 (external protein surface). The lower AFM image shows one honeycomb lattice. The inset area is 200 nm × 200 nm. This panel is adapted with permission from ref 143. Copyright 2019 Springer Nature.

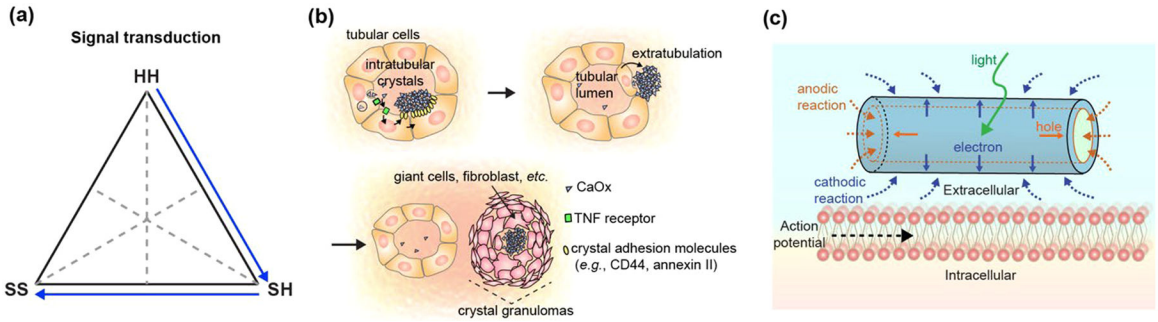

Figure 11.

Interaction framework–signal transduction can be verified with existing examples. (a) The interaction framework for the hard phase-initiated signal transduction. (b) The formation of kidney crystal granulomas is an example of cooperative and multiple interfacial processes in a soft–hard hybrid generation. (c) A photoelectrochemical process at a coaxial silicon nanowire/neuron interface can elicit action potential propagation in cells. Adapted with permission from ref 86. Copyright 2018 Springer Nature.

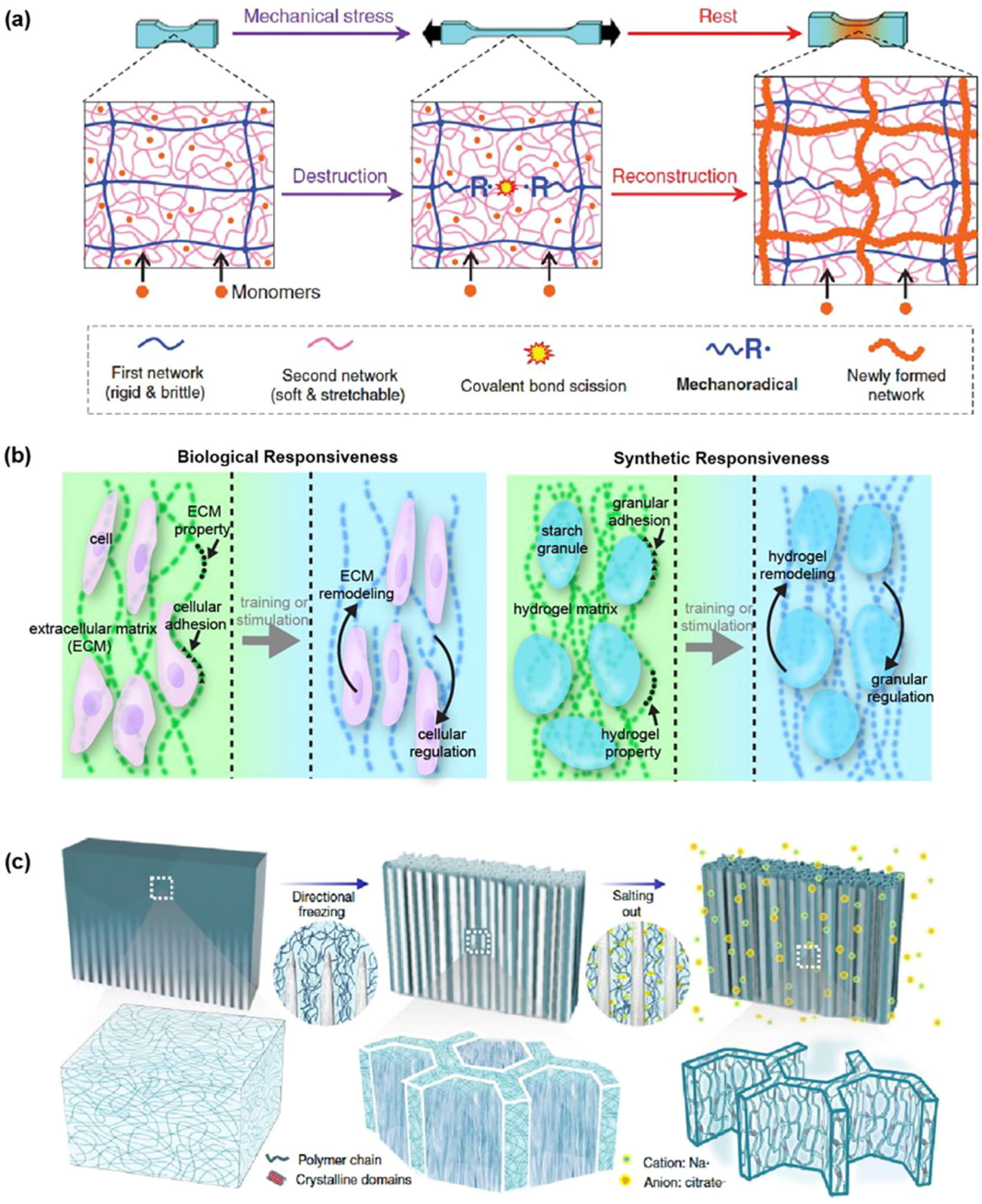

Figure 12.

Several strategies have been developed to produce soft tissue-like materials. (a) Self-growing muscle-like hydrogels. Reproduced with permission from ref 196. Copyright 2019 AAAS. (b) Granules-enabled tissue-like materials from granule/hydrogel composite. Reproduced with permission from ref 197. Copyright 2020 ELSEVIER. (c) A multilength-scale hierarchical hydrogel architecture that mimicks tendon was made by directional freezing and salting out methods. Reproduced with permission from ref 198. Copyright 2021 Springer Nature.

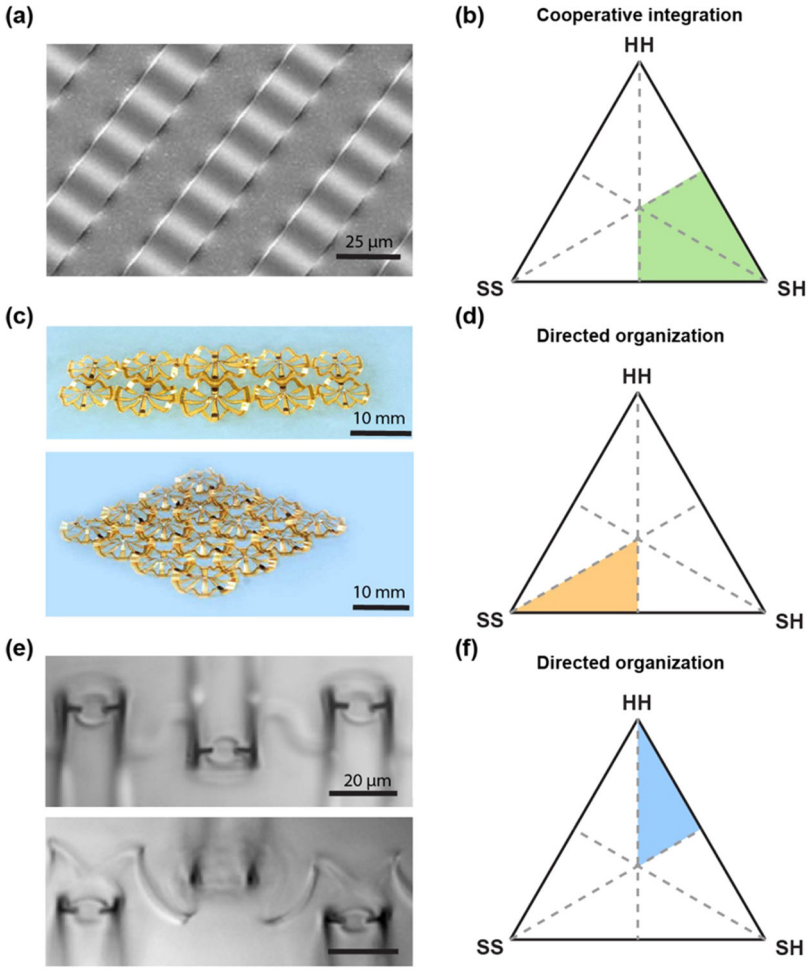

Figure 13.

Interaction between soft substrates and hard electronics produces stretchable and three-dimensional devices. (a) Interaction between the stretchable substrate and silicon material allows the formation of highly uniform ribbons. Reproduced with permission from ref 200. Copyright 2006 AAAS. (b) Cooperative integration, SH > SS, SH > HH. The wavy structure was formed through a biphasic cooperative process. This structure cannot form with PDMS or Si nanoribbon alone. (c) Arrays of three-dimensional multifunctional mesoscale frameworks for holding and recording electrical activity in spheroid organoids. Reproduced with permission from ref 211. Copyright 2021 AAAS. (d) Directed organization, SS > SH > HH. The local bonding sites and the elastomer substrate enable 2D-3D transformation. (e) Stress between the hard (metal) and soft (SU-8) materials allows for transistor positioning in a recording device. Reproduced with permission from ref 212. Copyright 2012 Springer Nature. (f) Directed organization, HH > SH > SS. The residual stress from multiple material layers enables the 2D–3D transformations.

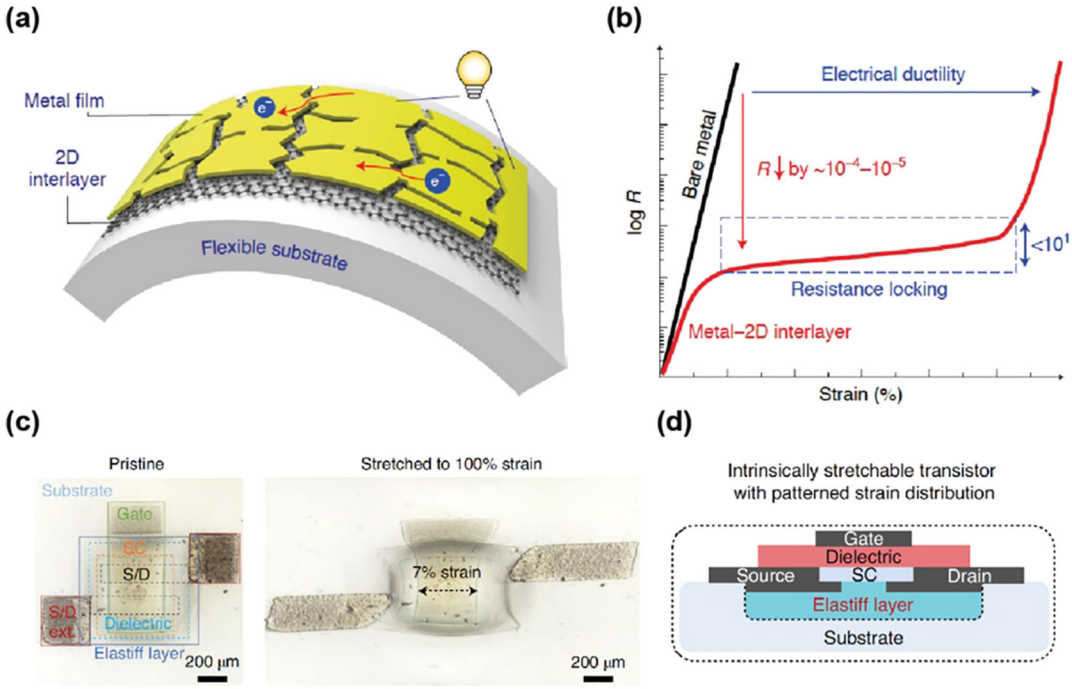

Figure 14.

Atomically thin-material interlayers enable strain-resilient electrodes. (a) Schematic of a fractured metal film on single-layer graphene forming the conductive and flexible electrode. (b) Conceptual plot comparing resistance in bare metal and metal-interlayer material in the function of applied strain. The metal-interlayer material possesses a large, stable “resistance locking” region. (c) Optical image of a flexible transistor array under 0% (left) and 100% (right) deformation. The varying concentration of cross-linkers in conductive polymers allows for the fabrication of the device with the prescribed stiffness allowing redistribution of strain to the nonactive areas. (d) Representative structure of a flexible transistor device. (SC, semiconductor material) Panels a and b were reproduced with permission from ref 245. Copyright 2021 Springer Nature. Panels c and d reproduced with permission from ref 218. Copyright 2021 Springer Nature.

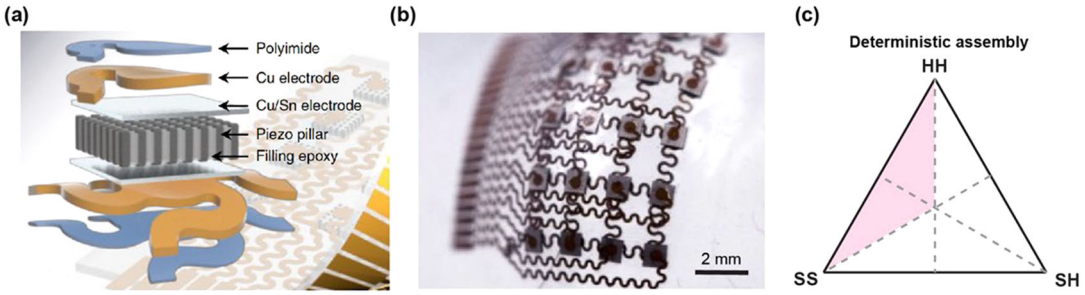

Figure 15.

Flexible ultrasonic device has high mechanical resilience and can conform to the skin enabling remote sensing of blood pressure. (a) Schematic of the ultrasonic device with the array of piezoelectric rods embedded in an epoxy matrix. (b) Optical image of the device under strain showing its high conformability. (c) The device was made by the deterministic assembly, where the properties of the soft and hard phases are well-defined. Reproduced with permission from ref 256. Copyright 2018 Springer Nature.

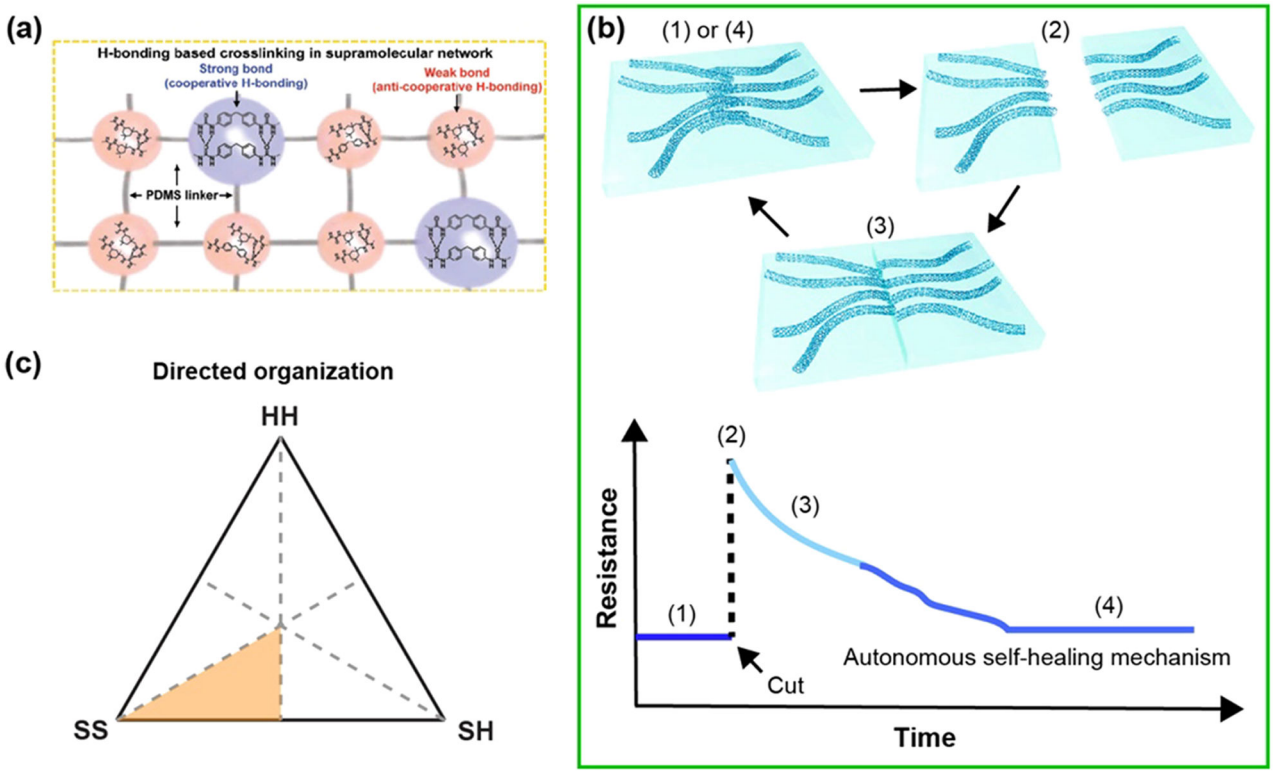

Figure 16.

Self-healing elastomers enable regeneration in electronic systems. (a) Schematic of hydrogen bonding combinations in the self-healable elastomer. Reproduced with permission from ref 261. Copyright 2018 Wiley. (b) Schematic of the autonomous resistance recovery in the carbon nanotube (CNT) network embedded in the self-healing polymer. (1) In the original state, the material possesses high conductivity due to interweaving CNTs in the network. (2) Mechanical damage (e.g., cut) increases the material's resistance. (3) Mechanical stability and conductivity are regained after contact between cut parts is established. (4) Due to the dynamic nature of the polymer, the CNT network recovers, and the cut part is indistinguishable from the pristine material. Adapted with permission from ref 221. Copyright 2018 Springer Nature. (c) Directed organization following SS > SH > HH can be used to describe the self-healing behavior of the 1D nanostructure-incorporated PDMS elastomer.

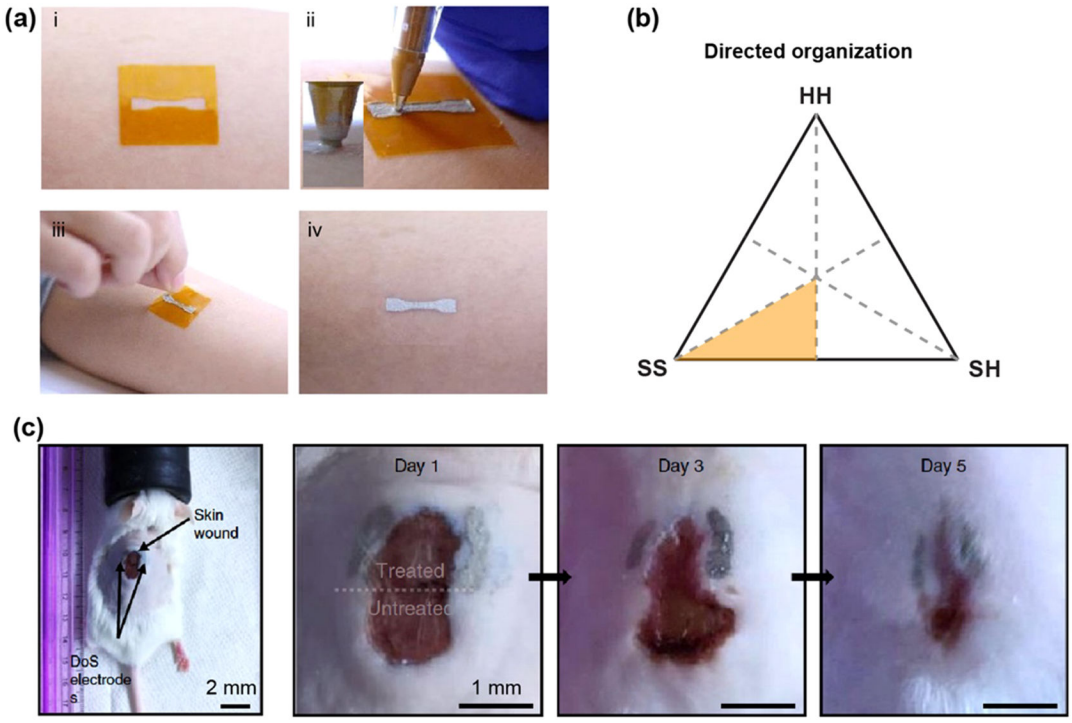

Figure 17.

Electronic inks enable the printing of electronic circuits directly on the skin and achieve unprecedented conformity. (a) A demonstration of an electronic ink deposition using polyimide stencil. (b) The material shows direct organization on the surface of the skin, following the directed organization pathway. (c) Drawn on skin electronics have been used to promote wound healing through electrical stimulation. The images show accelerated healing in the treated region (top part of the wound) compared to the untreated region (bottom part of the wound). Reproduced with permission from ref 223. Copyright 2020 Springer Nature.

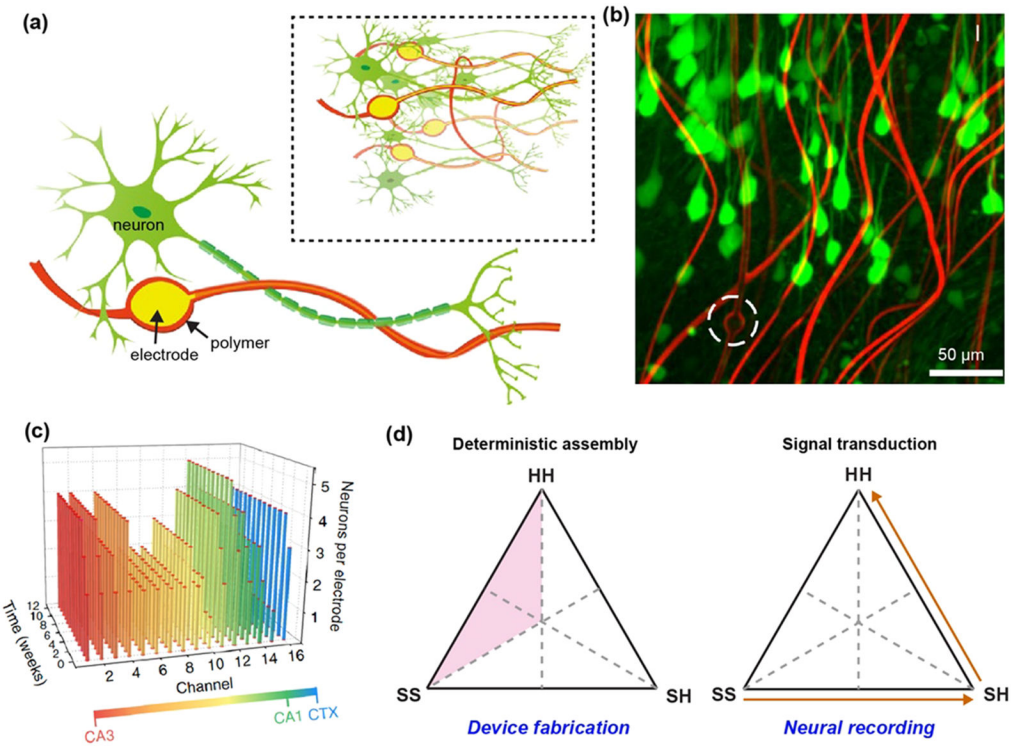

Figure 18.

Bioinspired architecture allows to produce minimally invasive and biocompatible neuron-like electrodes. (a) Schematics of neuron-like electronics (NeuE) and neurons showing their structural similarity at the subcellular level and the network level (inset). NeuE is fabricated using photolithography. Submicrometer-thick and a few micrometer-wide neurite-like SU-8/gold/SU-8 interconnects are connected to platinum electrodes. (b) Two-photon fluorescence image of the interface between neurons (green) and NeuE (red) at 6 weeks after injection into the mouse brain. The white dashed circle indicates an electrode. (c) Bar chart showing the number of neurons recorded by each electrode as a function of postimplantation time. Bar colors are coded according to the brain regions spanning from the cortex (CTX) to hippocampal CA1 and CA3. (d) While device fabrication follows deterministic assembling, the signal transduction for neural recording starts from a different soft system, i.e., neural tissues. Panels a–c are reproduced with permission from ref 224. Copyright 2020 Springer Nature.

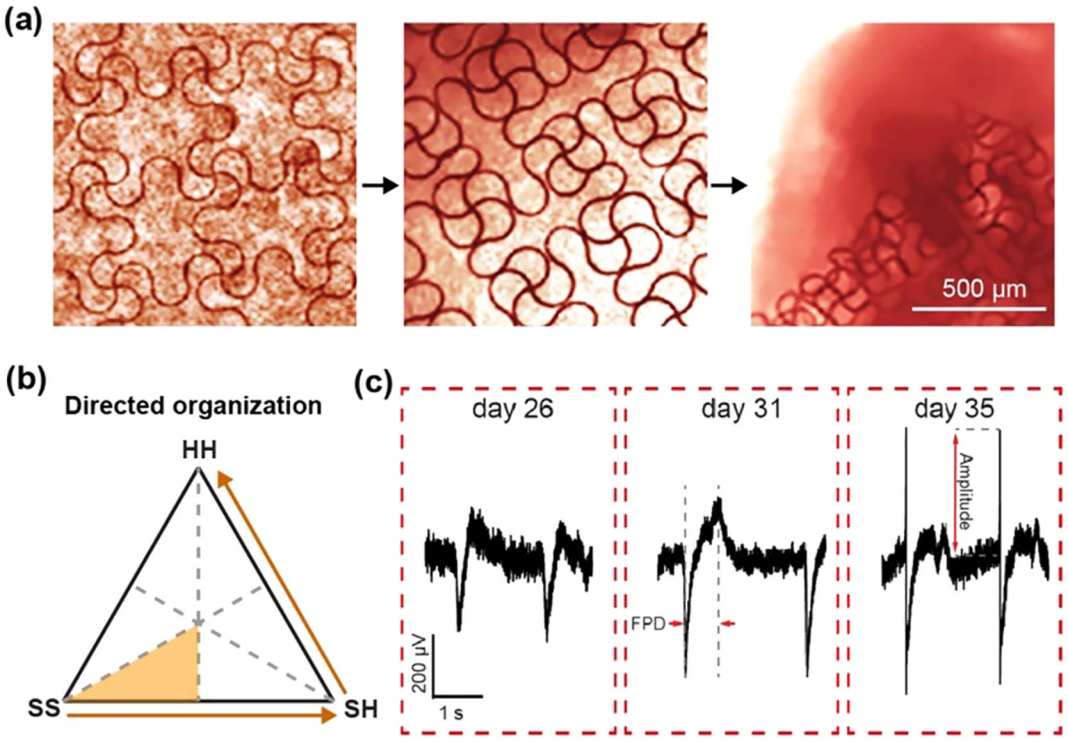

Figure 19.

Organogenesis can guide an organization of 3D mesh electronics. (a) Microscope images showing different types of deformations in the material throughout organogenesis. (b) Directed organization, following SS > SH > HH. Organoid development provided the driving force for the 2D to 3D device transformation. (c) Seamless integration enabled continuous chronic recording and analysis of spike dynamics revealed a change from an initially slow waveform to fast depolarization over the course of organogenesis. Reproduced with permission from ref 225. Copyright 2019 ACS.

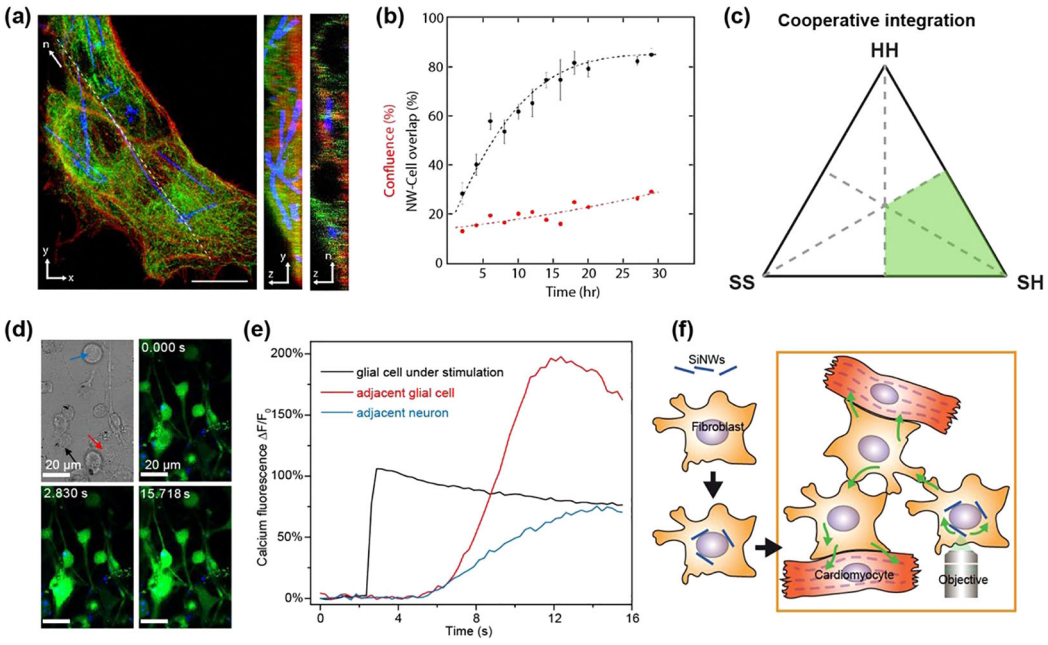

Figure 20.

Silicon nanowires can be spontaneously internalized by different types of cells, enabling optical modulation of cells. (a) Confocal microscope image of nanowires (blue, scattering channel) internalized by HUVEC cells. The confocal sections confirm nanostructure internalization. (b) The plot of area overlap between the nanowires and cell bodies and confluence over time. Overlap fraction larger than confluence suggests that nanowires are actively taken up by the cells. (c) soft–hard interaction framework follows SH > SS and SH > HH. (d) DIC microscopy image of nanowires internalized by glial cells. (black arrow–nanowire, red arrow–glial cell, blue arrow–neuron) Confocal microscope fluorescence time series shows calcium wave propagation after stimulation of an internalized nanowire using a laser. (e) Transients of calcium dynamics in the cellular assembly after stimulation. (f) Schematic of myofibroblast-cardiomyocytes assembly, which can be used to study intercellular signaling and perform pacing of muscle cells. Panels a and b were reproduced with permission from ref 226. Copyright 2016 AAAS. Panels d and e reproduced with permission from ref 85. Copyright 2018 Springer Nature. Panel f reproduced with permission from ref 228. Copyright 2019 PNAS.

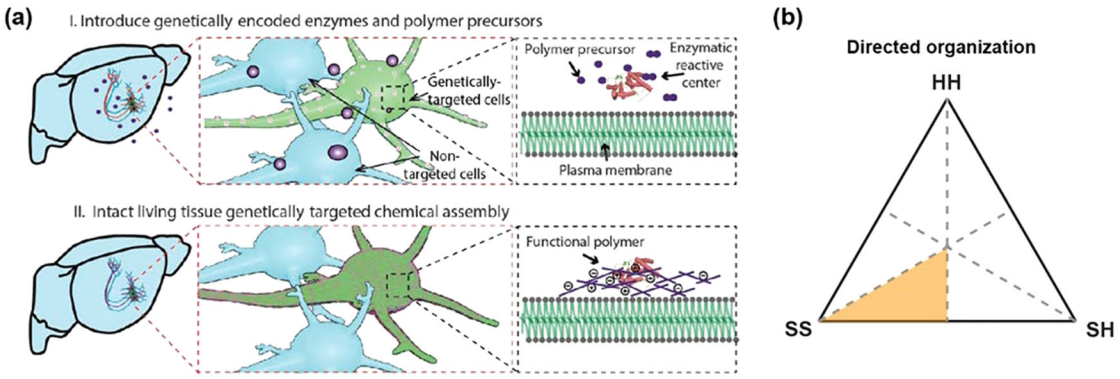

Figure 21.

Genetic encoding of the catalytic enzyme allows the synthesis of conductive polymers directly onto the cell membranes. (a) Genetic targeting allows modifying only a specific subset of neurons with the conductive polymer. Depending on the polymer conductivity, these materials can enhance or inhibit neuronal activity by modifying their membranes' capacitance. Reproduced with permission from ref 229. Copyright 2020 AAAS. (b) Directed organization following SS > SH> HH. Genetically modified neurons can guide the growth of the conducting polymers. In this case, the modulus of the conducting polymers are orders of magnitude larger than that of cell membranes. This process can be homologous to biomineralization, although no inorganic materials are formed.

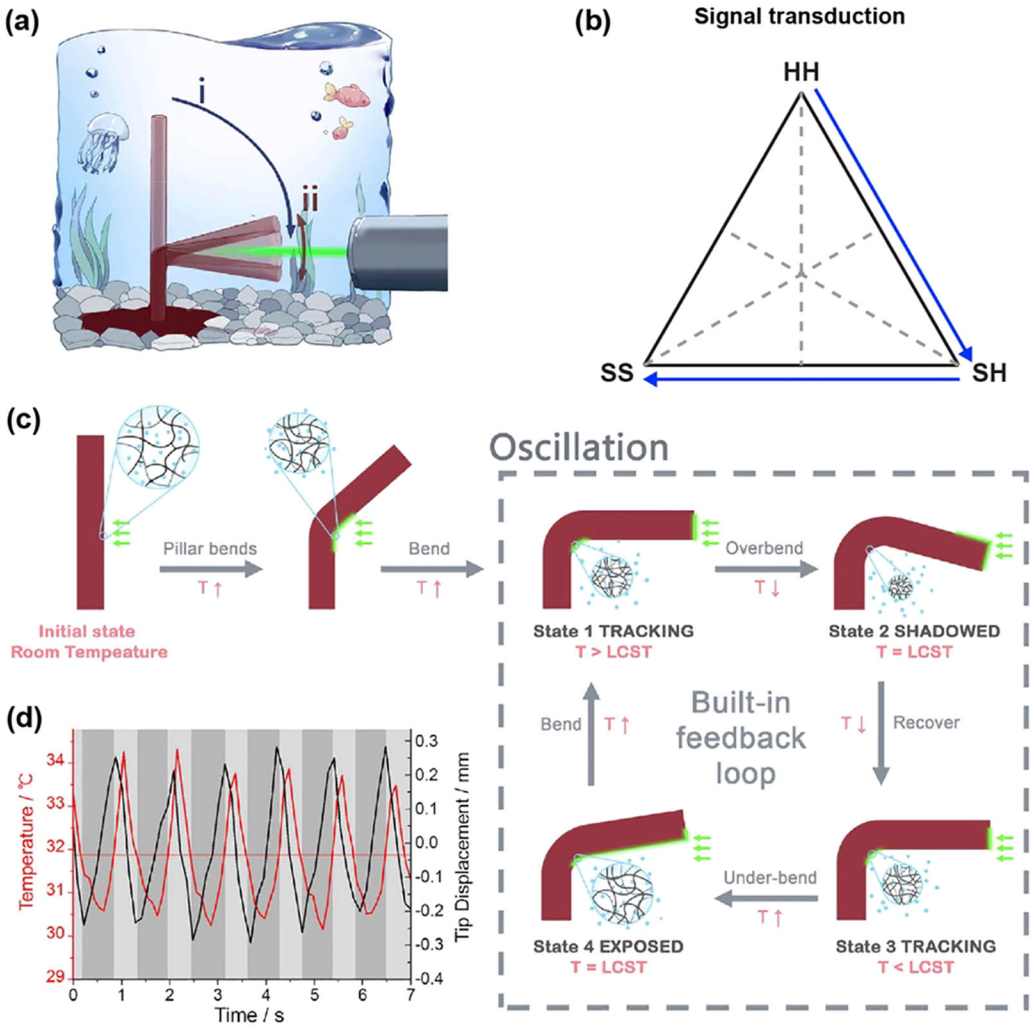

Figure 22.

Phototactic gels allow the creation of oscillators that can be used for light-driven motion. (a) Schematic of the laser-driven oscillating pillar made of the phototactic gel. (b) soft–hard interaction framework. The signal transduction follows HH > SH > SS. (c) Mechanism of oscillating motion. Self-shadowing of the pillar's inner surface creates out-of-equilibrium condition and negative loop driving the reciprocal motion. (d) Tip displacement and local temperature in the hinge during motion. The 90° shift between the curves is in agreement with the proposed motion mechanism. Reproduced with permission from ref 230. Copyright 2019 AAAS.

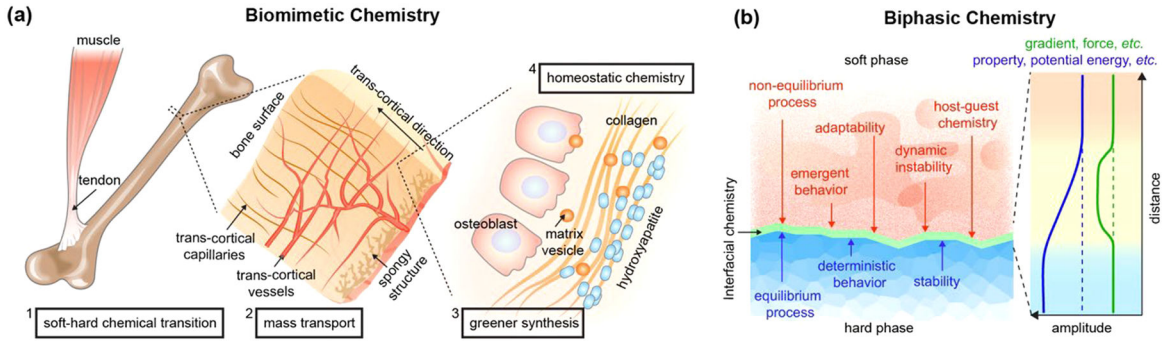

Figure 23.

Future exploration at soft–hard interfaces can yield numerous advances. (a) Bone formation presents several biomimetic chemical approaches. The chemical gradient in a tendon may suggest new ways of building load-bearing interfaces between implants and tissues. Transcortical vessels, the newly discovered trans-cortical capillaries, and the spongy structures indicate that building micro- or nanoscale networks within the hard-phase may improve mass transport to soft–hard interfaces. The biogenic synthesis and regulation of hydroxyapatites over the collagen matrix may address the need for greener and homeostatic chemical processes. (b) Property mismatches at soft–hard interfaces can be leveraged for unique chemical processes. For example, the “host–guest chemistry” from soft materials, when coupled with the deterministic electronic processing from the hard counterpart, may yield new chemical or biochemical sensor devices. Additionally, mismatches at interfaces can produce gradients and fields, which could trigger chemical or biochemical reactions in a highly efficient manner.

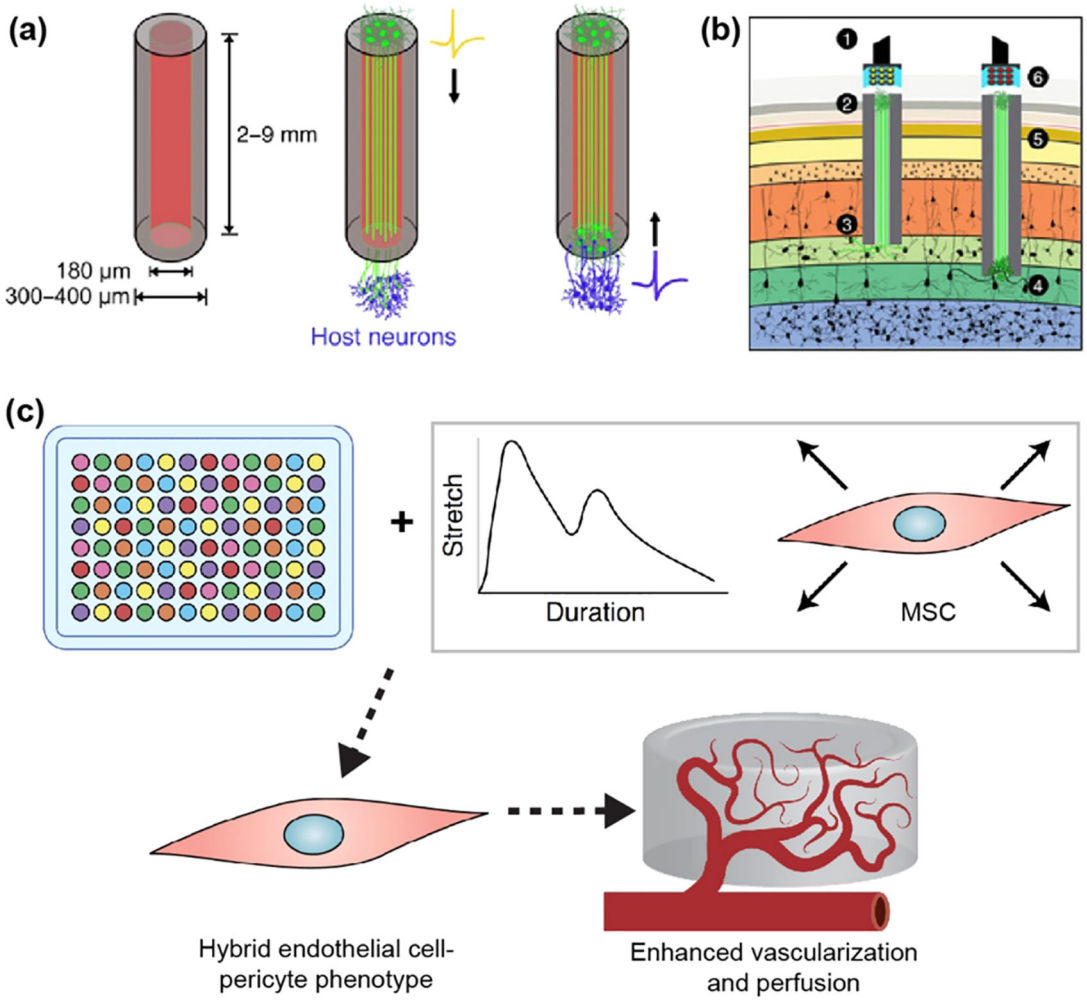

Figure 24.

New strategies for tissue engineering would enable future biointegrated electronics and robotics. (a) Hydrogel-directed axonal growth was used to generate living electrodes. Optogenetically active neurons were grown in a cylinder. After implantation, rapid axonal overgrowth allowed integration of the probe with the tissue. Partial overgrowth of host axons with the probe allows for the recording of neuronal activity. (b) Schematic of two probes of various lengths which can be implanted to distinct depth allowing stimulation of different parts of the brain using LED arrays. (c) High throughput mechano-pharmacological screen was used to produce mesenchymal stem-cell-derived endothelial cells, which promote vascularization and perfusion in the tissue after transplantation. Both chemical and mechanical stimuli were applied to generate appropriate cell phenotype. Panels a and b were reproduced with permission from ref 337. Copyright 2021 AAAS. Panel c reproduced with permission from ref 338. Copyright 2021 Springer Nature.

Table 1.

Characterization of Selected Chemical Processes at the Soft–Hard Interfaces[a]

	composite materials	soft components	hard components	characterization of the chemical processes
cooperative integration	mesoporous material synthesis[50]	surfactants or block copolymers	inorganic precursors, oligomers or their cross-linked network	SAXS, NMR, and TEM were used to capture the immediate products, biphasic self-assembly dynamics and material structures during the mesostructure formation.
	high water content hydrogel[23]	telechelic dendritic macro-molecules	clay nanosheets	rheology test and cryo-TEM showed that electrostatic interaction between positively charged guanidinium ion pendants and negatively charged clay nanosheets stabilizes the hydrogel.
	monolayer atomic crystal molecular superlattice[110]	lauryl- or cetyl- or octadecyl-trimethylammonium bromide	monolayers separated from black phosphorus, $WeSe_2$, SnSe, $NbSe_2$ etc.	cross-sectional TEM, XRD, XPS were used to study the interactions between the negatively charged monolayer atomic crystals and the positively charged surfactant layers.
	twin plane superlattice in nanowires[54,137]	gold-based alloy droplets	InAs, GaP, InP, etc.	environmental TEM showed that the variation of alloy/semiconductor interface geometry in a growing nanowire and surface energy minimization introduces periodic twin planes and sidewall faceting.
directed organization	*P. carterae* coccolith shell[19]	coccolith plate, soluble macromolecules	calcite nanocrystals	AFM, HAADF-STEM, EELS, and ATR-FTIR revealed that specific interactions between soluble macromolecules and coccolith plate direct calcite precursors for mineralization at the plate periphery.
	bone[138]	type I collagen matrix, osteoblast, etc.	apatite nanocrystals	Cryo-TEM, tomography and MD simulation suggest that the positive net charge close to the C-terminal end of the collagen promotes amorphous calcium phosphate infiltration, and that the charged amino acid clusters promote mineralization.
	squid beak[102]	hydrated chitin network	protein-cross-linked and dehydrated chitin network	SDS-PAGE, rheometry, and turbidity measurements revealed that the modulus gradient in squid beak is created by chitin-binding proteins (DgCBPs), histidine-rich proteins (DgHBPs) based coacervates, the dynamic interaction of these proteins with the chitin network, and hydration/dehydration.
	synthetic nacre[139]	chitosan, β-chitin, silk fibroin	aragonite ($CaCO_3$)	cross-sectional TEM confirmed that $Ca(HCO_3)_2$ decomposes in the presence of poly(acrylic acid) and Mg^{2+} within the scaffold.
	dodecahedral silica cage[45]	mesitylene-swelled CTAB micelles	primary silica cluster	Cryo-TEM and tomography showed that primary silica clusters are symmetrically assembled on the surface of oppositely charged surfactant micelles.
	2D Au–Si sheet over liquid alloy[80]	liquid Au–Si alloy droplet	Au–Si solid sheet	environmental TEM highlighted the crystallization of ordered layers of Au–Si over the alloy droplet surface near the eutectic temperature.
	2D metal oxides over liquid metal[140]	Ga–In–Sn liquid metal	HfO_2, Al_2O_3, Gd_2O_3, Ga_2O_3	TEM and AFM confirmed the formation of metal oxides over the liquid metal surface.
	photosynthetic bacteria[141]	*Moorella thermoacetica*	CdS nanoparticles	TEM and EDS showed that when Cd^{2+} and cysteine are supplied to the CO_2-reducing bacterium M. thermoacetica, CdS nanoparticles precipitate over the bacterium surface *in situ.*
	peptide nanowire arrays[142]	Tyr-Ser-Ala-Thr-Phe-Thr-Tyr peptides	MoS_2 substrate	AFM and MD simulation revealed the nucleation and growth dynamics of peptide array formation over MoS_2 substrate.
	protein arrays and patterns[143]	helicalrepeat (DHR) proteins	mica substrates with controlled K^+ lattice sites	de novo protein design, AFM, and SAXS were used to achieve nanowire and honeycomb arrays of proteins on mica.

Chem Rev. Author manuscript; available in PMC 2022 July 09.

	composite materials	soft components	hard components	characterization of the chemical processes
signal transductions	kidney crystal granulomas[82]	tubular cells, giant cells, fibroblasts, etc.	CaOx crystals	histology straining and TEM revealed kidney stone location and formation dynamics.
	cell/nanostructure interface[56]	cells (SK-MEL-2 and genome-edited SK-MEL-2 line)	quartz nanopillars and other nanostructures	immunostaining, FIB-SEM, and fluorescence imaging showed that positive curvature of nanostructures recruits clathrin-mediated endocytosis proteins, such as clathrin and dynamin.
	neuron/coaxial Si nanowire interface[86]	DRG neuron	p-type/intrinsic/n-type coaxial Si nanowire	APT and patch-clamp revealed that atomic gold at the coaxial Si nanowire surface promotes the photoelectrochemical reaction, which reduces the local electrochemical potential at the neuron/nanowire interface and elicits action potentials in neuron.

[a]SAXS: small-angle X-ray scattering; NMR: nuclear magnetic resonance; TEM: transmission electron microscopy; SEM: scanning electron microscopy; XPS: X-ray photoelectron spectroscopy; XRD: X-ray diffraction; AFM: atomic force microscopy; HAADF-STEM: High-angle annular dark field-scanning transmission electron microscopy; EELS: electron energy loss spectroscopy; ATR-FTIR; attenuated total reflection-Fourier transform infrared spectroscopy; EDS: energy-dispersive X-ray spectroscopy; SDS-PAGE: sodium dodecyl sulfate polyacrylamide gel electrophoresis; PCR: polymerase chain reaction; FIB: focused ion beam; APT: atom probe tomography.

Table 2.

Classification of Tissue-Like Systems with the Soft–Hard Interaction Framework

Soft–hard interfaces	soft components	hard components	Soft–hard interaction framework
wavy Si nanoribbon/PDMS interface[200]	PDMS or other elastomers	Si nanoribbons	cooperative integration: SH > SS and SH > HH
complex 3D structures through compressive buckling[214]	PDMS or other elastomers	diverse inorganic materials for electronic components	directed organization: SS > SH > HH
3D bendable nanoelectronics[216]	SU-8	metal layers that yield strong residual stress	directed organization: HH > SH > SS
intrinsically stretchable electronics through nanoconfinement effect[217]	elastomer phase	conjugated polymer	Cooperative integration: SH > SS and SH > HH
strain-insensitive intrinsically stretchable transistor array[218]	elastomer substrate with patterned stiffness	conjugated polymer	deterministic assembly: SS > SH and HH > SH
stretchable electronics for neonatal intensive care[203]	elastomer and ionic liquid	metal and other circuit components	deterministic assembly: SS > SH and HH > SH
PVA/Au nanomesh prior to PVA dissolution[219]	PVA nanofibers	Au layers	directed organization: SS > SH > HH
laser-engraved graphene-based sensor[220]	polyimide	graphene layers	directed organization: SS > SH > HH
self-healing electronics[221]	self-healing elastomer (e.g., PDMS-MPU0.4-IU0.6)	carbon nanotubes and Ag nanowires	directed organization: SS > SH > HH
stretchable hydrogel electronics[222]	hydrogel	electronic and optoelectronic devices	deterministic assembly: SS > SH and HH > SH
conductive on-skin tape through direct drawing[223]	skin and polymer components of the ink	Ag flakes	directed organization: SS > SH > HH
macroporous nanoelectronic scaffold[212]	SU-8	metal layers	deterministic assembly: SS > SH and HH > SH directed organization: HH > SH > SS
neuron-like electronics[224]	SU-8	metal layers	deterministic assembly: SS > SH and HH > SH
neural recording from the neuron-like electronics[224]	neurons	metal recording device	signal transduction: SS → SH → HH
multilayered Si membrane[85]	porous PDMS	Si nanostructured membrane	deterministic assembly: SS > SH and HH > SH
neuromodulation from the multilayered Si membrane[85]	isolated neurons or neural tissues	Si nanostructured membrane	signal transduction: SS → SH → HH
organogenesis-directed formation of 3D bioelectronics[225]	growing cardiac organoid	Au and Pt electrodes	directed organization: SS > SH > HH
nanowire-polymer mesh[188]	SU-8 mesh	Si nanowires	deterministic assembly: SS > SH and HH > SH
optically triggered cardiac training from nanowire-polymer mesh[188]	cardiomyocytes and cardiac tissues	Si nanowires	signal transduction: HH → SH→ SS
phagocytosis-enabled nanowire/cell composite[85,226-228]	mammalian cells	Si nanowires	cooperative integration: SH > SS and SH > HH
genetically targeted assembly of polymers[229]	neurons or neural tissues	conjugated polymers	directed organization: SS > SH > HH
phototactic actuation from a hydrogel composite pillar[230]	PNIPAAm	Au nanoparticles	signal transduction: HH → SH→ SS

Soft–hard interfaces	soft components	hard components	Soft–hard interaction framework
ferromagnetic soft continuum robot[231]	polymers and hydrogels	magnetic microparticles	signal transduction: HH → SH→ SS
magnetically steerable helical microswimmers[232]	mouse macrophages and primary splenocytes	helical magnetic microparticles	cooperative integration: SH > SS and SH > HH